
Electronic Thesis and Dissertation Repository

2-21-2017 12:00 AM

Cytosolic acetyl-CoA promotes histone H3 lysine 27 acetylation in Arabidopsis

Chen Chen, *The University of Western Ontario*

Supervisor: Dr. Yuhai Cui, *The University of Western Ontario*

Joint Supervisor: Dr. Susanne Kohalmi, *The University of Western Ontario*

A thesis submitted in partial fulfillment of the requirements for the Doctor of Philosophy degree in Biology

© Chen Chen 2017

Follow this and additional works at: <https://ir.lib.uwo.ca/etd>



Part of the [Molecular Biology Commons](#), and the [Plant Biology Commons](#)

Recommended Citation

Chen, Chen, "Cytosolic acetyl-CoA promotes histone H3 lysine 27 acetylation in Arabidopsis" (2017). *Electronic Thesis and Dissertation Repository*. 4423.
<https://ir.lib.uwo.ca/etd/4423>

This Dissertation/Thesis is brought to you for free and open access by Scholarship@Western. It has been accepted for inclusion in Electronic Thesis and Dissertation Repository by an authorized administrator of Scholarship@Western. For more information, please contact wlsadmin@uwo.ca.

Cytosolic acetyl-CoA promotes histone H3 lysine 27 acetylation in Arabidopsis

Chen Chen

Supervisor

Dr. Yuhai Cui Dr. Susanne Kohalmi

The University of Western Ontario

Graduate Program in Biology

A thesis submitted in partial fulfillment of the requirements for the degree in Doctor of Philosophy

© Chen Chen 2017

Follow this and additional works at: <http://ir.lib.uwo.ca/etd>

 Part of the [Molecular Biology Commons](#), and the [Plant Biology Commons](#)

Abstract

Acetyl-coenzyme A (acetyl-CoA) serves as a central metabolite in energy metabolism and biosynthesis. High level of acetyl-CoA can fuel the tricarboxylic acid (TCA) cycle to generate energy and store excess energy in fatty acids. Meanwhile, it also provides acetyl groups for protein acetylation, which normally occurs at the lysine or arginine residues. Acetylation regulates protein functions largely due to the change of total charges. Acetylation of histones, for example, can lead to loss of the interaction between histone and DNA, thus relaxing chromatin structure and potentially promoting gene expression. However, whether and how acetyl-CoA regulates plant chromatin remains unexplored. Here, I show that dysfunction of cytosolic acetyl-CoA carboxylase 1 (ACC1), a key enzyme for catalyzing the carboxylation of acetyl-CoA to malonyl-CoA, leads to elevated levels of acetyl-CoA and promotes histone acetylation in *Arabidopsis*. The increased accumulation of acetyl-CoA is also dependent on the activity of ATP-citrate lyase, a cytosolic enzyme which can generate cytosolic acetyl-CoA from citrate. In the wave of high levels of acetyl-CoA, hyperacetylation is mainly detected at lysine 27 of histone H3 (H3K27). Using a pharmacological approach, I demonstrate that this increase of H3K27 acetylation (H3K27ac) is dependent on the activity of histone acetyltransferase. Further, by generating and analyzing double mutants of *acc1* and mutants of each of the histone acetyltransferases, I found that General Control Non-depressible 5 (GCN5), a histone acetyltransferase of the GNAT family, is necessary for the increased H3K27ac in *acc1*. Consistently, the morphological phenotype of *acc1* can be partially rescued by knocking out *GCN5* and the H3K27ac levels in the double mutant (*gcn5 acc1*) are restored to WT levels at several selected genes. Finally, transcriptome analysis shows that increased H3K27ac in *acc1* can significantly promote transcription. Altogether, this study reveals that acetylation at H3K27 may be an important link between cytosolic acetyl-CoA level and gene expression in response to changes of the metabolic environments in plants.

Keywords

Acetyl-CoA, H3K27ac, metabolism, epigenetics, histone acetylation, GCN5, histone acetyltransferase, ChIP-seq, gene expression, *Arabidopsis*

Acknowledgments

First, I would like to express my sincere gratitude to my supervisor Dr. Yuhai Cui for his continuous support throughout my Ph.D. study, for his patience and encouragement. I am grateful to my co-supervisor Dr. Susanne Kohalmi and all my advisory committee members, Dr. Rima Menassa and Dr. Norm Hüner for their time, advice and encouragement.

My sincere thanks also go to Dr. Ali Hannoufa and Dr. Ying Wang, who provide the instruments and instructions to me for the measurement of acetyl-CoA. I also would like to thank Dr. Masao Tasaka and Dr. José Luis Micol for sharing seeds of *gk101* (*acc1-4*) and *elo3*, respectively. I am thankful to Nguyen Vi for helping with general lab work and DNA sequencing. I am also thankful to Alex Molnar for help with preparing figures.

I would also like to thank all my fellow labmates: Dr. Gang Tian, Dr. Chenlong Li, Dr. Saatian Behnaz, Jie Shu, and Raj Thapa. I am grateful for their warmth, encouragement, and helpful discussions.

In particular, I would like to thank Dr. Shangzhi Huang for enlightening me the first glance of research. I am also grateful to China Scholar Council for the financial support.

Last but not least, I would like to thank my wife and parents for supporting me spiritually throughout the five years study and my life in general.

Table of Contents

Abstract.....	ii
Acknowledgments.....	iii
Table of Contents.....	iv
List of Tables.....	vii
List of Figures.....	viii
List of Appendices.....	x
Abbreviation.....	xi
1 INTRODUCTION.....	1
1.1 Histone modifications regulate chromatin states and gene expression.....	1
1.1.1 Histone acetylation.....	2
1.1.2 Histone methylation.....	8
1.1.3 Other histone modifications.....	11
1.2 Metabolites bridge cellular environment and gene expression via histone modification.....	12
1.2.1 Central metabolites reflect cellular environment.....	12
1.2.2 Metabolites regulate histone modifications.....	14
1.3 Acetyl-CoA and histone acetylation.....	15
1.4 Scope of the Research and Objectives.....	19
2 MATERIALS AND METHODS.....	22
2.1 Plant materials and growth conditions.....	22
2.2 Next-generation mapping of <i>p1045</i>	22
2.3 Plasmid construction for plant transformation.....	23
2.4 GUS staining and microscopy.....	24
2.5 Acetyl-CoA measurement.....	24
2.6 Analysis of transcript levels.....	24

2.7	Western blotting.....	25
2.8	Chromatin immunoprecipitation (ChIP).....	26
2.9	ChIP-seq analysis.....	26
2.10	Statistical analysis.....	27
3	RESULTS	28
3.1	Identification of the <i>acc1-5</i> mutant.....	28
3.1.1	Mutation in <i>ANK^p</i> is not responsible for the <i>p1045</i> phenotype	28
3.1.2	Mutation in <i>NAC^p</i> is not responsible for the <i>p1045</i> phenotypes.....	28
3.1.3	Mutation in <i>ACCI</i> is responsible for the <i>p1045</i> phenotype.....	28
3.2	Subcellular localization and tissue specificity of ACC1.....	35
3.3	Increased accumulation of acetyl-CoA and histone H3K27 acetylation in <i>acc1</i> mutants.....	35
3.4	Genome-wide profiles of histone modifications in WT and <i>acc1-5</i> mutant plants	50
3.4.1	Increased genome-wide occupancy of H3K27ac in <i>acc1-5</i>	50
3.4.2	Genome-wide occupancies of other 7 histone acetylations in <i>acc1-5</i> and WT	57
3.4.3	Genome-wide profiling of H3K27ac in <i>acc1-5 acla-1i</i> conditional double mutant	57
3.4.4	Genome-wide analysis of H3K27me3 in <i>acc1-5</i>	64
3.5	GCN5/HAG1 is required for the increased H3K27ac in <i>acc1-5</i> on some genetic loci.....	71
3.6	Global profiling of transcripts in <i>acc1-5</i>	78
4	DISCUSSION	84
4.1	Mutation of <i>ACCI</i> disrupts fatty acids elongation and causes accumulation of acetyl-CoA	84
4.2	Cytosolic acetyl-CoA promotes H3K27ac in <i>Arabidopsis</i>	85
4.3	Interplay between H3K27ac and H3K27me3.....	89
4.4	Concluding remarks and perspectives	89

Appendices.....	93
References	103
Curriculum Vitae	118

List of Tables

Table 1: Allelic test of <i>ACCI</i> alleles.....	36
---	----

List of Figures

Figure 1: Comparison of putative histone acetyltransferases in <i>Arabidopsis</i>	4
Figure 2: Cytosolic acetyl-CoA biosynthesis in <i>Arabidopsis</i>	16
Figure 3: Physical distance of the region harboring <i>ANKp</i> , <i>NACp</i> , and <i>ACC1</i> on the first chromosome	20
Figure 4: Depletion of the expression of <i>NAC^p</i> by artificial microRNA	29
Figure 5: Characterization of different <i>acc1</i> alleles.....	31
Figure 6: Mutation of <i>ACC1</i> is responsible for <i>p1045</i> phenotypes	33
Figure 7: ACC1 protein in various <i>Arabidopsis</i> tissues.....	37
Figure 8: Partial complementation of <i>acc1-5</i> phenotypes by exogenous malonate.....	40
Figure 9: ACC1 affects the acetyl-CoA level and global histone H3K27 acetylation	42
Figure 10: Unchanged transcript levels of genes encoding ACL subunits in WT and <i>acc1-544</i>	
Figure 11: Artificial microRNA of <i>ACLA-1</i> in β -estradiol inducible system.....	46
Figure 12: ACL activity is required for the accumulation of acetyl-CoA and increased H3K27ac in <i>acc1-5</i>	48
Figure 13: High reproducibility and reliability of H3K27ac ChIP-seq	51
Figure 14: Genome-wide analysis reveals increased H3K27ac in <i>acc1-5</i>	53
Figure 15: Increased depositions of H3K27ac at selected genes in <i>acc1-4</i>	55
Figure 16: High reproducibility of histone acetylations ChIP-seq experiments in WT and <i>acc1-5</i>	58

Figure 17: Similar genome-wide occupancies of 7 histone acetylation marks in <i>acc1-5</i> to that in WT.....	60
Figure 18: Increased H3K27ac is dependent on the activity of ACL.....	62
Figure 19: H3K27me3 ChIP-seq analysis in WT and <i>acc1-5</i>	65
Figure 20: Genome-wide analysis of H3K27me3 in <i>acc1-5</i> and WT	67
Figure 21: Go terms analysis of two subgroup genes.....	69
Figure 22: Transcript levels of genes encoding histone acetyltransferases and deacetylases	72
Figure 23: Histone acetyltransferases activity is required for increased H3K27ac in <i>acc1</i> mutant.....	74
Figure 24: <i>GCN5</i> gene structure and expression in Col (WT) and <i>gcn5</i> mutant.....	76
Figure 25: GCN5 is involved in hyperacetylation of H3K27 in <i>acc1-5</i>	79
Figure 26: Hyperacetylation of H3K27 activates gene expression in <i>acc1-5</i>	82
Figure 27: A model showing how cytosolic acetyl-CoA affects H3K27ac in <i>Arabidopsis</i> ...	90

List of Appendices

Appendix A: Sequences of primers used	93
Appendix B: Accession number and corresponding protein	99
Appendix C: The reads number of all ChIP-seq samples	101

Abbreviation

Note: SI units are not listed

Abbreviation	Full Name
½ MS	half strength of MS medium
2HG	2-hydroxyglutarate
ABRC	<i>Arabidopsis</i> Biological Resource Center
ACC	acetyl-CoA carboxylase
ACL	ATP-citrate lyase
ACLA	ATP-citrate lyase subunit A
ACLB	ATP-citrate lyase subunit B
Alpha-KG	α -ketoglutarate
AMP	adenosine monophosphate
ANOVA	analysis of variance
ASH1	absent, small, or homeotic discs 1
ATP	adenosine triphosphate
ATX1	<i>Arabidopsis</i> trithorax 1
AURORA3	a member of aurora protein kinase family
CBP	CREP-binding protein
cDNA	complementary DNA
ChIP	chromatin immunoprecipitation

ChIP-chip	ChIP followed by DNA microarray analysis
ChIP-qPCR	ChIP followed by quantitative real-time PCR
ChIP-seq	ChIP followed by massively parallel DNA sequencing
CoA	coenzyme A
Col-0	columbia ecotype 0
CTAB	Cetyltrimethyl ammonium bromide
DAG	day after germination
DNA	deoxyribonucleic acid
E(Z)	enhancer of zeste
ELP3	elongator complex protein 3
EMS	ethyl methanesulfonate
FLC	flower locus C
GAPDH	glyceraldehyde 3-phosphate dehydrogenase
GCN5	general control nonderepressible 5
gDNA	genomic DNA
GFP	green fluorescent protein
GlcNAc	N-acetylglucosamine
GNAT	GCN5-related N-terminal acetyltransferase
GSNO	S-nitroso-glutathione
GUS	β -glucuronidase

H2A	histone 2A
H2B	histone 2B
H3	histone 3
H4	histone 4
HAC	histone acetyltransferases of the CBP family
HAF	histone acetyltransferases of the TAFII250 family
HAG	histone acetyltransferases of the GNAT family
HAM	histone acetyltransferases of the MYST family
HAT	histone acetyltransferase
HDA	histone deacetylase
HDAC	histone deacetylase
HDT	histone deacetylase of the HD-tuins family
HD-tuins	histone deacetylase- tuins
HKMT	histone lysine methyltransferase
HP1	heterochromatin protein 1
HPLC	high-performance liquid chromatography
IDH	isocitrate dehydrogenase
IGB	integrated genome browser
kb	kilo base pair
Ler-0	Landsberg erecta ecotype 0

MACS	model-based analysis for ChIP-Seq
MB-3	α -methylene- γ -butyrolactone
MEF	mouse embryonic fibroblast
mESC	mouse embryonic stem cell
MS	Murashige and Skoog medium
MYST	MOZ, Ybf2/Sas3, Sas2 and Tip60
NAC	no apical meristem
NAD	nicotinamide adenine dinucleotide
NADP	nicotinamide adenine dinucleotide phosphate
NGM	next-generation mapping
NO	nitric oxide
PCR	polymerase chain reaction
PEG100	pEarly gate 100
PHD	plant homeodomain
pH(i)	intracellular pH
PI	propidium iodide
PRC2	polycomb repressive complex 2
qPCR	quantitative real-time PCR
qRT-PCR	quantitative reverse-transcription PCR
RNA	ribonucleic acid

RNAi	RNA interference
RNA-seq	RNA sequencing
RPD3	reduced potassium dependency 3
RT-PCR	reverse transcription PCR
SAH	<i>S</i> -adenosylhomocysteine
SAM	<i>S</i> -adenosylmethionine
SD	standard deviation
SDG8	SET domain group protein 8
SDS	sodium dodecyl sulfate
SET	su(var)3-9 and enhancer of zeste
SICER	spatial clustering for identification of ChIP-enriched regions
SNF	sucrose non-fermenting
SNP	single-nucleotide polymorphism
SRT	sirtuin
SWI	switch
TAFII250	transcription initiation factor TFIID 250kDa
TAZ	transcription adaptor putative zinc finger
TCA	tricarboxylic acid
Tdh	threonine dehydrogenase
T-DNA	transfer DNA

TRX	trithorax
VLCFAs	very long chain fatty acids
w/v	weight/volume percent
WIG	wiggle
WT	wild type

1 INTRODUCTION

1.1 Histone modifications regulate chromatin states and gene expression

In eukaryotic nuclei, genomic DNA is packed in a highly organized DNA-protein complex known as chromatin which is composed of nucleosomal subunits. The nucleosome core particle consists of approximately 147 base pairs of DNA wrapped in 1.67 left-handed superhelical turns around a histone octamer consisting of 2 copies each of the core histone 2A (H2A), histone 2B (H2B), histone 3 (H3) and histone 4 (H4) (Luger et al., 1997). A high-resolution X-ray structure of the nucleosome (Luger et al., 1997) indicates that highly basic histone amino (N)-terminal tails can protrude from the octamer and make contact with adjacent nucleosomes. The histone tails can be covalently modified by adding small groups to some amino acid residues, such as methyl group to lysine (Kme, me represents methylation) and arginine (Rme), acetyl group to lysine (Kac, ac represents acetylation), and phosphate to serine, threonine, and tyrosine.

These modifications can regulate the chromatin states via at least two main mechanisms. The first involves influencing the overall structure of chromatin by neutralizing the positive charge of the histone tail and then affecting the interactions between histones and DNA, such as acetylation and phosphorylation. The second involves the modifications regulating the binding of effector molecules. For example, the chromatin remodeler SWITCH2/SUCROSE NON-FERMENTING 2 (SWI2/SNF2) can target acetylated histones by its bromodomain. In turn, this recruits the SWI/SNF remodeling complex to 'open' the chromatin (Hassan et al., 2002). In addition to acetylation, di/tri-methylation of histone 3 lysine 9 (H3K9me2/H3K9me3) can be recognized by HETEROCHROMATIN PROTEIN 1 (HP1) dimers and then maintain constitutive heterochromatin such as centromeres and telomeres (Trojer and Reinberg, 2007). Chromatin states are partially regulated through dynamic modification of histones, such as acetylation, methylation, phosphorylation, ubiquitination and sumoylation (Lu and Thompson, 2012). Although a complete understanding of the precise mechanisms by which these modifications to histone tails influence chromatin structure remains elusive,

some specific alterations have been studied in detail. For example, di-/tri-methylation of histone 3 lysine 27 (H3K27me₂/ H3K27me₃) are associated with repressed transcription while acetylation of lysine residues of histone tail and trimethylation of histone 3 lysine 4 (H3K4me₃) and monomethylation of histone 3 lysine 36 (H3K36me₁) are normally linked to activated chromatin (Lu and Thompson, 2012). Phosphorylation of histone 3 serine 10 and 28 are associated with condensed chromatin, while the combination of phosphorylation of serine 10 and acetylation of lysine 14 on histone 3 is a sign of active transcription (Tan et al., 2011). Similar to H3K27me₃, ubiquitination of H2A and H2B is also associated with repression of transcription (Tan et al., 2011). Those modifications, in many cases, are heritable and are thought to provide a dynamic linkage between extracellular environment and gene regulation.

1.1.1 Histone acetylation

Histone acetylation plays critical roles in the global regulation of chromatin architecture and gene expression (Berr et al., 2011; Verdin and Ott, 2015). Acetylated lysine residues of histones, on one side, can provide binding sites for proteins with bromodomains, such as several ATP-dependent nucleosome remodeling complexes which can either remove or exchange histone dimers (Venkatesh and Workman, 2015; Verdin and Ott, 2015). On the other side, additional acetyl group effectively remove the positive charge of histone, which can reduce the interaction between histone tail and nucleosome and relieve DNA from its condensed state (Venkatesh and Workman, 2015; Verdin and Ott, 2015). The level of histone acetylation is dynamically regulated through the antagonistic actions between histone acetyltransferases (HATs) and histone deacetylases (HDACs), which both acts on targeted regions of chromatin to regulate specific gene expression and in a global manner (Kurdistani and Grunstein, 2003).

1.1.1.1 Structure and function of histone acetyltransferases

According to their subcellular localization, HATs have been divided into two classes: Type A and Type B (Brownell and Allis, 1996; Roth et al., 2001). Type A class HATs are localized in the nucleus and responsible for acetylation of nucleosomal core histones. They function as transcriptional co-activators and therefore play an important role in the

regulation of gene expression. Type A HATs can be further subdivided into four families that include the GENERAL CONTROL NONDEREPRESSIBLE 5 (GCN5)-related N-terminal acetyltransferases (GNATs), the MYST (MOZ, Ybf2/Sas3, Sas2 and Tip60)-related HATs, p300/CREP-binding protein (CBP) HATs and transcription initiation FACTOR TRANSCRIPTION INITIATION FACTOR TFIID (TAFII-250) (Boycheva et al., 2014).

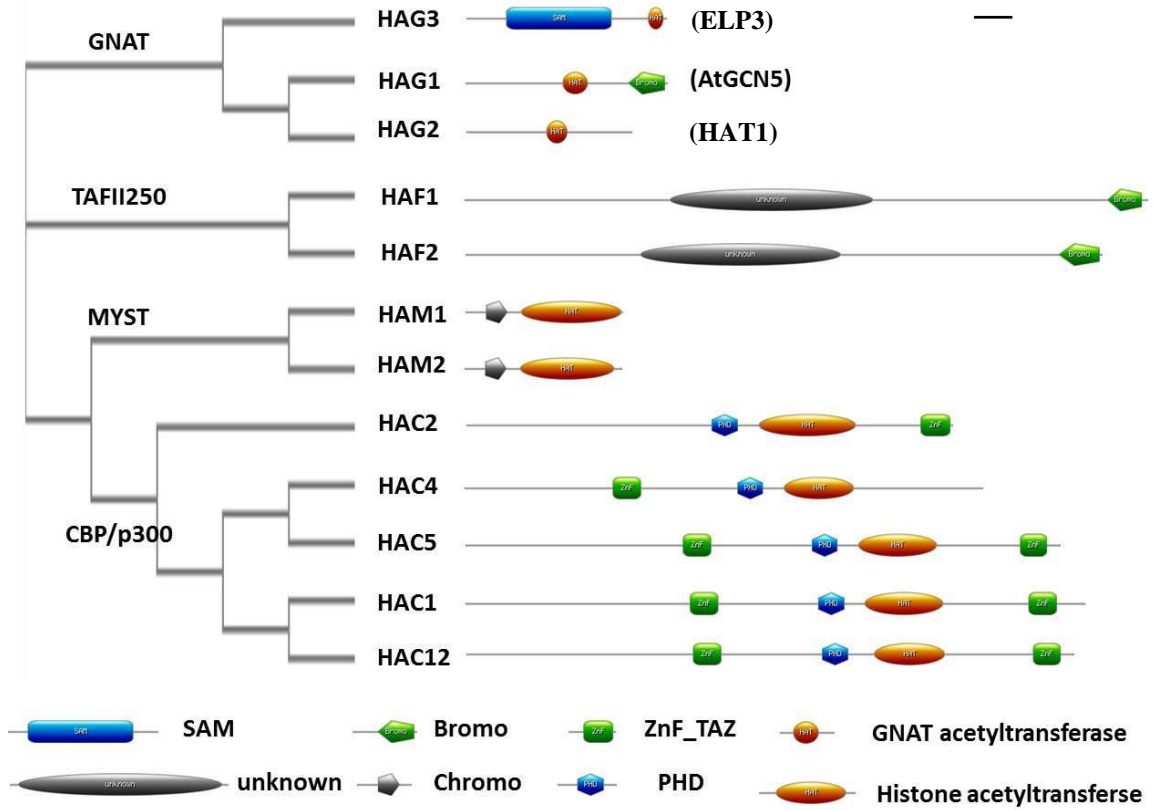
Type B HATs, on the other side, have long been considered cytoplasmic enzymes and catalyze acetylation of free histones which are not associated with DNA (Parthun et al., 1996; Verreault et al., 1998). However, a type B HAT identified in maize was shown to form a heterodimeric complex and acetylate of histone 4 lysine 5 and lysine 12 (H4K5 and H4K12) (Eberharter et al., 1996; Lusser et al., 1999). This type B HAT from maize is not only localized in the cytoplasm but also accumulates in nuclei, suggesting additional nuclear functions of the plant type B HAT (Lusser et al., 1999).

In higher eukaryotes, the GNAT family can be further divided into three subfamilies: ELONGATOR COMPLEX PROTEIN 3 (ELP3), GCN5 and HAT1. In *Arabidopsis*, there are homologs corresponding to each of the subfamilies: HISTONE ACETYLTRANSFERASES OF THE GNAT FAMILY 3 (HAG3), *Arabidopsis* GCN5 (AtGCN5)/ACETYLTRANSFERASES OF THE GNAT FAMILY 1 (HAG1) and ACETYLTRANSFERASES OF THE GNAT FAMILY 2 (HAG2) (Pandey et al., 2002). Besides, two MYST genes have been identified in *Arabidopsis* genome, named *HISTONE ACETYLTRANSFERASES OF THE MYST FAMILY 1 (HAM1)* and *HISTONE ACETYLTRANSFERASES OF THE MYST FAMILY 2 (HAM2)* (Earley et al., 2007). At last, there are five p300/CBP genes: *HISTONE ACETYLTRANSFERASES OF THE CBP FAMILY (HAC1, HAC2, HAC4, HAC5 and HAC12)* and two TAFII250 genes: *HISTONE ACETYLTRANSFERASES OF THE TAFII250 FAMILY (HAF1 and HAF2)* (Bertrand et al., 2005) (Figure 1).

Structural and functional studies on HATs have revealed the fundamental mechanism of histone binding and histone acetylation (Marmorstein, 2001; Boycheva et al., 2014). As shown in Figure 1, the CBP/p300 family contains a histone acetyltransferase domain and

Figure 1: Comparison of putative histone acetyltransferases in *Arabidopsis*

All the protein sequences (HAG3: Q93ZR1, HAG1: Q9AR19, HAG2: Q9FJT8, HAF1: Q8LRK9, HAF2: Q6PUA2, HAM1: Q9FLF7, HAM2: Q9LXD7, HAC1: F4IDH2, HAC2: Q9FYH1, HAC4: NP_564706, HAC5: Q9LE42, and HAC12: Q9FWQ5) were obtained from The *Arabidopsis* Information Resource (TAIR) without any change and aligned by Clustal Omega with the default setting. The conserved domains were drawn according to domain information in TAIR. Bar= 100 amino acids. Sam domain: reductively cleave *S*-adenosylmethionine (SAM) to methionine and a 5'-deoxyadenosyl radical; Bromo and chromo domains: functional domains recognize acetylated lysine of histone; PHD: Plant homeodomain; ZnF_TAZ: TAZ-type of zinc finger domain.



a plant homeodomain (PHD) finger that is considered to be an H3K4me3 reader (Li et al., 2006). The TAZ-type of zinc finger domain presented in CBP/p300 family participates in the protein-protein interactions with transcription factors (Ponting et al., 1996). The MYST family contains a C-terminal HAT domain and an N-terminal chromodomain which is responsible for remodeling and manipulation of chromatin (Min et al., 2003a). In the TAFII250 family, both proteins contain a C-terminal bromodomain that is considered to be a targeting motif (Dhalluin et al., 1999). Although no typical HAT domain has been identified in this family, both HAF1 and HAF2 were shown to have histone acetyltransferase activity *in vivo* (Bertrand et al., 2005; Benhamed et al., 2006).

The GNAT family shows less similarity among family members compared to other histone acetyltransferase families. In addition to the HAT domain, HAG1 contains a C-terminal bromodomain and HAG3 contains an N-terminal SAM domain which can reductively cleave *S*-adenosylmethionine (SAM) to methionine and a 5'-deoxyadenosyl radical (Frey et al., 2008).

Histone acetyltransferases play a crucial role in the determination of cell fate and maintaining cell cycle, responses to environmental conditions and gene interactions. An analysis of the transfer DNA mutants of *HAG1* reveals that this gene participates in plant development pathways and the responses to environmental stimuli, like light and cold (Servet et al., 2010). Mutants of *HAG1* show pleiotropic defects such as dwarfism, loss of apical dominance, smaller, upward-curved leaves, abnormal roots, aberrant meristem function, reduced fertility and expression of light- and cold-inducible genes (Bertrand et al., 2003; Vlachonasios et al., 2003; Long et al., 2006; Kornet and Scheres, 2009).

The CBP/p300 family is involved in the vegetative and reproductive development of *Arabidopsis*. Mutation in *HAC1* leads to a late-flowering phenotype and a *hac1 hac5* double mutant shows a further delay in flowering time. In addition, *hac1 hac5* also has a small plant size, twisted and enlarged pistils, underdeveloped petals and reduced fertility (Han et al., 2007).

Single mutants of MYST family members show indistinguishable phenotypes compared with wide-type (WT) plants (Latrasse et al., 2008). However, a *ham1 ham2* double

mutant exhibits severe defects in the formation of male and female gametophytes, resulting in an arrest of mitotic cell cycle at early stages of gametogenesis (Latrasse et al., 2008). In addition, mutations in the *Arabidopsis HAF2* gene can affect the photoperiod pathway and leaf greening (Bertrand et al., 2005) and knock out *HAF1* affects the viability of the male gametophyte and causes infertility (Waterworth et al., 2015).

1.1.1.2 Specificity of histone acetyltransferases

In *Arabidopsis*, multiple lysine residues of histone tails can be acetylated, such as lysine 9, 14, 18, 23, 27 of H3 and lysine 5, 8, 12 and 16 of H4. Previous *in vitro* work found that CBP/p300 family shows broad-specificity and can acetylate most of the lysine residues of H3 and H4 tails (Earley et al., 2007). In addition, HAG1 is responsible for adding acetyl group on histone 3 lysine 14 and lysine 27 (H3K14 and H3K27) (Benhamed et al., 2006; Earley et al., 2007). MYST family is mainly involved in acetylation of lysine residues of H4 both *in vitro* and *in vivo* (Earley et al., 2007; Xiao et al., 2013). In fact, CBP/p300 family acetyltransferases not only modify histones but also non-histone proteins, affecting multiple cellular processes (Sterner and Berger, 2000).

1.1.1.3 Histone deacetylases

The histone acetylation status is the result of the balance between activities of acetyltransferases and deacetylases. In *Arabidopsis*, 18 HDAC have been predicted based on their sequence similarity to known HDAC proteins in other organisms (Pandey et al., 2002; Hollender and Liu, 2008; Berr et al., 2011). The HDACs can be grouped into three types. The first type is homologous to the yeast REDUCED POTASSIUM DEFICIENCY 3 (RPD3), which is present throughout eukaryotes and is most widely studied. The second type, the HISTONE DEACETYLASE-TUINS (HD-tuins), appears to be present only in plants (Lusser et al., 1997; Wu et al., 2000; Dangl et al., 2001). The structurally-distinct third type is homologous to the yeast sirtuin 2 protein, which is a nicotinamide adenine dinucleotide (NAD) dependent enzyme.

The type I (RPD3-like) group contains 12 putative members in *Arabidopsis* (Pandey et al., 2002). All the members have a characteristic histone deacetylase domain. According to sequence similarity, this family can be further divided into 3 subgroups (Pandey et al.,

2002). Group I contains HDA19, HDA6, HDA7 and HDA9. Group II includes HDA5, HDA15, and HDA18. HDA2 and its two isoforms comprise group III. Remaining members such as HDA8, HDA14, HDA10 and HDA17 are unclassified in the RPD3-like superfamily. The type II (HD-tuins) group contains four members: HISTONE DEACETYLASE OF THE HD-TUINS FAMILY1-4 (HDT1-4) (Wu et al., 2000; Dangl et al., 2001; Pandey et al., 2002). This family has a conserved N-terminal EFWG motif which is required to repress the following central acidic region rich in glutamic and/or aspartic acid (Hollender and Liu, 2008). The type III group (sirtuin) includes two sirtuin proteins in *Arabidopsis*, SRT1, and SRT2 (Frye, 2000; Pandey et al., 2002).

Similar to HATs, HDACs also play critical roles in plant development. Loss-of-function *hda19* mutants show reduced numbers of petals, shorter stamens, reduced male and female fertility, and smaller siliques that often contain aborted seeds (Hollender and Liu, 2008). In addition to development, HDA19 also regulates the plants' response to their environment. *Hda19* loss-of-function lines are late flowering under long day conditions (Tian et al., 2003). A double mutant of *hda19 had6* causes the derepression of embryogenesis-related genes after germination (Tanaka et al., 2008).

1.1.2 Histone methylation

Unlike histone acetylation which only adds acetyl groups to the side chain of lysine residues, histone methylation mainly occurs on lysine and arginine residues. Since a methyl group does not change the charge of a histone protein, histone methylation may not directly affect chromatin structure. However, histone methylation has higher complexity than acetylation: lysine residues can be mono-, di- or tri-methylated (simplified as Kme1/Kme2/Kme3, respectively), whereas arginine residues can be mono, symmetrically or asymmetrically di-methylated (Liu et al., 2010).

The first histone lysine methyltransferase (HKMT) was identified in 2000 which can catalyze methylation of H3K9 (Aagaard et al., 2000). Numerous HKMTs have since been identified, most of which contain a so-called SET domain that harbors the enzymatic activity. However, one exception is the DOT1 enzyme which catalyzes the methylation of H3K79 for maintaining telomeric silencing and does not contain a SET domain (Min et

al., 2003b). In *Arabidopsis*, there are 41 putative SET domain proteins encoded in the genome (Gendler et al., 2008). Based on their homology to the SET domains in animals, and the characteristic of cysteine-rich regions and additional conserved domains, SET domain proteins in *Arabidopsis* are divided into four families: (I) SU(VAR)3-9 groups [including SU(VAR)3-9 homologs and SU(VAR)3-9 related proteins], (II) ENHANCER OF ZESTE [E(Z)] homologs, (III) TRITHORAX (TRX) groups (TRX homologs and TRX-related proteins), and (IV) ABSENT, SMALL, OR HOMEOTIC DISCS 1 (ASH1) groups (ASH1 homologs and ASH1-related proteins) (Baumbusch et al., 2001; Springer et al., 2003; Zhao and Shen, 2004). There is no homolog of DOT1 in the genome and no H3K79 methylation has been detected in *Arabidopsis* (Zhang et al., 2007a).

1.1.2.1 Specificity of histone methyltransferases

Unlike the broad-specificity of histone acetyltransferases, methyltransferases show high specificity to the lysine residues of histones. A typical example is the Trithorax group proteins which are responsible for histone 3 lysine 4 tri-methylation (H3K4me₃). In *Arabidopsis*, *ARABIDOPSIS* TRITHORAX 1 (ATX1), a homolog of histone H3K4 methyltransferase TRX, is a histone methyltransferase specific for histone H3K4 (Alvarez-Venegas et al., 2003). Mutations in *ATX1* lead to abnormal floral organ identity and early flowering (Alvarez-Venegas et al., 2003; Pien et al., 2008). ATX1 directly interacts with the promoter and the first exon of *FLOWER LOCUS C* (*FLC*) locus and catalyzes H3K4 tri-methylation modification (Pien et al., 2008). Consistent with ATX1 being an H3K4me₃ methyltransferase, H3K4me₃ at *FLC* was reduced but H3K4 di-methylation (H3K4me₂) remained unchanged in *atx1* mutants (Pien et al., 2008). Another example is methylation of histone H3K36 which is specifically methylated by histone methyltransferase ASH1 in mammals and *Drosophila* (Berger, 2007; Li et al., 2007). In *Arabidopsis*, SET DOMAIN GROUP 8 (SDG8) is the major H3K36 methyltransferase *in vivo* required for global H3K36me₂/H3K36me₃ deposition (Dong et al., 2008; Xu et al., 2008). Mutations in *SDG8* cause early flowering, increased shoot branching and altered carotenoid composition, indicating a broader role of SDG8 in regulating other developmental or physiological processes (Dong et al., 2008; Liu et al., 2010; Tang et al., 2012).

1.1.2.2 Histone methylation can regulate gene expression

While histone methylation is a process to add a methyl group to lysines or arginines of histones, it shows different effects on gene expression. Immunostaining of nuclei and chromatin immunoprecipitation (ChIP) assays found that H3K9 mono-methylation (H3K9me1) and H3K9 di-methylation (H3K9me2) is enriched in centromeres, indicating a conservation of histone marks in silenced chromatin among different species (Jackson et al., 2004; Mathieu et al., 2005; Fuchs et al., 2006). Consistent with the primary function of H3K9me2 in repressing transposon activities, genome-wide ChIP assays coupled with high-resolution microarray analysis (ChIP-chip) revealed that H3K9me2 is enriched in transposon and repeated sequences in plants (Bernatavichute et al., 2008; Cartagena et al., 2008).

Similar to H3K9 methylation, H3K27 methylation is also considered as a repressive mark in both animals and plants. H3K9me1/2 and H3K27me1 are enriched at constitutively silenced heterochromatin in *Arabidopsis* (Mathieu et al., 2005; Fuchs et al., 2006). However, H3K27me3 is enriched at euchromatin. In *Arabidopsis*, H3K27me3 modification preferentially localizes to the transcribed regions of genes, with a remarkable bias towards those immediately upstream of promoters and the 5' end of transcribed regions of genes, consistent with a role in transcriptional repression (Turck et al., 2007; Zhang et al., 2007b). In addition, a large number of genes (~17% of the coding genes) were found to be marked with H3K27me3, indicating that H3K27me3 is a major gene silencing mechanism in *Arabidopsis* (Zhang et al., 2007b). H3K27me3 deposition is mediated by a protein complex called POLYCOMB REPRESSIVE COMPLEX 2 (PRC2). In *Arabidopsis*, at least three distinct PRC2 core complexes regulate common target genes with specific functions, including regulating cell proliferation and differentiation and controlling developmental phase transition upon environmental changes (Kohler et al., 2003; Pien and Grossniklaus, 2007; Liu et al., 2010).

Unlike H3K9 and H3K27 methylation, H3K4 and H3K36 methylation are associated with actively transcribed genes. In *Arabidopsis*, all three types of H3K4me (mono-, di-, and tri-) are predominantly located in exons and/or introns, and more than two-thirds of the annotated genes are marked by at least one type of H3K4 methylation in a given

tissue, developmental stage and environmental condition (Zhang et al., 2009).

H3K4me_{2/3} are predominantly enriched in the promoters and transcription starting sites (TSSs), whereas H3K4me₁ is found in the entire gene (Zhang et al., 2009; Roudier et al., 2011; Sequeira-Mendes et al., 2014). Relative to H3K4 methylation, H3K36me₃ levels are highest in the 5'-half of actively transcribed genes (Sequeira-Mendes et al., 2014). H3K36me₂ levels, on the other hand, mainly enriched in the 3'-end of expressed genes and are associated with the processivity of RNA polymerase II (Sequeira-Mendes et al., 2014).

1.1.3 Other histone modifications

In addition to histone acetylation and methylation, multiple serine and threonine residues of histones are subject to phosphorylation by a wide array of kinases (Baek, 2011). A study shows that serine 10 and serine 28 of histone 3 can be phosphorylated *in vitro*, and probably *in vivo*, by the kinase AURORA3. Both phosphorylations correlate with chromosome segregation and metaphase/anaphase transition (Kurihara et al., 2006). In addition, H3 threonine 3 and threonine 11 also can be phosphorylated *in vitro* (Kurihara et al., 2011).

Ubiquitination is the result of a concerted action of the ubiquitin-activating enzyme E1, the ubiquitin-conjugating enzyme E2, and the ubiquitin-protein ligase E3 (Pickart, 2001). During this process, a small and highly conserved protein named ubiquitin is covalently attached to the target protein. Nucleosomal core histones, linker histones, and several histone variants were reported to be mono-ubiquitinated (Hicke, 2001). However, most studies were focused on H2A and H2B mono-ubiquitination (H2Aub1 and H2Bub1) (Zhang, 2003; Weake and Workman, 2008). In *Arabidopsis*, H2Aub1 is mediated by POLYCOMB REPRESSIVE COMPLEX 1 (PRC1)-like complexes and is required for the silencing of genes (Xu and Shen, 2008; Bratzel et al., 2010; Chen et al., 2010). In contrast, H2Bub1 is mainly associated with transcriptional activation (Zhang, 2003; Weake and Workman, 2008).

Besides the modifications mentioned above, histone lysine propionylation, butyrylation, malonylation, succinylation, 2-hydroxyisobutyrylation, and crotonylation have all been

identified by tandem mass spectrometry proteomic analysis over the past several years (Chen et al., 2007; Tan et al., 2011; Xie et al., 2012; Dai et al., 2014). These discoveries have revealed the potential complexity of histone lysine modifications and have prompted interest in investigating the functional consequence of these different modifications on histones.

1.2 Metabolites bridge cellular environment and gene expression via histone modification

Living organisms and individual cells continuously adapt to changes in their environment. The ability of survival and maintaining function in various environments is called cellular phenotypic plasticity (Feinberg, 2007). Cellular plasticity relies on the precise coordination of transcriptional programs that allow the cell to adapt to a changing environment. How to sense the environmental changes and determine which genes are activated by transcription factors at a certain time and in a specific cellular context are the key questions to be addressed to understand the mechanisms underlying cellular plasticity. One of the answers to the question would be the change of metabolites.

1.2.1 Central metabolites reflect cellular environment

From prokaryotic to eukaryotic cells, carbon sources or energy serve as one of the basic factors to allow cell growth and division. To gradually release the energy stored in carbon sources, cells have developed two major catabolic pathways: glycolysis and oxidative phosphorylation. In eukaryotic cells, by combining the actions of glycolysis and oxidative phosphorylation, 1 molecule of glucose will release about 30 to 38 molecules of adenosine triphosphate (ATP) which is a small molecule used in the cell as an energy source and carrier. One key metabolite between these two metabolic pathways is acetyl-CoA which is generated from pyruvate, the end product of glycolysis. In addition, acetyl-CoA serves as the basic building block to the synthesis of lipids which are not only the main component of the membrane system but can also store the excess of energy released from a carbon source. A good example to illustrate the central role of acetyl-CoA in a metabolic pathway is the oscillatory change of acetyl-CoA in the budding yeast *Saccharomyces cerevisiae*. Most of the laboratory strains are cultured in media with

abundant nutrient supply. In this environment, yeast takes up extracellular nutrients to fuel cell growth and proliferation at a logarithmic rate. However, under restricted conditions with one or more nutrients being limited, the growth of yeast displays an oscillatory metabolic behavior with distinct phases characterized by robust changes in oxygen consumption (Chance et al., 1964). This metabolic oscillation can vary from minutes to hours depending on yeast strains and experimental conditions and is independent of the cell cycle (Slavov et al., 2011). Interestingly, global transcriptome analyses revealed that nearly 60% of the genes were expressed in a similarly cyclic fashion when yeast grew in such limiting conditions (Klevecz et al., 2004; Tu et al., 2005). Levels of acetyl-CoA were found to oscillate dynamically and peak during the oscillatory growth phase (Tu et al., 2007; Cai et al., 2011). These metabolic oscillations can be effectively induced by adding different precursors of acetyl-CoA, such as ethanol, acetate, and lactate (Cai et al., 2011). This evidence supports the idea that acetyl-CoA might represent a metabolic signal to affect the entire metabolic network.

Except for acetyl-CoA, the amount of ATP is not only an indicator of cellular energy state but also provides the phosphate group to phosphorylate proteins and regulate enzyme activity. During the process of releasing energy or phosphorylation, ATP can be hydrolyzed to adenosine diphosphate plus Pi or adenosine monophosphate (AMP) plus 2 Pi. The ratio of AMP:ATP can be sensed by metabolic enzymes including (1) glycogen phosphorylase and 6-phosphofructo-1-kinase in muscles, which are activated by increasing AMP:ATP ratios, switching on two catabolic pathways (glycogenolysis and glycolysis) (Hardie, 2011), and (2) fructose-1,6-bisphosphatase in the liver, which is inhibited by increasing AMP:ATP ratios, switching off an anabolic pathway (gluconeogenesis) (Hardie, 2011). Most other processes sense the energy change indirectly from the AMP-activated protein kinase system (Hardie, 2011).

Energy state can also be linked with the metabolism of glutamine/glutamate via α -ketoglutarate (α -KG) which is an intermediate metabolite in the TCA cycle. This is a crucial step to maintain the balance between carbon and nitrogen in the cell. Glutamate can be generated from α -KG by glutamine oxoglutarate aminotransferase. And then, glutamate provides a molecular backbone to assimilate ammonia and to generate

glutamine by glutamine synthetase. Thus, the amount of α -KG represents the state of cell energy and nitrogen metabolism.

1.2.2 Metabolites regulate histone modifications

Intermediate metabolites are needed as substrates for many histone modifications at specific amino acid residues. For example, SAM and ATP provide methyl group and Pi, respectively, for histone methylation and phosphorylation. O-linked N-acetylglucosamine (GlcNAc), an intermediate metabolite of glycolysis, serves as the substrate for histone GlcNAcylation (Lu and Thompson, 2012). In addition, most of the substrates are also linked to specific metabolic pathways. So, environmental change can be translated into the fluctuation of metabolites, and the metabolite changes can regulate histone modifications and affect gene expression subsequently. In fact, a certain composition of metabolites in a cell reflects the homeostasis between a given environment and a gene expression program. In other words, the metabolite composition in a cell determines the cell's identity and function. It has been reported that threonine sourced SAM provides the methyl group for maintaining H3K4me3 in mouse embryonic stem cells (mESCs) (Shyh-Chang et al., 2013). The key enzyme for converting threonine to SAM is threonine dehydrogenase (Tdh), which is highly accumulated in mESCs rather than mouse embryonic fibroblasts (MEFs) (Mikkelsen et al., 2008; Wang et al., 2009). After providing the methyl group for histone methylation, SAM will be converted to S-adenosylhomocysteine (SAH). Further research has found that the ratio of SAM/SAH rather than the absolute amount of SAM will determine the H3K4me3 level in mESCs and MEFs (Shyh-Chang et al., 2013).

Metabolites can not only serve as substrates but also as cofactors to affect histone modifications. The best example is the linkage between mutation of isocitrate dehydrogenase (IDH) and histone methylation. IDH1 and IDH2 are NADP⁺ dependent enzymes that interconvert isocitrate and α -KG in the cytosol and mitochondria, respectively (Lu and Thompson, 2012). α -KG serves as a cofactor of histone and DNA demethylases to remove methyl groups (Klose and Zhang, 2007). Mutants of IDHs display a neomorphic activity of producing 2-hydroxyglutarate (2HG) from α KG (Dang

et al., 2009; Ward et al., 2010). As a structural analog of α KG, 2HG inhibits activities of histone demethylases and maintain high levels of H3K9me3 and H3K27me3 (Lu et al., 2012). The results suggest that metabolites can serve as signal molecules to link the cellular environment to histone modifications and gene transcription.

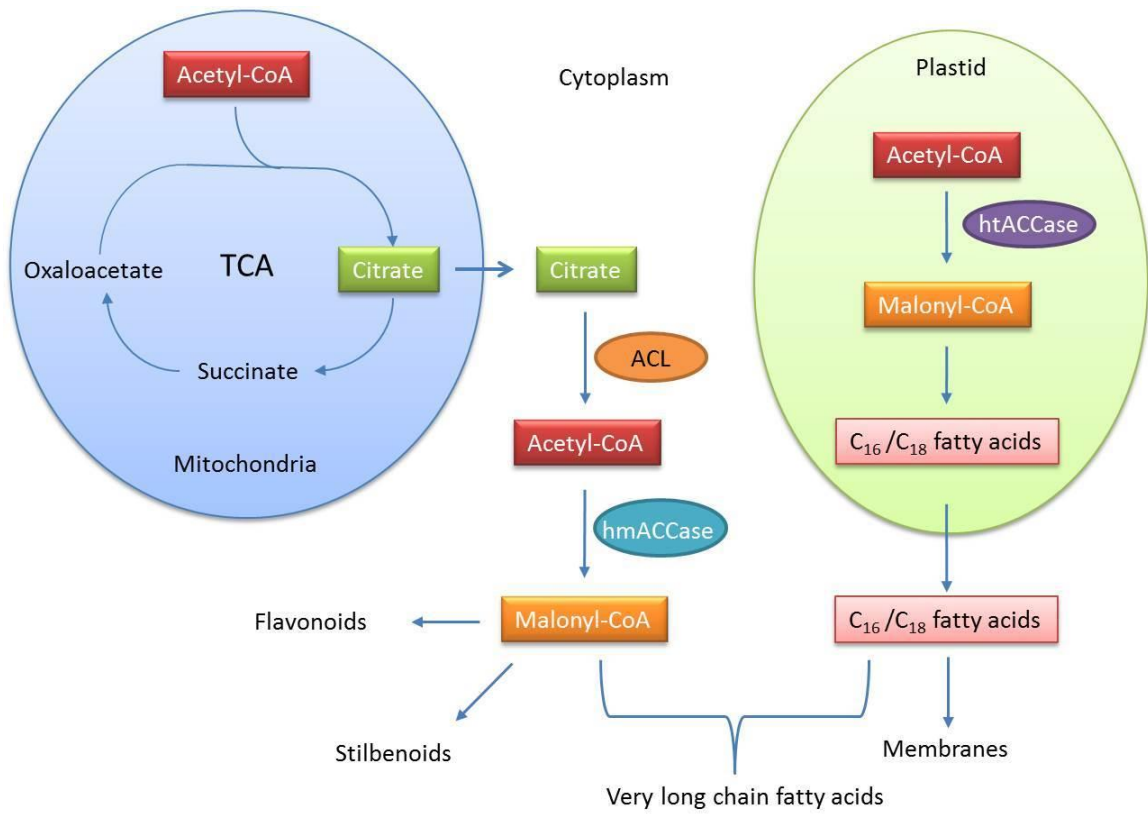
1.3 Acetyl-CoA and histone acetylation

Histone acetylation level is also affected by energy and the metabolic state of cells. Studies on the nicotinamide adenine dinucleotide (NAD⁺) dependent sirtuins (class III HDACs), which recognizes acetylated histones and non-histone proteins, have shown that deacetylation is responsive to the metabolic state (Cohen et al., 2004; Yang et al., 2007; Sack and Finkel, 2012; Guarente, 2013). Although the activities of HATs have not been reported to be regulated by metabolic states, histone acetylation is highly sensitive to the level of cytosolic acetyl-CoA in mammalian, yeast, and *Drosophila* cells (Takahashi et al., 2006; Wellen et al., 2009; Cai et al., 2011; Galdieri and Vancura, 2012; Lee et al., 2014). Increased levels of cytosolic acetyl-CoA in yeast cause hyperacetylation at multiple lysine residues of histone H3 and H4 and there seems to be no preference in terms of which lysine residue is acetylated in response to elevated acetyl-CoA levels. Similar to the cytosolic acetyl-CoA, in mammalian cells, mitochondrial sourced acetylcarnitine can be transported into the nucleus, where it can then be converted to acetyl-CoA to fuel the nuclear acetyl-CoA pool in the nucleus (Madiraju et al., 2009). In addition, pyruvate can also be converted to acetyl-CoA in the nucleus by a pyruvate dehydrogenase complex which is translocated from mitochondria in mammalian cells (Sutendra et al., 2014).

As shown in Figure 2, cytosolic acetyl-CoA is mainly produced by ATP-citrate lyase (ACL), a $\alpha_4\beta_4$ heteromeric enzyme composed of two different subunits, ACLA and ACLB (Fatland et al., 2002). Reduction of ACL activity leads to complex, bonsai phenotypes such as miniaturized organs, reduced cell size and cuticular wax deposition (Fatland et al., 2005). These phenotypes are similar to some HAT mutants such as *hag1/gcn5* mutant with dwarf stature, small leaves, and short roots (Bertrand et al., 2003; Vlachonasios et al., 2003), *hag3/elp3* mutant with reduced organ growth and cell

Figure 2: Cytosolic acetyl-CoA biosynthesis in *Arabidopsis*

To obtain cytosolic acetyl-CoA, citric acid is escaped from the TCA cycle and carried across mitochondrial membranes into the cytosol and cleaved by ACL into acetyl-CoA. The cytosolic acetyl-CoA can be carboxylated by homomeric ACCase (hmACCase) to form malonyl-CoA, which is a substrate required for elongation of fatty acids and biosynthesis of flavonoids and stilbenoids. The plastid localized heteromeric ACCase (htACCase) can carboxylate acetyl-CoA to malonyl-CoA for *de novo* fatty acids biosynthesis. (Figure was drawn based on the information from Fatland et al., (2005)).



proliferation rate (Genoveva et al., 1999), and *hac1 hac5* double mutant with small plant size, twisted and enlarged pistils, and reduced fertility (Han et al., 2007). Cytosolic acetyl-CoA can be either converted to malonyl-CoA by acetyl-CoA carboxylase (ACCase) for synthesizing elongated fatty acids, flavonoids, and malonyl derivatives or condensed to acetoacetyl-CoA for synthesizing precursors of isoprenoids (Oliver et al., 2009; Jin et al., 2012).

In plants, two forms of ACCase have been found: the heteromeric ACCase (htACCase) located in plastids is responsible for *de novo* fatty acids synthesis, and the homomeric (hmACCase) in the cytosol that carboxylates acetyl-CoA to malonyl-CoA for elongating the plastid-produced fatty acids (Figure 2). Two tandem genes, *ACC1* (*ATIG36160*) and *ACC2* (*ATIG36170*), encode two hmACCase isoforms in *Arabidopsis* (Yanai et al., 1995). Although both *ACC1* and *ACC2* show ubiquitous expression, no visible phenotype has been observed in *acc2* mutants while knocking out *ACC1* can disrupt embryo development (Baud et al., 2003; Kajiwara et al., 2004). Studying weak *acc1* mutant alleles uncovered that ACC1 is responsible for the production of very-long-chain fatty acids (VLCFAs) and their derivatives such as sphingolipids, waxes, and cuticles (Faure et al., 1998; Baud et al., 2004; Lu et al., 2011b). Defects in VLCFAs biosynthesis affect cell plate formation, polar auxin transport, and cytokinin synthesis (Roudier et al., 2010; Bach et al., 2011; Nobusawa et al., 2013).

In a previous study conducted by Dr. Tian (Tang et al., 2008; Lu et al., 2010; Tang et al., 2012), *Arabidopsis* seeds were treated with ethyl methanesulfonate (EMS) to screen for repressor(s) of seed-specific genes. The mutagen, EMS, can induce chemical modification of nucleotides that results in mispairing and base changes, producing G/C to A/T transitions (Lindgren et al., 1965). One mutant, initially named p1045, shows unorganized cell proliferation in vegetative organs. Staining of this mutant with Sudan red, a yellowish red lysochrome azo dye which is used for coloring fats and oils (Brundrett et al., 1991), indicated that storage lipids are ectopically synthesized in cells. The p1045 mutation is a recessive mutation and the potential mutation site(s) were mapped to the centromere region of chromosome 1 by combining rough mapping and a

whole genome sequencing-based approach (Austin et al., 2011). In this region, three genes, encoding a putative ANKYRIN (ANK) repeat family protein (ANKp, p for putative, AT1G34050), a putative NO APICAL MERISTEM (NAC) domain transcriptional regulator (NACp, AT1G35890) and an ACETYL-COA CARBOXYLASE (ACCase) (ACC1, AT1G36160), were identified as candidates potentially responsible for the *p1045* mutant phenotype (Figure 3).

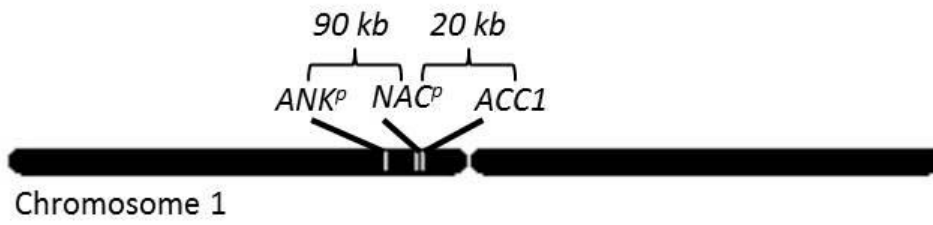
1.4 Scope of the Research and Objectives

I hypothesize that: 1) The mutation of *ACC1* is responsible for the phenotype of *p1045*. 2) Dysfunctional acetyl-CoA carboxylase 1 leads to accumulation of acetyl-CoA in *p1045*. 3) Changed acetyl-CoA affects histone acetylation and transcription. To test these hypotheses, the following specific objectives were addressed:

1. To identify which gene(s) is(are) responsible for the phenotypes of *p1045*
2. To compare the acetyl-CoA levels in *p1045* and WT
3. To examine the effects of changed acetyl-CoA on histone acetylation
4. To examine the effects of changed acetyl-CoA in *p1045* on global transcription

Figure 3: Physical distance of the region harboring *ANKp*, *NACp*, and *ACCI* on the first chromosome

The physical distances among the three genes were obtained from TAIR and the map was drawn by using Chromosome Map Tool in TAIR with default settings.



2 MATERIALS AND METHODS

2.1 Plant materials and growth conditions

Ethyl methanesulfonate (EMS) mutants, *acc1-4* and *elp3*, were described previously (Kajiwara et al., 2004 and Genoveva et al., 1999). Seeds of SALK_055428 (*acc1-6*), SALK_070277 (*hac1*), SALK_152684C (*hac5*), SALK_052490 (*hac12*), SALK_051832C (*hac7*), and SALK_042287 (*gcn5*) were obtained from the *Arabidopsis* Biological Resource Center (ABRC) at the Ohio State University. All used *Arabidopsis* seeds are in *Col-0* (Columbia) background, except *acc1-4* that is in the *Ler-0* (*Landsberg erecta*) background. All the seeds were sterilized by incubating in wash buffer (20% bleach and 0.1% [w/v] SDS) and rotating for 10 mins. After spin down, wash buffer were removed and replaced with sterilized water. Following four times wash by sterilized water, seeds were incubated in sterilized water at 4 °C for 2 days. And then, seeds were sown and grown in half strength of Murashige and Skoog (½ MS) medium (0.5 × MS salts, 1.5% [w/v] sucrose, and 0.8% agar [pH 5.8]) or soil under 16h/8h light/dark cycle at 23°C. To complement *acc1-5* by exogenous malonate, WT and *acc1-5* seeds were directly sown in to ½ MS plate absence or in the presence of 1 mM malonate (sigma) for 12 days. For activating the inducible promoter, 17β-estradiol (Sigma) was dissolved in dimethylsulfoxide at 20 mM and diluted 1,000-fold into the medium. To induce artificial microRNA, 11-day old seedlings were transferred into mediums with or without 17β-estradiol for 24h. For inhibitor treatment, seeds were germinated in ½ MS medium for 3 days and then transferred into mediums absence or in the presence of 100 μM MB-3 (Sigma) for 9 days.

2.2 Next-generation mapping of *p1045*

To map the *p1045* mutation, 50 two-week-old *p1045* F2 mutant seedlings were pooled and the genomic DNA (gDNA) was isolated using cetyltrimethylammonium bromide (CTAB) protocol (Clarke, 2009). Pooled gDNA was sequenced on the Illumina HiSeq (Illumina, USA) using 100 nt paired-end sequencing. To identify the single-nucleotide polymorphism (SNP), caused by ethyl methanesulfonate (EMS) in *p1045*, a next-generation mapping (NGM) approach (Austin et al., 2011) was used. Previous rough

mapping analysis narrowed down the mutation(s) into a 250kb genomic region which is close to the centromere of chromosome 1. Combining those results, all non-synonymous SNPs, caused by EMS, were identified within the candidate region on chromosome 1 using a web-based tool (<http://bar.utoronto.ca/NGM/>). The *p1045* heterozygous plants were backcrossed with WT plants (Col-0) for 4 generations to remove other potential mutations.

2.3 Plasmid construction for plant transformation

All the cloning steps are following the instructions of Gateway technology (12535-019, Invitrogen) which includes two series of recombination reactions: BP (attB and attR) and LR (attL and attR). In the BP reactions, PCR-product with flanking attB sites is incubated with donor vector containing attP sites in the presence of BP clonase for overnight. During the incubation, recombination between attB and attP occurs and PCR-product is replaced into donor vector to generate entry clone with new flanking attL sites. Following with the first reaction, the second recombination is occurred by incubating entry clone and destination vector (contains attR sites) for overnight and the finally expression clone is generated. The 2-kb promoter and genomic region of *ACC1* were PCR-amplified from genomic DNA and cloned into the Gateway donor Vector pDONR221 (Invitrogen) by a BP reaction. Then LR reactions were performed with the destination vectors pMDC107 and pMDC163 (Curtis and Grossniklaus, 2003) to generate binary vectors carrying the fusion constructs with *GFP* (*ProACC1:ACC1-GFP*) and *GUS* (*ProACC1:ACC1-GUS*). A fragment encoding an artificial microRNA targeting *ALCA-1* was designed and amplified as previously described (Schwab et al., 2006). The amplified fragment (*ACLA-Ii-1*) was cloned into pDONR221 by a BP reaction. Then an LR reaction was conducted with the destination vector pMDC7 (Curtis and Grossniklaus, 2003). An artificial microRNA targeting *NAC* (*NACi*) was designed and amplified with the same method and was inserted into the destination vector pEarly Gate 100 (pEG100) (Earley et al., 2006). All transgenic plants were generated by following the *Agrobacterium*-mediated floral dip method (Zhang et al., 2006). The *Agrobacterium* strain GV3101 (Hellens et al., 2000) was used for plant transformations.

2.4 GUS staining and microscopy

β -glucuronidase (GUS) staining was performed following a previously described method (Adachi et al., 2009). Briefly, plant tissues were incubated in 90% acetone at -20 °C overnight and washed in 100 mM sodium phosphate buffer (pH 7.0) for three times. And then, samples were incubated in the staining solution (100 mM sodium phosphate, 5 mM potassium ferrocyanide, 5 mM potassium ferricyanide, and 0.5 mg/mL 5-bromo-4-chloro-3-indolyl- β -D-glucuronide) at 37 °C for 24h. After staining, seedlings were transferred to glass slides and photographed using stereo microscopy (Zeiss). To detect green fluorescence signal, root tips were cut from 7-day old seedlings and transferred onto glass slides with 50 μ L propidium iodide (PI) solution (1 μ g/mL). The green fluorescence was detected by confocal microscopy (Leica) with excitation at 488 nm and emission at 505 to 525 nm.

2.5 Acetyl-CoA measurement

To measure the levels of acetyl-CoA in *Arabidopsis* seedlings, 100 mg of the 12 DAG seedlings was homogenized followed by resuspension in 300 μ L of ice-cold 5% perchloric acid. 150 μ L of supernatant was collected from each sample after thorough vortexing and centrifugation at 18,000 g at 4 °C for 5 mins. High-performance liquid chromatography (HPLC) was used for the measurements using the column and method previously described by Tsuchiya et al. (2014). Acetyl-CoA standard (A2056, Sigma) was used for peak identification. The peak areas were obtained and quantified using Agilent ChemStation software (Agilent Technologies, USA). Absolute quantities of acetyl-CoA were calculated by normalizing the peak area with the weight of the tissue used in each sample. Four independent biological replicates are included.

2.6 Analysis of transcript levels

Total RNA was extracted from *Arabidopsis* seedlings grown on ½ MS medium for ten days after germination (DAG) using the RNeasy Plant Total RNA Isolation kit (Qiagen). Genomic DNA was removed by treating with DNase TURBO (Ambion). For RT-qPCR, the first-strand complementary DNA (cDNA) was synthesized from 200 ng of total RNA using random primers in a 20 μ L reaction volume using the ABI cDNA synthesis kit.

Quantitative PCR was performed with a CFX96 Real-time PCR Instrument (Bio-Rad) using the SYBR Green I master mix (Bio-Rad) in a volume of 10 μ L. Data were analyzed using CFX Manager 3.1 software (Bio-Rad). Three independent biological replicates were included. For RNA-seq, libraries were prepared using the TruSeq RNA sample preparation kit (Illumina) following the manufacturers' protocol. All the libraries were sequenced on Illumina Hiseq 2500 platform using a paired-end scheme (2×50 bp) with TruSeq v3 chemistry. The sequencing reads were mapped to the TAIR10 version of the *Arabidopsis thaliana* genome using Tophat version 1.4.0 (Kim et al., 2013) with the minimum and maximum intron length setting being 20 bp and 4000 bp, respectively. Then, mapped reads were assembled according to the TAIR10 version of genome annotation using cufflinks version 2.1.1 (Trapnell et al., 2010) with default settings. To analyze differential expression, the assembled transcripts from three independent biological replicates in WT (Col-0) and *acc1-5* were included and compared by using cuffdiff version 2.1.1 (Trapnell et al., 2010) with default settings. Genes with at least two-fold changes in expression ($p < 0.001$) were considered to be differentially expressed.

2.7 Western blotting

Fifty mg of 12 DAG seedlings grown on $\frac{1}{2}$ MS medium was homogenized followed by resuspension in $3 \times$ SDS loading buffer. The mixture was sonicated for 15 secs with power 30 (Fisher scientific model-50) and then boiled for 10 mins. The supernatant was collected by centrifugation at 15,000 g for 10 mins. To separate histone proteins, the supernatant was loaded onto 16% sodium dodecyl sulfate polyacrylamide gel and run in electronic field for 100 mins at 150 Volts. Then proteins were transferred to polyvinylidene fluoride (PVDF) membrane following the Abcam transfer protocol. After blocking with 5% non-fat milk/ tris-buffered saline with Tween 20 (TBST) solution, the membrane was incubated in primary antibody solution with recommended dilution overnight. The primary antibodies are listed below: anti-H3: ab1791 (Abcam), anti-H3K9ac: 07-352 (Millipore), anti-H3K14ac: 07-353 (Millipore), anti-H3K18ac: 07-354 (Millipore), anti-H3K27ac: 07-360 (Millipore), anti-H4K5ac: 07-327 (Millipore), anti-H4K8ac: 07-328 (Millipore), anti-H4K12ac: 07-595 (Millipore), anti-H4K16ac: 07-329

(Millipore), anti-H3K27me3:07-449 (Millipore). After removing the primary antibody and washing the membrane three times with TBST buffer, the membrane was incubated in secondary antibody (A0545, Sigma) solution for 1 h. After 3 times washing with TBST buffer, Western blotting detection kit (RPN2016, GE Healthcare) was used and chemiluminescence was captured on X-ray film (Curix ultra, AGFA). The intensities of immunoblot were quantified by using ImageJ. The loading amount of each sample was adjusted according to detected H3 intensity. All the Western blots were repeated three times with independent samples and typical images are presented in figures.

2.8 Chromatin immunoprecipitation (ChIP)

ChIP was performed as previously described (Gendrel et al., 2005) with minor changes. Briefly, 2 g of 12 DAG Arabidopsis seedlings grown on ½ MS medium were collected and cross-linked with 1% formaldehyde for 15 mins under vacuum and then ground into fine powder in liquid nitrogen. Chromatin was isolated and sheared into 200 to 800 bp fragments by sonication. The sonicated chromatin was incubated with 5 µL antibody overnight at 4 °C. All the used antibodies for ChIP were the same as those for western blotting. The ChIP DNA was used for Illumina single-end sequencing (1 × 50) or qPCR. ChIP-qPCR was performed with three biological replicates, and results were calculated as a percentage of input DNA or normalized with histone H3 signals at same genomic loci. The primers used for qPCR were listed in Appendix A. One region (PLT7-2) without H3K27ac modification was used as negative controls. To collect enough plant materials of the *acc1-5 gcn5* double mutants for the H3K27ac ChIP assay, for each biological replicate we identified around 50 *acc1-5 gcn5* double mutant seedlings from ~800 progenies of the *acc1-5^{+/-} gcn5^{+/-}* double heterozygous parental plants by PCR and sequencing-based genotyping. Since both *acc1-5* and *gcn5* mutant plants fail to set seeds, we had to make crosses between the *acc1-5^{+/-}* and *gcn5^{+/-}* parental plants and select double heterozygous plants (*acc1-5^{+/-} gcn5^{+/-}*) to propagate seeds.

2.9 ChIP-seq analysis

Ten nanograms of ChIP DNA were used for library preparation using the Illumina Genomic DNA Sample Prep kit according to the manufacturer's protocol. Two biological

replicates were prepared and sequenced for each ChIP-seq experiment. An Illumina HiSeq 2500 instrument was used for high-throughput sequencing of the ChIP-seq libraries. The reads were aligned to the TAIR10 assembly using the Bowtie program (Illumina) (Langmead et al., 2009). Only perfectly and uniquely mapped reads were retained for further analysis. A summary of the number of reads for each replicates is given in Appendix C. To determine the correlation of each biological replicates, Pearson correlation was computed using deepTools2 (Ramirez et al., 2016) on normalized signal intensity. And then, the MACS program (Zhang et al., 2008) was used to convert mapped reads to the wiggle (WIG) format, which could be visualized with the Integrated Genome Browser (IGB) (Nicol et al., 2009). The SICER program (Zang et al., 2009) (window size = 200 and gap size = 200) was used to identify H3K27ac enriched domain and quantitatively compare H3K27ac levels in WT and *acc1-5*. According to the TAIR10 genome information, the H3K27ac enriched regions were converted to a gene list using the PeakAnalyzer program (Salmon-Divon et al., 2010). The final gene list was manually checked to remove false positives caused by the 200 bp window size used in the SICER program and incorrect conversion in the PeakAnalyzer program. All The genome-wide occupancies were analyzed using the seqMINER program (Ye et al., 2011).

2.10 Statistical analysis

Simple univariate statistics (means, standard deviations, and quartiles) were computed or find using Excel 2010 (Microsoft Corp., Redmond, Washington). The student t-test (two-tailed) was used to calculate the significance of differences between two independent data sets. For the data with non-normal distribution, Mann-Whitney test (two-tailed) was used to calculate significant differences. To compute significant differences among more than two samples, one-way ANOVA (analysis of variance) with post-hoc Tukey HSD Test was used (http://astatsa.com/oneway_anova_with_TukeyHSD/). A p-value of 0.05 or less indicated statistically significant differences.

3 RESULTS

3.1 Identification of the *acc1-5* mutant

3.1.1 Mutation in *ANK^p* is not responsible for the *p1045* phenotype

Based on the physical distance between *ANK^p* and the other two mutated loci (Figure 3), one recombination is expected to occur between *ANK^p* and *NAC^p* among every 150 segregating progenies. Luckily, one mutant with the following genotype, *ANK^p^{-/+} NAC^p^{-/-} ACC1^{-/-}* was isolated from 50 analyzed mutants. While this mutant contains a functional allele of *ANK^p*, it still showed the same phenotypes as *p1045*. Thus, this result clearly indicates that the *p1045* phenotype is not caused by a mutation in *ANK^p*.

3.1.2 Mutation in *NAC^p* is not responsible for the *p1045* phenotypes

The short distance between *NAC^p* and *ACC1* (Figure 3) makes it extremely rare for homologous recombination to occur between them. In addition, there are no T-DNA insertion lines available for *NAC^p* from ABRC. Thus, five *NAC^p* knock down/out transgenic lines were generated by using artificial microRNA (Figure 4a) which were designed according to a published procedures (Schwab et al., 2006; Ossowski et al., 2008). The expression of *NAC^p* in those transgenic lines was examined using semi-quantitative RT-PCR. Expression of *NAC^p* was decreased in four transgenic lines and completely silenced in one transgenic line (Figure 4b). However, there are no observable morphological differences in any of the transgenic lines following germination compared to WT (Figure 4c). This result suggests that the mutation in *NAC^p* is not responsible for the *p1045* phenotype.

3.1.3 Mutation in *ACC1* is responsible for the *p1045* phenotype

To confirm that *p1045* is allelic to *ACC1*, I first checked the phenotypes of two other *acc1* mutants: *gk101* (renamed hereafter *acc1-4*), an EMS mutant in *Ler-0* (Kajiwara et al., 2004), and SALK_055428 (renamed *acc1-6*), a T-DNA insertion line (Figure 5a). Compared with WT (Figure 6a to 6d), both *acc1-4* and *acc1-6* showed similar defects during embryogenesis to *p1045* (Figure 5b, 5c and Figure 6e, 6f). At the seedling stage,

Figure 4: Depletion of the expression of *NAC^p* by artificial microRNA

a: Map of *NAC^p* microRNA fragment (NACi) inserted into the pEG100 vector backbone. The microRNA is driven by the 35S promoter. LB and RB indicate left and right border of T-DNA, respectively. Basta represents a bialaphos resistance gene for selection of transgenic lines.

b: Semi-quantitative RT-PCR analysis of the expression of *NAC^p* in five RNAi transgenic lines and corresponding phenotype of 7-day old seedlings. The gene encoding glyceraldehyde 3-phosphate dehydrogenase (GAPDH) serves as loading control.

c: Phenotypes of wild-type and five RNAi transgenic lines at 7 DAG. Bar = 500 μ m

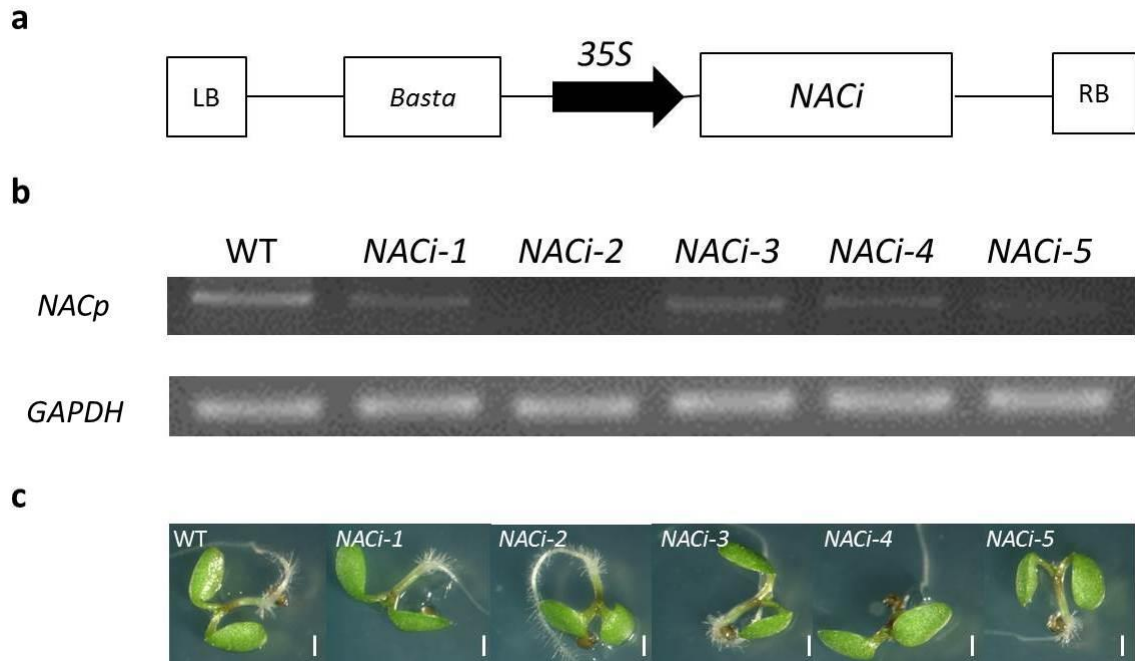


Figure 5: Characterization of different *acc1* alleles

a: A diagram showing the gene structure of *ACC1* with the EMS mutation and T-DNA insertion sites of three *acc1* mutant alleles indicated by arrows. Black boxes: exons; lines: introns.

b: 7 day-after-pollination embryos of *acc1-4*. Bar = 100 μ m

c: 7 day-after-pollination embryos of *acc1-6*. Bar = 100 μ m

d: 7 DAG seedlings of *acc1-4*. Bar = 1 mm

e: 7 DAG seedlings of *acc1-6* with severe mutant phenotype. Bar = 1 mm

f: 7 DAG seedlings of *acc1-6*. Bar = 0.5 mm

g: 12 DAG seedlings of WT, *acc1-4*, and *acc1-6*. Bar = 10 mm

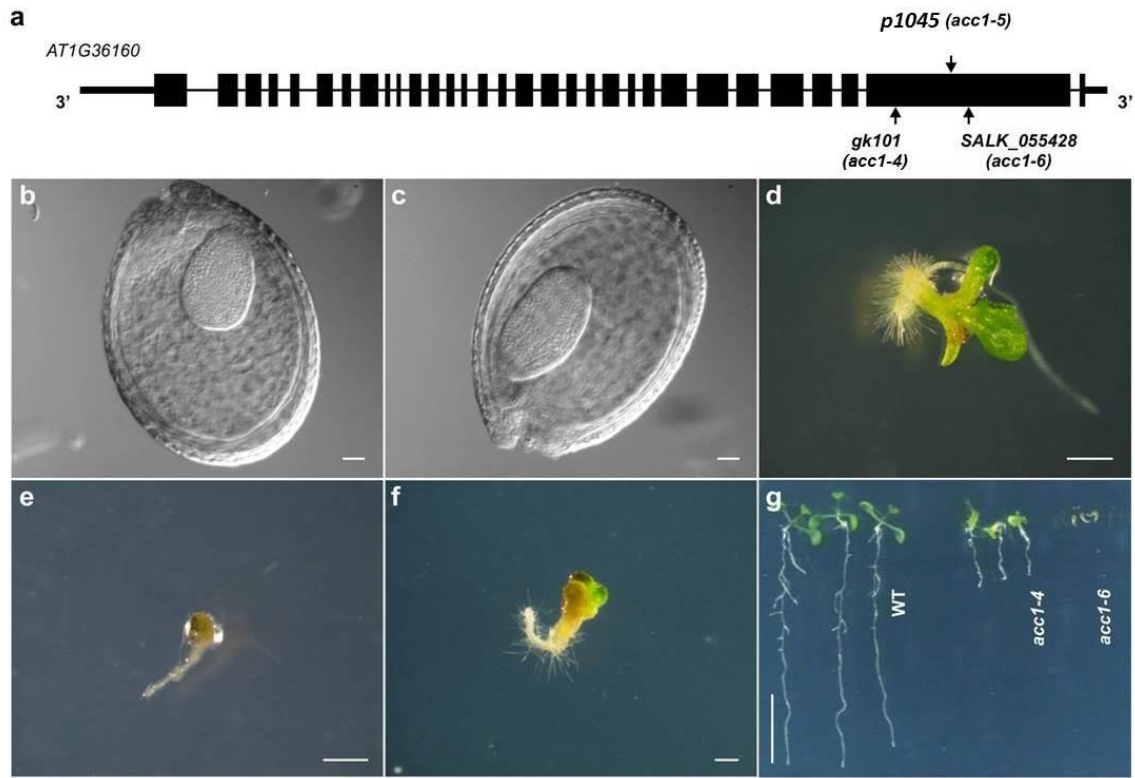


Figure 6: Mutation of *ACCI* is responsible for *p1045* phenotypes

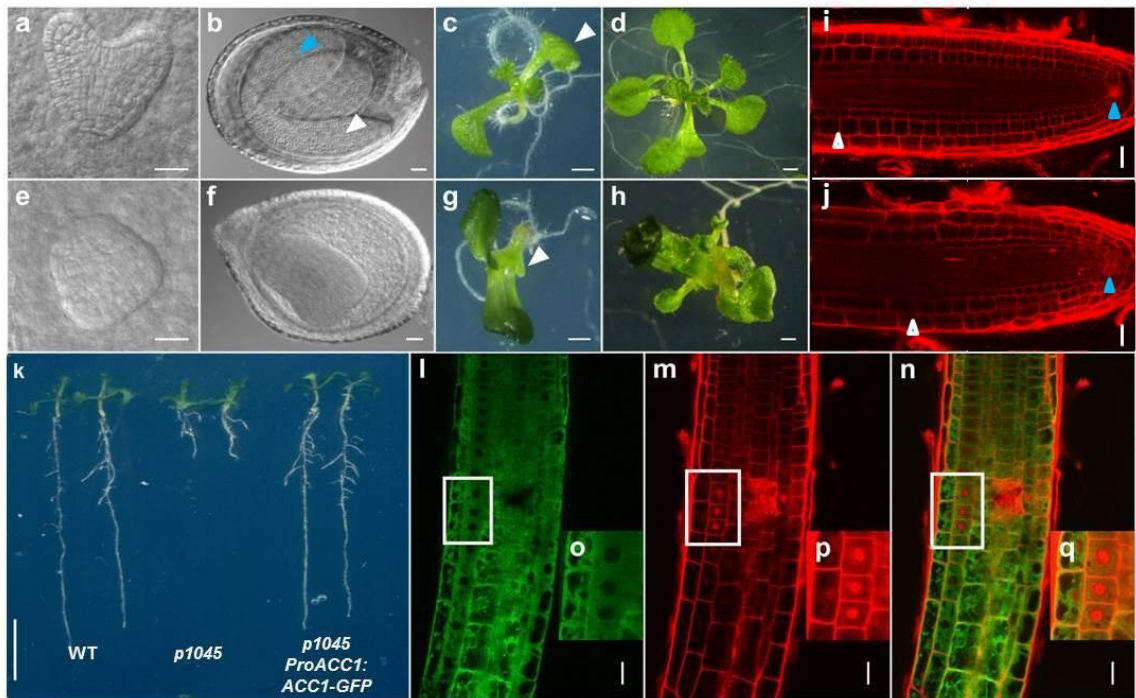
a to d: WT embryo at heart stage (3 day-after-pollination). Bar = 50 μm (a) and maturation (7 day-after-pollination). Blue and white arrows indicate embryonic cotyledon and root, respectively. Bar = 100 μm (b); seedlings at 7 DAG. White arrow represents cotyledon. Bar = 1 mm (c) and 14 DAG. Bar = 1 mm (d).

e to h: *p1045* embryo at heart stage (3 day-after-pollination). Bar = 50 μm (e) and maturation (7 day-after-pollination). Embryonic cotyledon and root are failed to differentiate in the *p1045* mutant. Bar = 100 μm (f); seedlings at 7 DAG. White arrow indicates deformed cotyledon. Bar = 1 mm (g) and 14 DAG. Bar = 1 mm (h).

i to j: Root meristems of 6 DAG Col-0 WT (i) and *p1045* (j). Root meristem was defined as the region of cortex cells between the cortex stem cell (blue arrow) and the first elongated cortex cell (white arrow). Bar = 20 μm .

k: 12 DAG seedlings of WT, *p1045*, and *p1045 ProACCI:ACCI-GFP*. Bar = 10 mm

l to q: *ProACCI:ACCI-GFP* distribution in 5 DAG root. GFP signal (l), propidium iodide staining (m), and merged (n). (o) to (q) enlarged views of indicated areas corresponding to (l), (m), and (n), respectively. Bar = 20 μm



both *p1045* and *acc1-4* showed deformed cotyledons and leaves and short primary roots on ½ MS media (Figure 5e to 5g and Figure 6g to 6k). The *acc1-6* seedlings failed to form cotyledons and true leaves, developed very short primary roots, and showed arrested growth after germination (Figure 5d to 5g). Then, I performed an allelic test by crossing heterozygous *p1045* with heterozygous *acc1-6* plants. In the F1 generation, 24.7% of the seedlings showed the same phenotype as *p1045* (Table 1). The mutant ratio is similar to that observed in the F1 generation of heterozygous *acc1-6* self-pollination. In addition, WT version of *ACC1* (fused with the GFP coding sequence) under its native promoter (*ProACC1:ACC1-GFP*) fully rescued the phenotypes of the *p1045* mutant seedlings (Figure 6k). Together, these data indicate that *p1045* are allelic to *ACC1* which cause amino acids change from aspartic acids to asparagine. Therefore, I renamed it as *acc1-5*.

3.2 Subcellular localization and tissue specificity of ACC1

ACC1 was proposed to be an endoplasmic reticulum-associated protein within the VLCFAs (very-long-chain fatty acids) elongase complex (Roudier et al., 2010) which includes multiple enzymes for fatty acids elongation. To examine the subcellular localization of ACC1, I visualize the GFP signals in the *ProACC1:ACC1-GFP acc1-5* roots. Most of the GFP signal was detected in the cytosol but not in the nucleus (which is stained by propidium iodide (PI)) (Figure 6l to 6q), suggesting that ACC1 is a cytosolic localized protein. I also generated a transgenic line expressing an ACC1-GUS fusion protein under its native promoter (*ProACC1:ACC1-GUS*) to examine ACC1's tissue distribution pattern. Consistent with previous data obtained with *ACC1* promoter-GUS fusion (Lu et al., 2011b). ACC1 protein was detected in many tissues including embryo, root, leaf, stem, and flower (Figure 7). In particular, the strongest signals were detected in actively dividing cells such as root and shoot meristems (Figure 7a and 7b).

3.3 Increased accumulation of acetyl-CoA and histone H3K27 acetylation in *acc1* mutants

The malfunction of ACC1 results in insufficient VLCFAs (Baud et al., 2003; Lu et al., 2011b), which have been shown to cause pleiotropic defects during plant development (Baud et al., 2004; Bach et al., 2008; Roudier et al., 2010; Nobusawa et al., 2013). To

Table 1: Allelic test of *ACCI* alleles

Parental genotype (P)	Number of total progeny (F1)	Number of mutants	% Mutants
<i>p1045</i> ^{+/-} X <i>p1045</i> ^{+/-}	216	52	24.1%
<i>acc1-6</i> ^{+/-} X <i>acc1-6</i> ^{+/-}	502	126	25.1%
<i>p1045</i> ^{+/-} X <i>acc1-6</i> ^{+/-}	316	78	24.7%

Figure 7: ACC1 protein in various *Arabidopsis* tissues

GUS stainings of ProACC1:ACC1-GUS transgenic plants were performed on various tissues. ACC1-GUS fusion proteins are indicated as blue color after staining. Bar = 1mm

a: 5 DAG seedling. Black arrow indicates shoot meristematic regions.

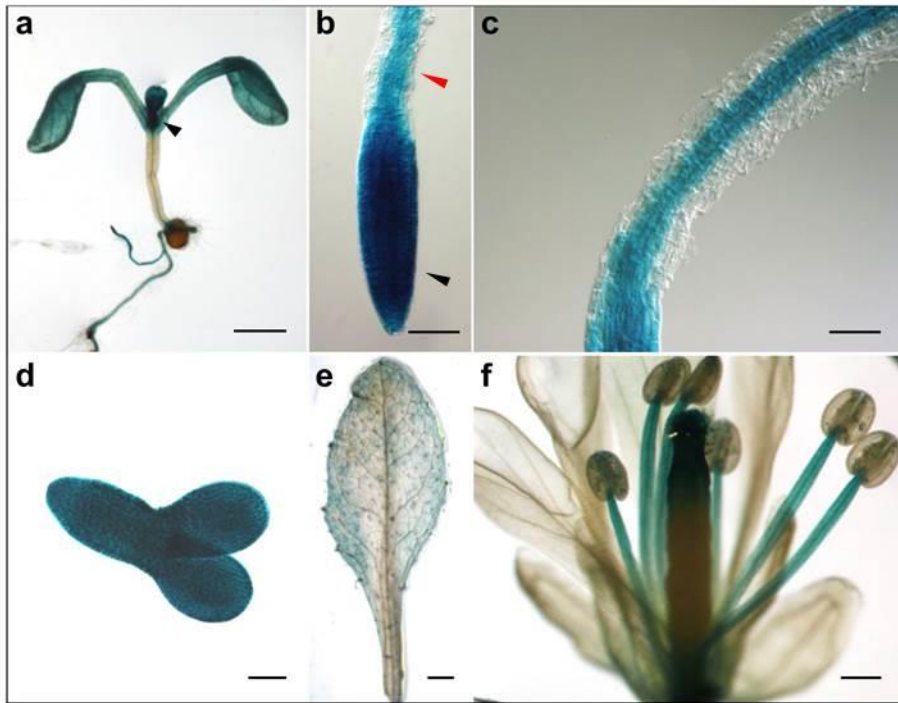
b: Root tip of 5 DAG seedling. Black and red arrows represent root meristematic and elongated zones, respectively.

c: Root elongation zone of 5 DAG seedling

d: Embryo dissected from 5 day-after-pollination silique. Bar = 100 μ m

e: Rosette leaf

f: Flower



examine whether the phenotypes of *acc1-5* resulted from the shortage of VLCFAs, I grew WT and *acc1-5* seedlings in the presence of malonate which can be converted to malonyl-CoA by malonyl-CoA synthetase (Baud et al., 2004). As shown in Figure 8, exogenous malonate can partially rescue the short root of *acc1-5*. It suggests that other defects also contribute the phenotypes of *acc1-5*.

Since ACC1 catalyzed fatty acid elongation serves as one of the pathways to utilize cytosolic acetyl-CoA, the mutation of *ACC1* may lead to accumulation of acetyl-CoA in the cell. To examine whether the level of acetyl-CoA is altered in *acc1* mutants, I measured the total amount of acetyl-CoA using HPLC. As shown in Figure 9a, the level of acetyl-CoA was significantly higher in *acc1-5* compared to that in WT. A similar result was also found in *acc1-4* (Figure 9a). Because acetyl-CoA is the substrate for histone acetylation, I hypothesized that accumulated acetyl-CoA in *acc1* can promote histone acetylation. I analyzed the levels of histone acetylation at 8 different lysine residues of histone tails in *acc1-4* and *acc1-5* by immunoblotting (Figure 9b). Increased acetylation was detected at H3K27, but not at the other 7 lysine residues in *acc1* mutants compared to that in WT (Figure 9b).

Previously, ACL has been characterized as a nonredundant source of cytosolic acetyl-CoA (Fatland et al., 2002) (Figure 2). Repressing the expression of the cytosolic enzyme ACL reduces the accumulation of cytosolic acetyl-CoA-derived metabolites (Fatland et al., 2005). It suggests that the amount of cytosolic acetyl-CoA is determined by the activity of ACL. Thus, the accumulated acetyl-CoA might contribute by increased transcription of genes encoding ACL subunits in *acc1* mutants. However, no significant differences were found in the expression of the five genes encoding ACL subunits in *acc1-5* compared to that in WT plants (Figure 10). To examine whether the accumulation of acetyl-CoA resulted in the increased H3K27ac in *acc1* mutants, I repressed the synthesis of cytosolic acetyl-CoA by conditionally knocking down the transcripts of *ACLA-1* that encodes one subunit of ACL. An artificial microRNA designed specifically against *ACLA-1* (*acla-1i*) was expressed in the *acc1-5* background under the control of a β -estradiol inducible promoter (Zuo et al., 2000) (Figure 11). After 24h induction, the expression of *ACLA-1* was reduced to ~35% of the WT level (Figure 12a) and the levels

Figure 8: Partial complementation of *acc1-5* phenotypes by exogenous malonate

a: Growth of WT and *acc1-5* seedlings at 10 DAG in mocking treatment. The short roots and deformed leaves were shown in *acc1-5*. Bar = 10 mm

b: Growth of WT and *acc1-5* seedlings at 10 DAG in 1 mM malonate treatment. Partially recovered roots growth was shown in *acc1-5* after treating with malonate. Bar = 10 mm

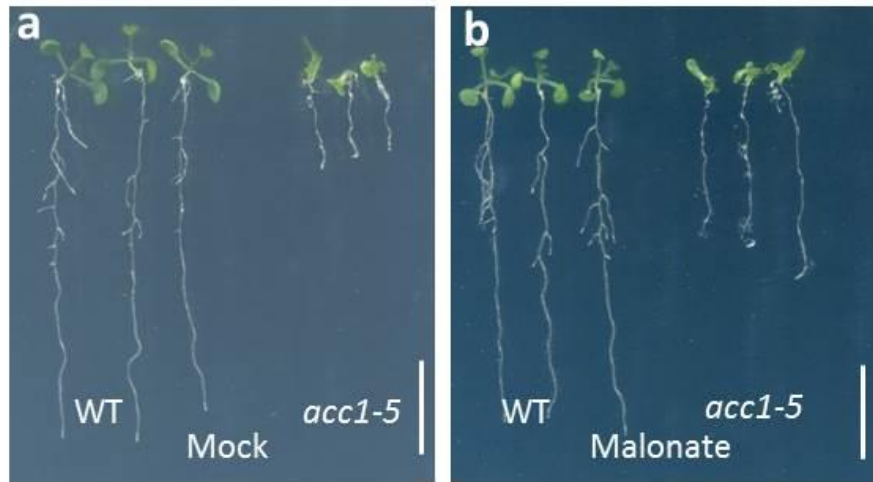


Figure 9: ACC1 affects the acetyl-CoA level and global histone H3K27 acetylation

a: Box plot of the acetyl-CoA levels in 12 DAG seedlings of WT (*Col-0* and *Ler-0*), *acc1-4*, and *acc1-5*. Four independent replicates are included; two-tailed student t-test, * $p = 0.012$; ** $p = 0.0013$.

b: Western blotting analysis of total protein extracts from 12 DAG seedlings. Antibodies used to identify various modifications on H3 and H4 are indicated on the left. Loading amounts of each sample were adjusted according to H3 blotting signals. Corresponding antibodies are listed as below: anti-H3: ab1791 (Abcam), anti-H3K9ac: 07-352 (Millipore), anti-H3K14ac: 07-353 (Millipore), anti-H3K18ac: 07-354 (Millipore), anti-H3K27ac: 07-360 (Millipore), anti-H4K5ac: 07-327 (Millipore), anti-H4K8ac: 07-328 (Millipore), anti-H4K12ac: 07-595 (Millipore), anti-H4K16ac: 07-329 (Millipore). Three independent extracts were performed for all the samples and one representative immunoblotting image is presented. The intensities of blotting signals were quantified by using ImageJ software and the average intensities from three independent extracts were shown.

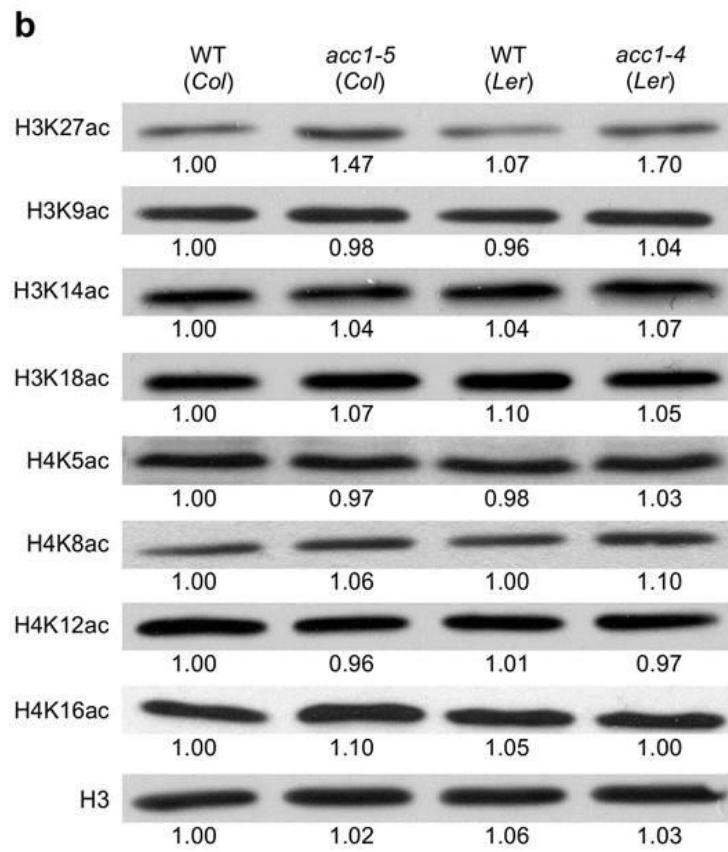
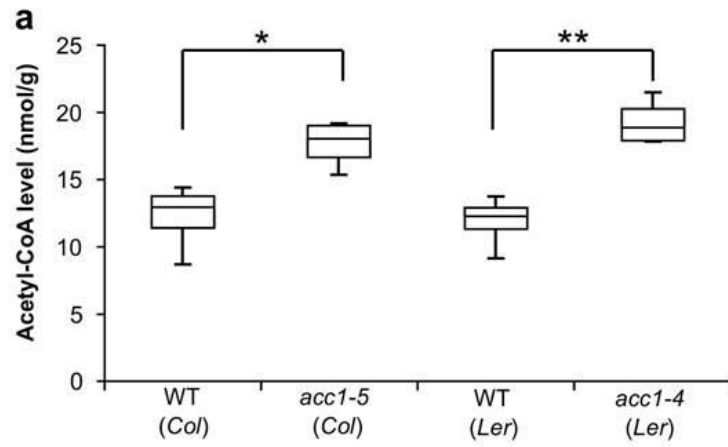


Figure 10: Unchanged transcript levels of genes encoding ACL subunits in WT and *acc1-5*

Quantitative RT-PCR determines the expression levels of ACL encoding genes in WT and *acc1-5*. The expression levels are normalized using *Actin 7 (ACT7)*. Three biological replicates were included and two-tailed student t-test was performed. There are no significantly different expressions of tested genes between WT and *acc1-5*.

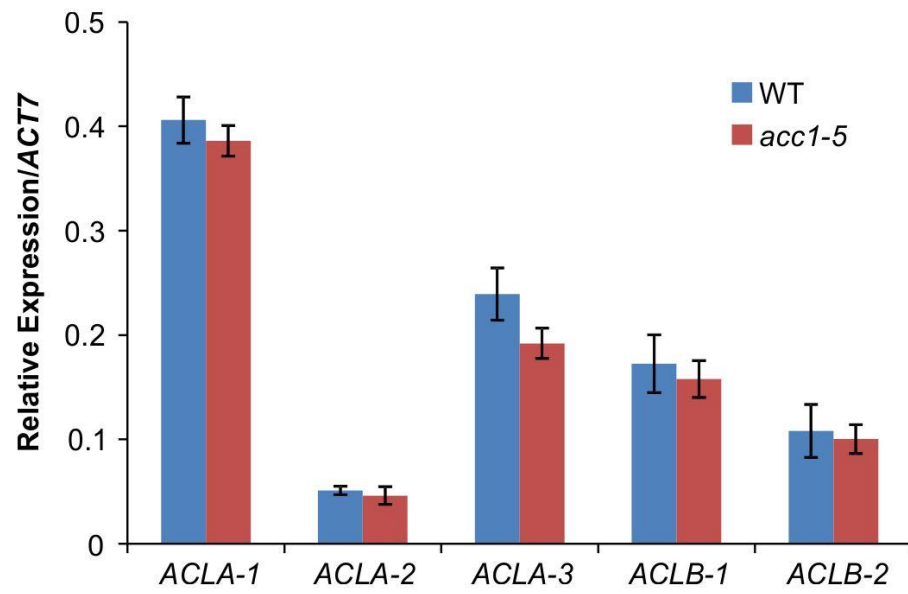


Figure 11: Artificial microRNA of *ACLA-1* in β -estradiol inducible system

In this inducible system, the expression of a chimeric transcription activator, XVE, is controlled by a constitutive promoter *G10-90*. And then, a LexA operator fused to 35S minimal promoter controls the expression of *ACLA-1* artificial microRNA (*ACLA-1i*). The dimerization of XVE protein is required to activate the LexA operator. In uninduced condition, the XVE transcription activator fails to form a dimer and the artificial microRNA cannot be transcribed. After treating with β -estradiol, the dimerized XVE protein can bind the LexA operator and activate downstream transcription. The transcribed microRNA will bind to *ACLA-1* mRNA and down-regulate *ACLA-1* transcript levels.

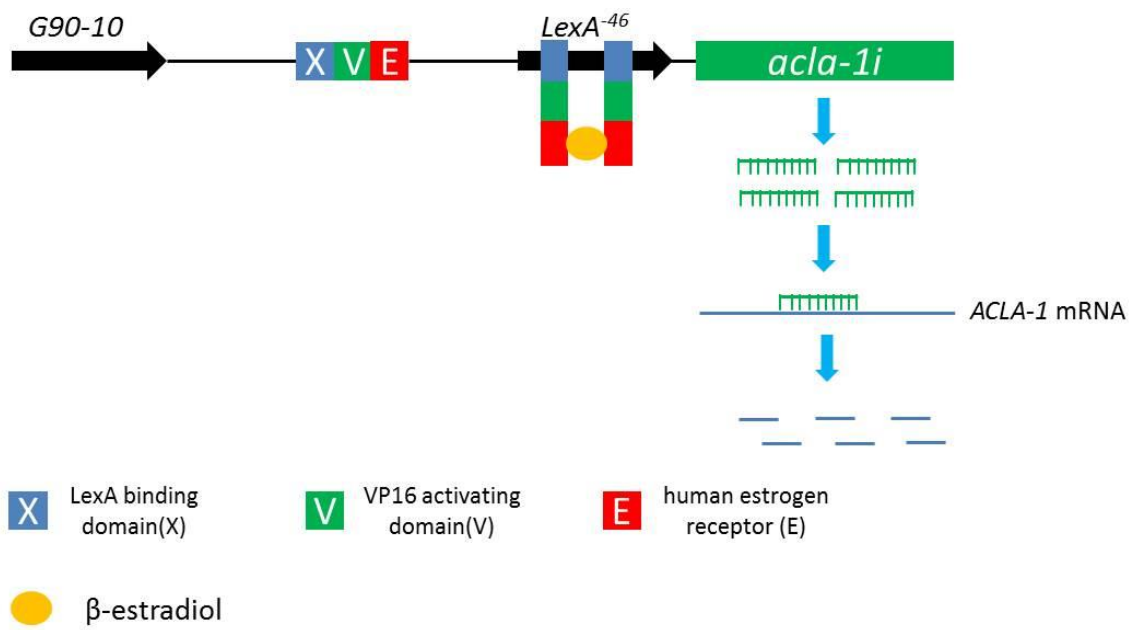
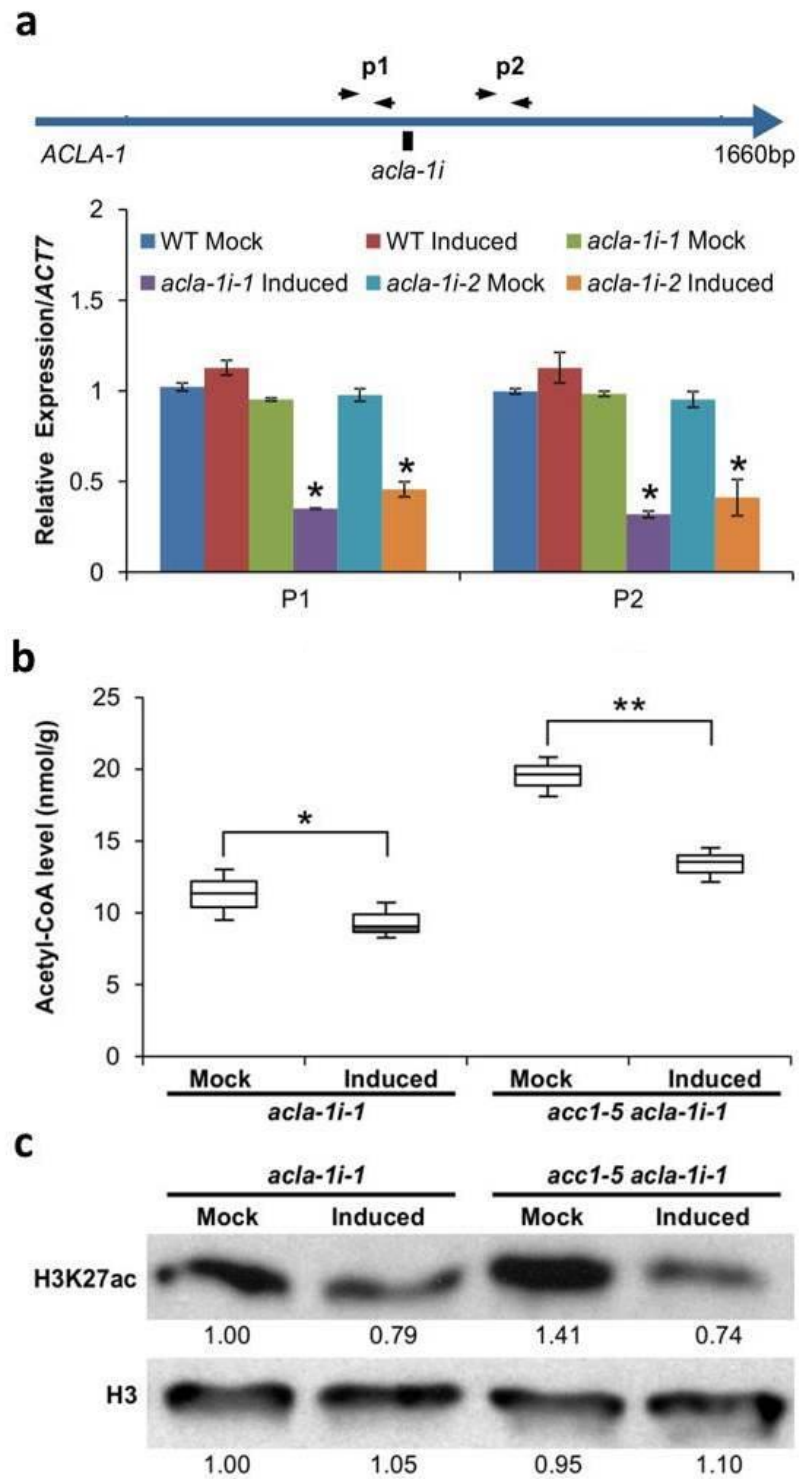


Figure 12: ACL activity is required for the accumulation of acetyl-CoA and increased H3K27ac in *acc1-5*

a: qRT-PCR measurement of the transcript level of *ACLA-1* after 24 h induction with 20 μ M 17 β -estradiol or same amount of distilled water (mock groups). All the expression levels are normalized to that of *ACT7*. The diagram at the top indicates the targeted positions of artificial microRNA and primers. Two independent transgenic lines were tested (*acla-li-1* and *acla-li-2*). Mean \pm SD; Three biological replicates are included; two-tailed student t-test, * $p < 0.02$.

b: Box plot of acetyl-CoA level in *acla-li-1 acc1-5* and *acla-li-1* after 24 h mock treatment or induction with 20 μ M 17 β -estradiol. Four biological replicates are included; two-tail student t-test, * $p = 0.035$, ** $p = 0.012$.

c: Western blot analysis of total protein extracts after 24 h induction with 20 μ M 17 β -estradiol, probed with anti-H3K27ac and anti-H3 antibodies. Three independent extracts were performed for all the samples and one representative immunoblotting image is presented. The intensities of blotting signals were quantified by using ImageJ software and the average intensities from three independent extracts were shown.



of acetyl-CoA and H3K27ac were also decreased in the *acc1-5 acla-li-1* induced group compared to that in the *acc1-5 acla-li-1* mock group (Figure 12b and 12c). Taken together, these data support that histone H3K27 acetylation is associated with the amount of acetyl-CoA in plants.

3.4 Genome-wide profiles of histone modifications in WT and *acc1-5* mutant plants

3.4.1 Increased genome-wide occupancy of H3K27ac in *acc1-5*

Having established that changes in the levels of acetyl-CoA affect histone acetylation, I next performed ChIP-seq analyses to determine the role of ACC1 in genome-wide locations of H3K27ac. To check assess the quality of our ChIP-seq data, firstly, I performed Pearson correlation analysis between the two replicates of each sample and found that both replicates of WT and *acc1-5* are highly correlated (Figure 13a). Secondly, I compared my H3K27ac binding target genes identified in WT to those identified in a previous ChIP-chip study (Charron et al., 2009) and found that 87.6% of the previously identified genes were re-identified in my work (Figure 13b). To compare the global H3K27ac levels in *acc1-5* and WT, I randomly extracted an equal number of reads from the H3K27ac ChIP-seq in *acc1-5* and WT and found that the levels of H3K27ac around transcriptional starting sites (TSS) was significantly increased in *acc1-5* relative to that in WT ($p = 3.52 \times 10^{-10}$, two-tailed, Mann-Whitney test) (Figure 14a). This result is consistent with the immunoblotting estimation of H3K27ac levels in *acc1-5* shown in Figure 9b. A total of 802 genes showed at least a 1.5 fold increase ($p < 0.001$) of H3K27ac deposition in the *acc1-5* mutant compared to WT. The increase in H3K27ac levels at selected genes in *acc1-5* is shown in Figure 14b and validated by ChIP-quantitative PCR (ChIP-qPCR) (Figure 14c). To determine whether the levels of histone H3 may be altered in *acc1-5*, I performed ChIP-qPCR with anti-H3 antibodies on the genomic regions selected above. As shown in Figure 13d, there were no significant alterations of H3 levels on these chromatin regions in *acc1-5* compared to WT. Consistently, the increased depositions of H3K27ac on those chromatin regions can also be detected in *acc1-4* compared to *Ler-0* WT (Figure 15a and 15b). Furthermore, Gene Ontology analysis indicated that the genes

Figure 13: High reproducibility and reliability of H3K27ac ChIP-seq

H3K27ac ChIP-seq experiments were performed by using 2g of WT and *acc1-5* 12 DAG seedlings. Two biological replicates were included for each sample.

a: Pearson correlation analyses of H3K27ac ChIP-seq within two replicates of WT and *acc1-5*. Pearson correlation values for WT and *acc1-5* are 0.95 and 0.91, respectively.

b: Venn diagram showing the overlap of genes bearing H3K27ac revealed in this work with those identified in a previous study (Charron et al., 2009). In total, 87.6% of the previously identified genes were re-identified in my work.

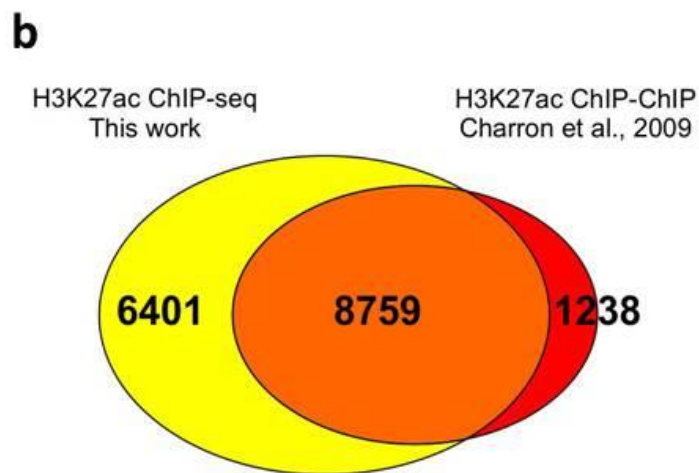
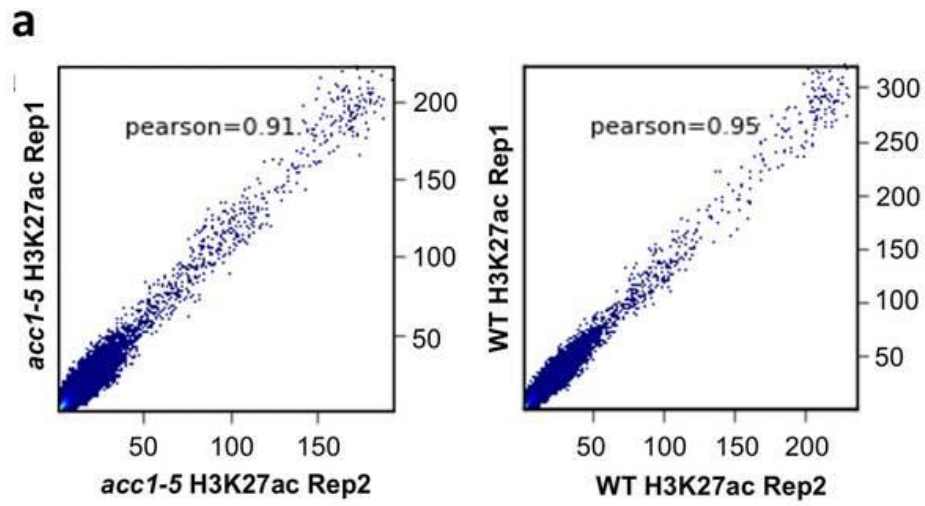


Figure 14: Genome-wide analysis reveals increased H3K27ac in *acc1-5*

a: WT and *acc1-5* H3K27ac ChIP-seq reads density are around ± 2.5 kb of 33,301 transcriptional starting sites (TSS). 3 million reads from each dataset were used. $p = 3.52 \times 10^{-10}$, two-tailed, Mann-Whitney test.

b: The Integrated Genome Browser (IGB) was used to visualize H3K27ac ChIP-seq signals on representative genes in WT and *acc1-5*. The scale was kept identical for the different tracks and the blue diagram indicates gene structure and white bar represents tested region in ChIP-qPCR. The y-axis scales represent shifted merged MACS tag counts for every 10-bp window

c: Validation of individual peaks using ChIP-qPCR (normalized to histone H3). The region 2 of *PLT7* and *ATIG01190* served as negative and non-change region controls, respectively. Mean \pm SD; n=3; two-tailed student t-test, * $p < 0.05$, ** $p < 0.03$.

d: Relative occupancy of histone H3 in WT and *acc1-5* at indicated genomic regions (relative to total input genomic DNA). Mean \pm SD; n=3; two-tailed student t-test.

e: Gene Ontology analysis of the 802 genes with increased H3K27ac in the *acc1-5* mutant.

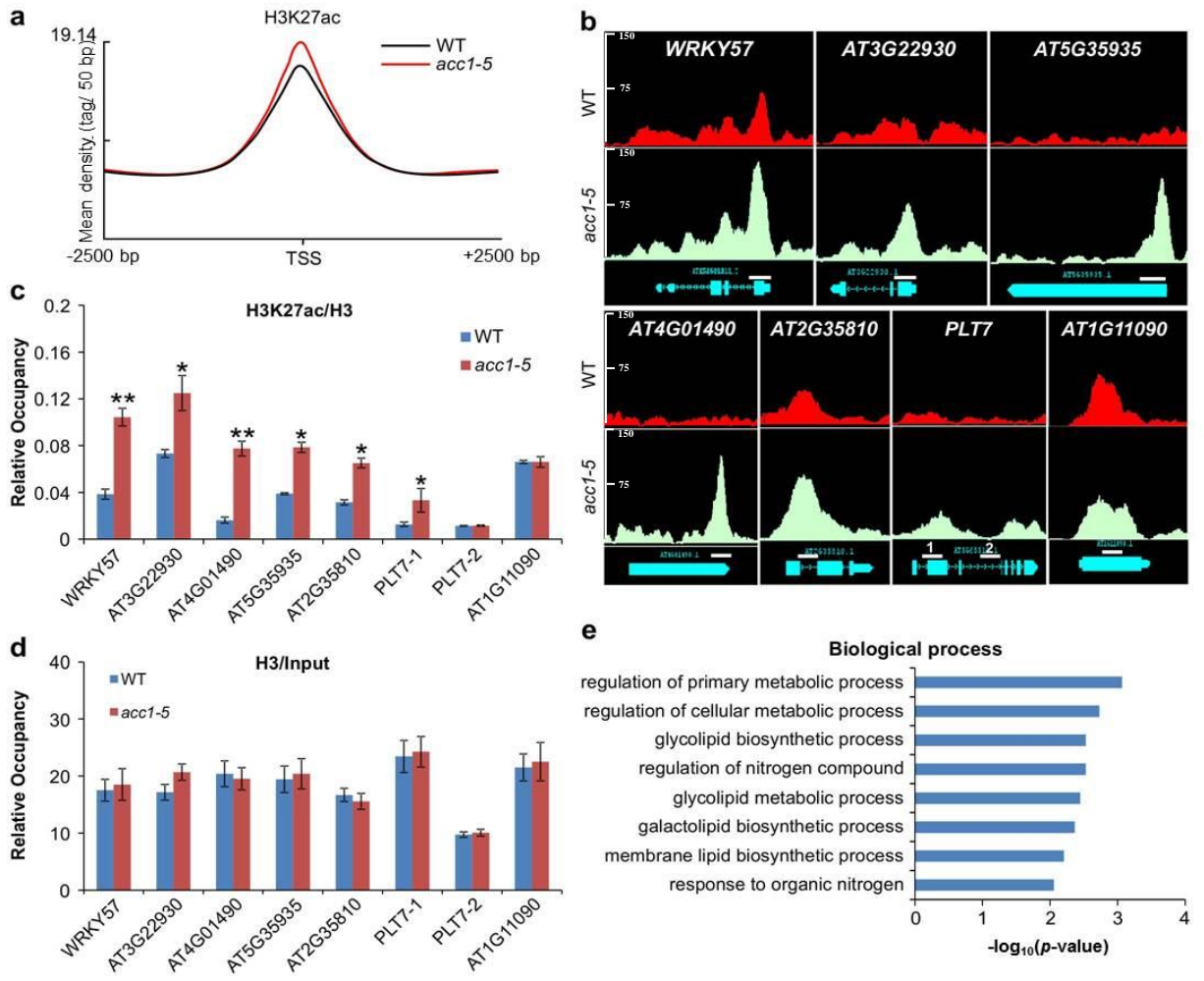
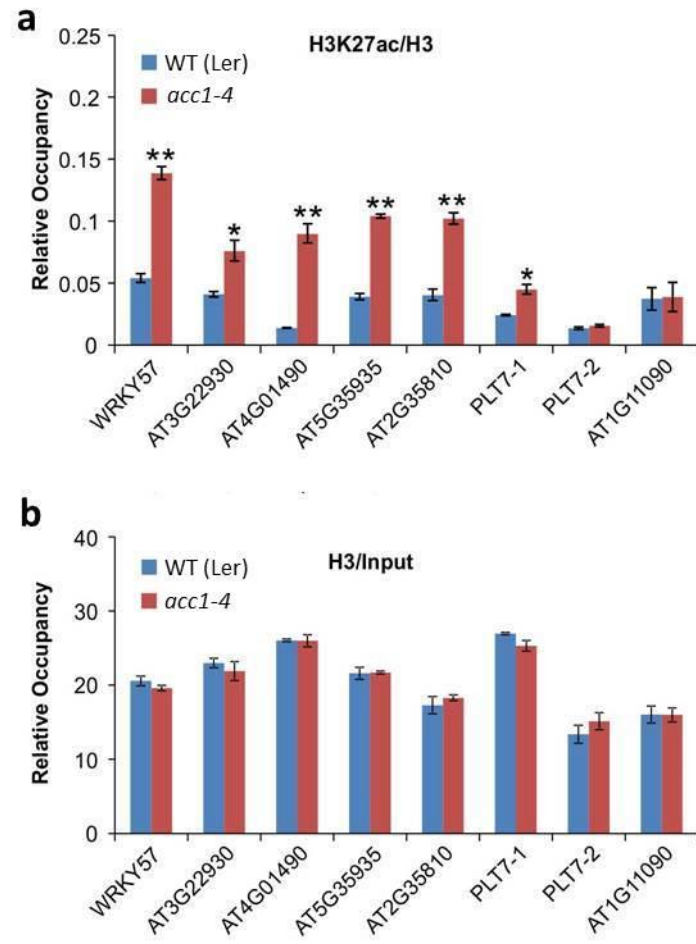


Figure 15: Increased depositions of H3K27ac at selected genes in *acc1-4*

a: Relative occupancy of H3K27ac (normalized to histone H3) in WT (*Ler*) and *acc1-4*. The region 2 of *PLT7* and *AT1G11090* serve as a negative control and a control locus without changes under all conditions, respectively. Mean \pm SD; n=3; two-tailed student t-test, * p < 0.05, **p < 0.03.

b: Relative occupancy of histone H3 in WT (*Ler*) and *acc1-4* at indicated genomic regions. Mean \pm SD; n=3; two-tailed student t-test. No significant differences were observed.



with increased H3K27ac were enriched in metabolic and nitrogen compound biosynthetic processes (Figure 14e). Therefore, I conclude that malfunction of ACC1 causes the increased deposition of H3K27ac at hundreds of genomic loci.

3.4.2 Genome-wide occupancies of other 7 histone acetylations in *acc1-5* and WT

ChIP-seq experiments were also performed in WT and *acc1-5* to examine whether ACC1 affects genome-wide histone acetylation patterns at the other 7 lysine residues (H3K9, H3K14, H3K18, H4K5, H4K8, H4K12, and H4K16). All the ChIP-seq data show high reproducibility between the two biological replicates (Figure 16). The genome-wide enrichments of each of the histone acetylation were analyzed by using an equal number of reads in WT and *acc1-5*. There were no significant differences of acetylation enrichments between WT and *acc1-5* on all the 7 acetylation marks (Figure 17). These results are consistent with the immunoblotting estimation of acetylation levels at these 7 lysine residues of histone H3 and H4 in *acc1-5* as shown in Figure 9b and suggest that elevated cytosolic acetyl-CoA levels are mainly associated with the increased H3K27ac deposition of over hundreds of genomic loci.

3.4.3 Genome-wide profiling of H3K27ac in *acc1-5 acla-1i* conditional double mutant

My immunoblotting data shown in Figure 11c indicate that increased H3K27ac in *acc1-5* is dependent on the availability of cytosolic acetyl-CoA. To investigate whether increased H3K27ac in *acc1-5* indeed resulted from the accumulation of acetyl-CoA, I performed H3K27ac ChIP-seq analyses with the *acc1-5 acla-1i-1* conditional double mutant. As controls, mock treated *acc1-5 acla-1i-1* double mutant and WT *Col-0* plants were also examined in parallel. After 24 h induction, I observed that the global H3K27ac level in induced *acc1-5 acla-1i-1* was similar to that level in WT (Figure 18a). The ChIP-seq data for selected genes are shown in Figure 17b and validated by ChIP-qPCR (Figure 18c). This result is consistent with my earlier observation that there were decreased levels of acetyl-CoA in the induced conditional double mutant relative to the *acc1-5* single mutant plants (Figure 12b). These findings further support a direct link between the accumulation of acetyl-CoA and the increase of H3K27ac in the *acc1-5* mutant.

Figure 16: High reproducibility of histone acetylations ChIP-seq experiments in WT and *acc1-5*

Pearson correlation analyses of H3K9ac, H3K14ac, H3K18ac, H4K5ac, H4K8ac, H4K12ac, and H4K16ac ChIP-seq within two replicates of WT and *acc1-5*. In WT samples, Pearson correlation values for H3K9ac, H3K14ac, H3K18ac, H4K5ac, H4K8ac, H4K12ac, and H4K16ac are 0.97, 0.92, 0.87, 0.96, 0.96, 0.95, and 0.95, respectively. In *acc1-5* samples, Pearson correlation values for H3K9ac, H3K14ac, H3K18ac, H4K5ac, H4K8ac, H4K12ac, and H4K16ac are 0.97, 0.92, 0.87, 0.95, 0.97, 0.94, and 0.95, respectively.

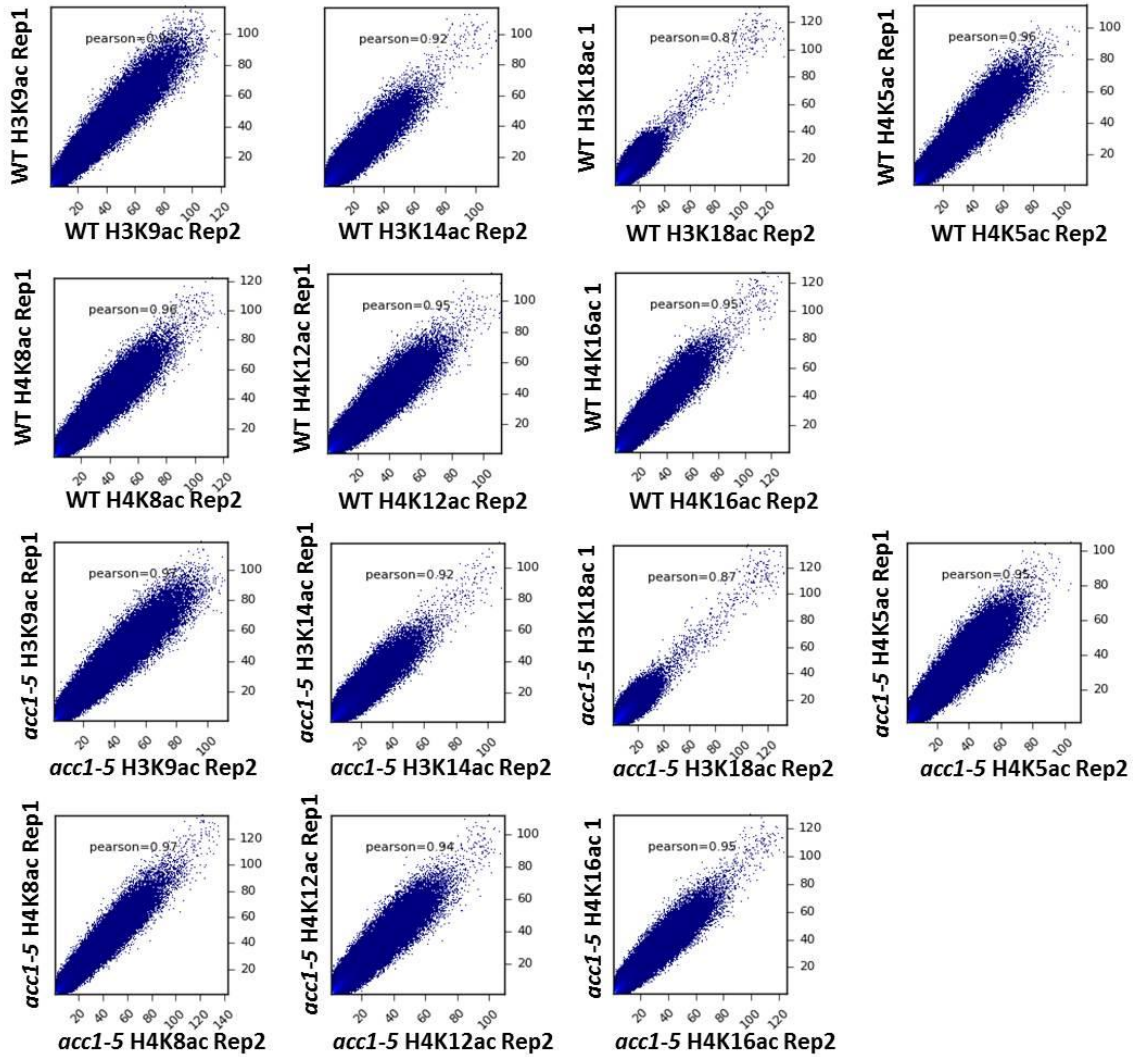


Figure 17: Similar genome-wide occupancies of 7 histone acetylation marks in acc1-5 to that in WT

Reads of each of the histone acetylation marks were plotted around ± 2.5 kb of TSS. One million of reads from each dataset was used. Two-tailed, Mann-Whitney test: H3K9ac, $p = 0.493$; H3K14ac, $p = 0.234$; H3K18ac, $p = 0.526$; H4K5ac, $p = 0.082$; H4K8ac, $p = 0.076$; H4K12ac, $p = 0.107$; H4K16ac, $p = 0.326$. With $p < 0.05$ is considered as significant difference.

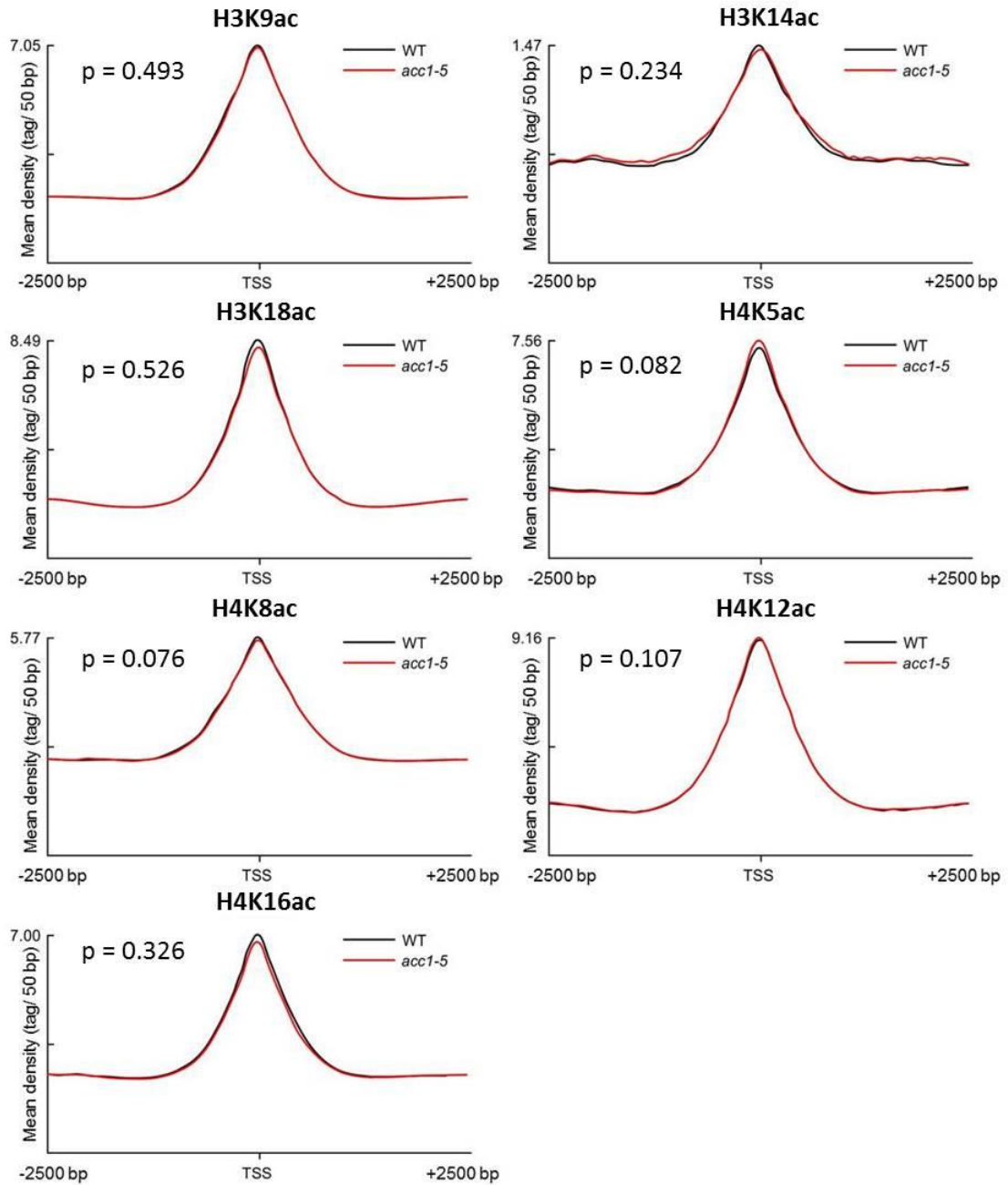
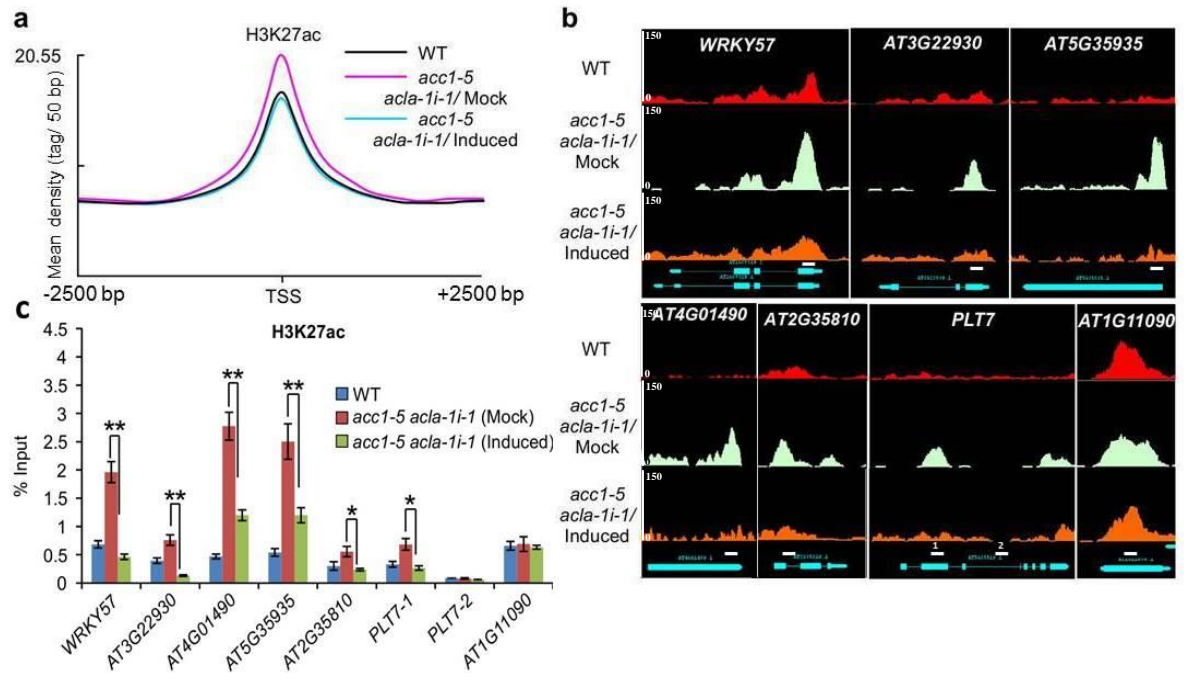


Figure 18: Increased H3K27ac is dependent on the activity of ACL

a: Peak distribution of H3K27ac relative to around ± 2.5 kb of TSS for WT, *acc1-5 acla-li-1* mock treated, and *acc1-5 acla-li-1* after 24 h induction. Three million reads from each dataset were used.

b: The IGB was used to visualize H3K27ac ChIP-seq signals on representative genes in WT, *acc1-5 acla-li-1* mock treated, and *acc1-5 acla-li-1* after 24 h induction. The scale was kept identical for the different tracks. The blue diagram indicates gene structure and the white bars represent tested region in ChIP-qPCR. *AT1G01190* serves as a control gene that exhibits no change of H3K27ac level under all conditions.

c: Validation of the occupancy of H3K27ac (normalized to histone H3) at 8 different regions after conditionally depleting *ACL* in *acc1-5*. The region 2 of *PLT7* and *AT1G01190* serve as a negative control and a control locus without changes under all conditions, respectively. Mean \pm SD; n=3; two-tailed student t-test, *p < 0.05, **p < 0.01



3.4.4 Genome-wide analysis of H3K27me3 in *acc1-5*

It has been shown that histone H3 lysine 27 trimethylation (H3K27) can antagonize H3K27ac during regulation of gene expression (Tie et al., 2009). Since these two histone modifications occur on the same lysine residue, it would be interesting to see whether the global level of H3K27me3 is also affected in the wave of H3K27 hyperacetylation in *acc1* mutants (Figure 9b). Therefore, I conducted a ChIP-seq analysis to profile H3K27me3 in WT and *acc1-5* plants. I identified 8,112 genes that were marked by H3K27me3 in WT with a large overlap with those identified in previous ChIP-seq studies (Lu et al., 2011a; Li et al., 2015) (Figure 19a). Interestingly, in *acc1-5*, genome-wide deposition of H3K27me3 was markedly decreased compared to WT ($p = 2.14 \times 10^{-11}$ two tail, Mann-Whitney test) (Figure 19b). To examine whether the H3K27ac increase and the H3K27me3 decrease occurred over the same genomic loci in *acc1-5*, I compared the H3K27me3 density between *acc1-5* and WT at the previously identified 802 hyperacetylated genes (section 3.4.1). Based on the levels of H3K27me3 in WT, the 802 genes were further clustered into 2 subgroups: group 1 contained 650 genes which were marked by H3K27ac only; while group 2 contained 152 genes which were co-marked by both H3K27ac and H3K27me3 (Figure 20a). Comparing the deposition of H3K27me3 on these two groups of genes, there was a significant decrease of H3K27me3 deposition in group 2 ($p = 0.0003$, two-tailed, Mann-Whitney test) (Figure 20b). ChIP-seq peaks for the selected genes in each group are shown in Figure 20c. The decreased H3K27me3 and increased H3K27ac at these genes were validated by ChIP-qPCR (Figure 20d). Gene ontology analysis showed that both groups of genes were mainly enriched in metabolic processes (Figure 21a and 21b). Interestingly, some of the genes in group 2 were also enriched in the regulation of gene expression and transcription, which was not the case for group 1 genes (Figure 21b). These observations suggest that the acetylation and trimethylation of H3K27 may be dynamically modulated on chromatin of the same gene loci in response to the changes of cellular acetyl-CoA levels.

Figure 19: H3K27me3 ChIP-seq analysis in WT and *acc1-5*

a: Venn diagrams showing the overlap of genes bearing H3K27me3 revealed in this work with those identified in two previous studies (Lu et al., 2011a; Li et al., 2015).

b: Peak distribution of H3K27me3 relative to around ± 2.5 kb of TSS in WT and *acc1-5*. Three million reads from each dataset were used. $p = 2.14 \times 10^{-11}$, two tail, Mann-Whitney test

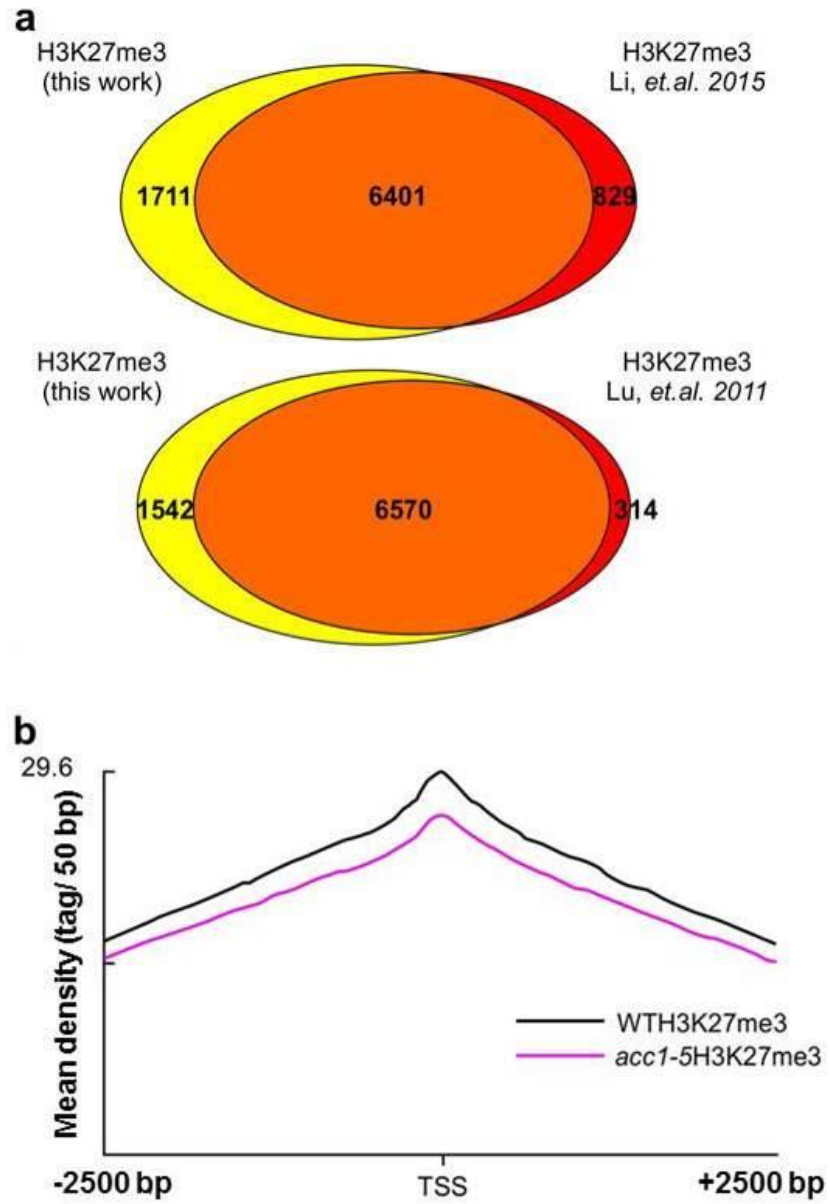


Figure 20: Genome-wide analysis of H3K27me3 in *acc1-5* and WT

a: Heat map of the enrichments of H3K27ac and H3K27me3 in WT and *acc1-5* at ± 2.5 kb of the 802 TSS sites, which showed H3K27 hyperacetylation in *acc1-5*. The red intensity represents an enrichment of reads and each line represents a genomic region. Two groups of genes were clustered based on reads density of H3K27me3.

b: Peak distribution of H3K27me3 and H3K27ac in group1 and group 2 relative to ± 2.5 kb around TSS for WT and *acc1-5*. Three million reads from each dataset were used.

c: H3K27ac and H3K27me3 ChIP-seq signals on example genes in WT and *acc1-5*. The scale was kept identical for the different tracks and the blue diagram indicates gene structure and white bars represent tested regions in ChIP-qPCR. The first three genes belong to group 1 which is only marked by H3K27ac and the last three genes are examples for gene group 2 which is co-marked by H3K27ac and H3K27me3. Region 2 of *PLT7* served as a negative control region.

d: Validation of the occupancy of H3K27ac and H3K27me3 (normalized to histone H3) at 7 different regions. Region 2 of *PLT7* (*PLT7-2*) served as a negative control region. Mean \pm SD; n=3; two-tailed student t-test, *p < 0.05, **p < 0.01.

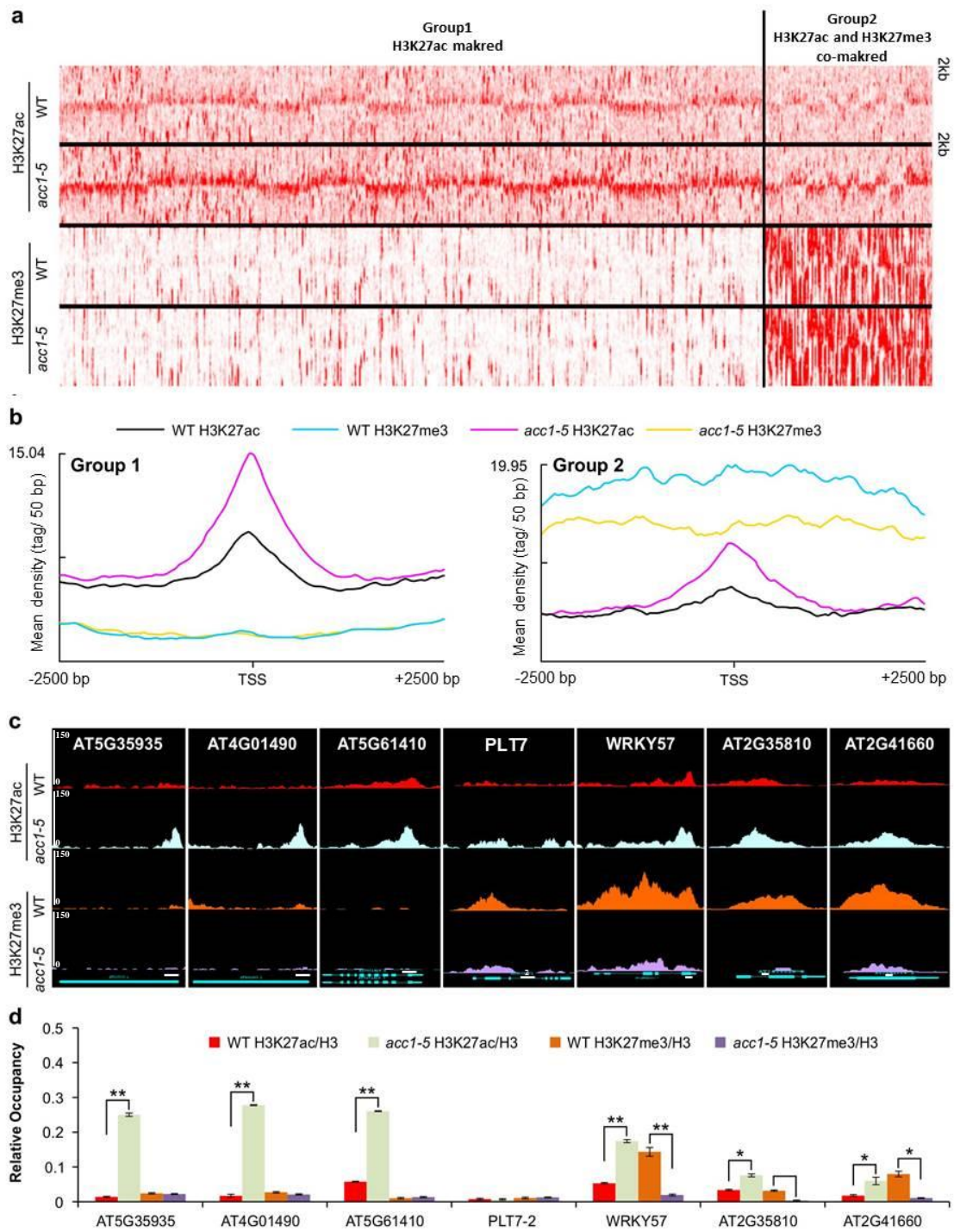
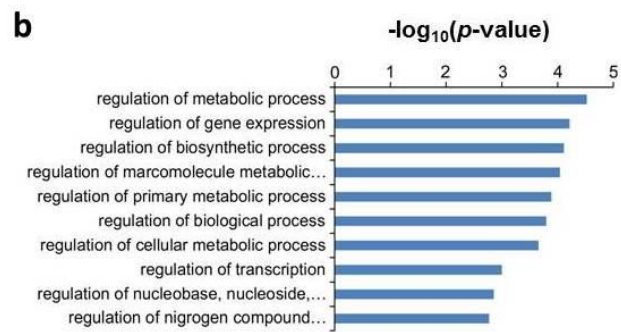
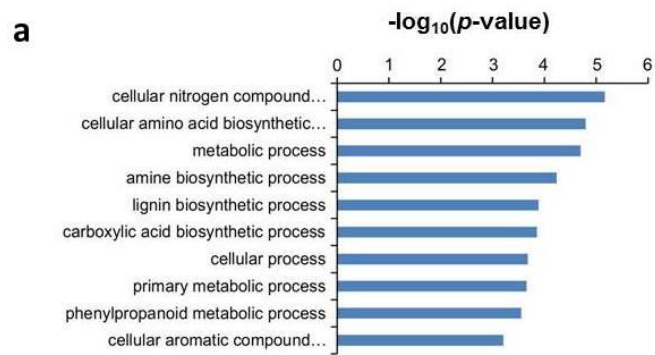


Figure 21: Go terms analysis of two subgroup genes

a: GO terms analysis of group 1 genes ($p < 0.001$), which are only marked by H3K27ac.

b: GO terms analysis of group 2 genes. ($p < 0.001$), which are co-marked by H3K27ac and H3K27me3.



3.5 GCN5/HAG1 is required for the increased H3K27ac in *acc1-5* on some genetic loci

The state of histone acetylation in a cell is determined by the balance of histone acetyltransferases and histone deacetylases. Thus, the increased H3K27ac in *acc1-5* may be due to misregulation of the genes encoding histone acetyltransferases and/or deacetylases. To test this possibility, the transcript levels of 12 genes encoding histone acetyltransferases and 18 genes encoding histone deacetylases were measured and no significant difference was detected in the transcript levels of these genes between the *acc1-5* mutant and WT plants (Figure 22). Next, to examine whether the activities of existing acetyltransferases are required for the hyperacetylation of H3K27 in *acc1-5*, α -methylene- γ -butyrolactone (MB-3), an inhibitor of histone acetyltransferase which is designed to compete with acetyl-CoA to interact with GNAT family acetyltransferases (Biel et al., 2004; Malapeira et al., 2012), was applied to *acc1-5* mutant and found that the increased H3K27ac in *acc1-5* (mock group) were restored to WT level on all the selected genes in *acc1-5* MB-3 (treated group) (Figure 23). This result suggests that the activity of acetyltransferase is required for the increased H3K27ac in *acc1-5*.

Since 12 putative HATs have been found in *Arabidopsis* (Figure 1), it is interesting to know which acetyltransferases are involved in the hyperacetylation of H3K27 driven by increased acetyl-CoA. According to previous studies, GCN5/HAG1 in the GNAT family and members of the CBP/p300 family, show H3K27ac activity (Benhamed et al., 2006; Tie et al., 2009). In the CBP/p300 family, *HAC4* is likely to be an expressed pseudogene that lacks HAT function (Earley et al., 2007) and the HAT domain of *HAC2* was shown to lack HAT activity (Bordoli et al., 2001). So, three HATs (*HAC1*, *HAC5*, and *HAC12*) of the CBP/p300 family and *GCN5* are the potential HATs which may be involved in hyperacetylation of H3K27 in *acc1-5*. Based on a previous study (Han et al., 2007), the corresponding null alleles of *HAC1*, *HAC5*, and *HAC12* were ordered from ABRC. For *GCN5*, a new T-DNA line (*gcn5*) was ordered from ABRC (Figure 24a), since all the published mutant lines are not in the Col-0 background (Bertrand et al., 2003; Vlachonasios et al., 2003; Benhamed et al., 2006). Similar to the published phenotypes of *GCN5* mutants, homozygous *gcn5* plants show dwarf stature, small leaves, short roots,

Figure 22: Transcript levels of genes encoding histone acetyltransferases and deacetylases

a: qRT-PCR analysis of the transcript levels of the 12 histone acetyltransferase genes in *Arabidopsis*. Expression levels are relative to the expression of *ACT7*. Mean \pm SD; n=3 two-tailed Student t-test.

b: qRT-PCR analysis of the transcript levels of the 18 histone deacetylases genes in *Arabidopsis*. Expression levels are relative to the expression of *ACT7*. Mean \pm SD; n=3 two-tailed Student t-test.

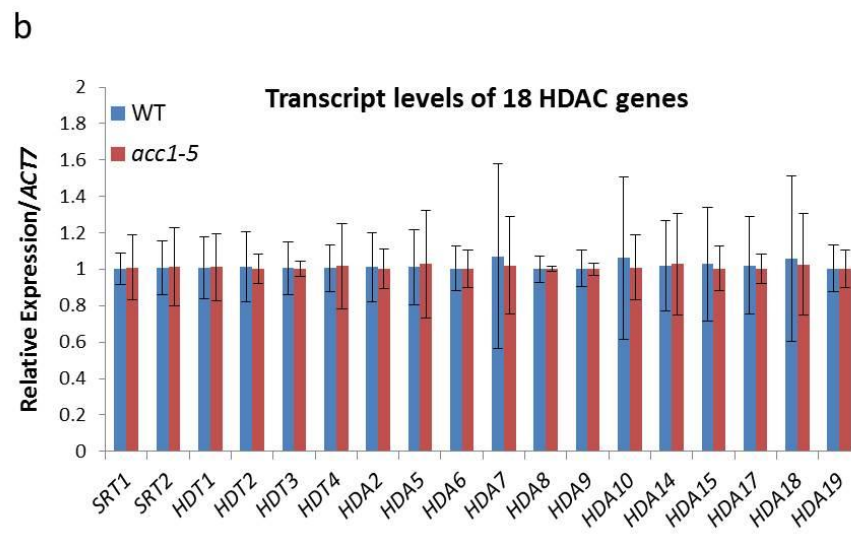
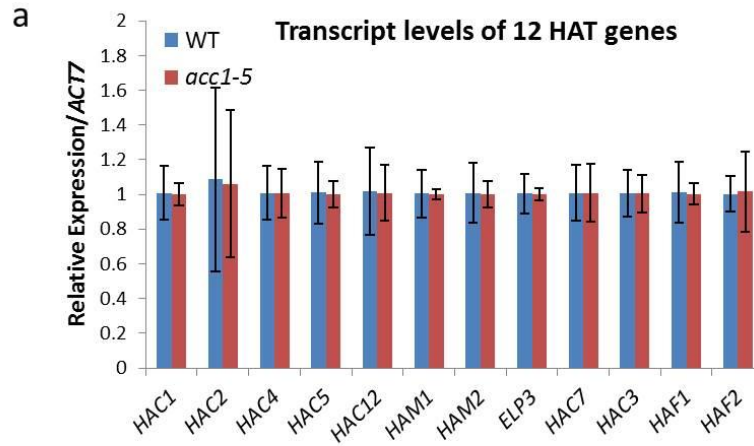


Figure 23: Histone acetyltransferases activity is required for increased H3K27ac in *acc1* mutant

The occupancies of H3K27ac at 8 different regions before and after treating with MB-3 (acetyl-transferases inhibitor). Seedlings were germinated in ½ MS medium for 3 days and then transferred into mediums absence or in the presence of 100 µM MB-3 for 9 days. The H3K27ac levels were normalized with histone H3 at each genomic region. Mean ± SD; n = 3. Lowercase letters indicate significant differences between genetic backgrounds, as determined by the post hoc Tukey's HSD test. $p < 0.01$

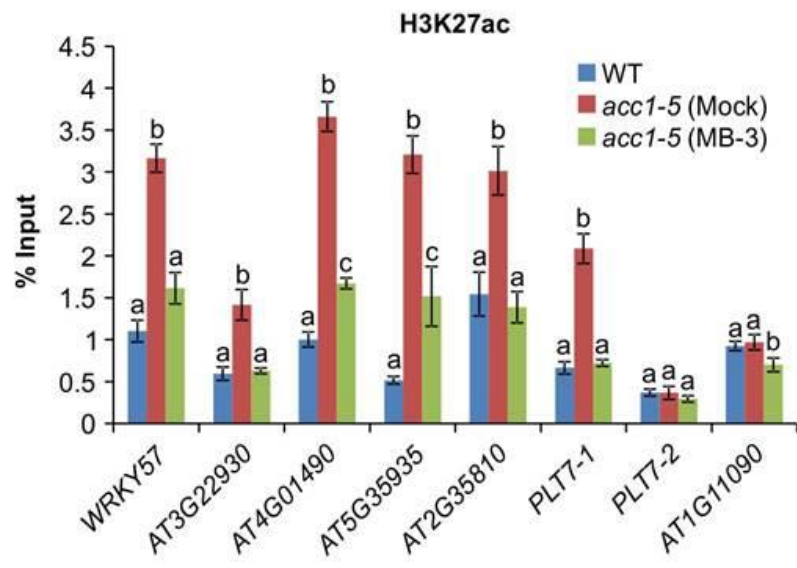
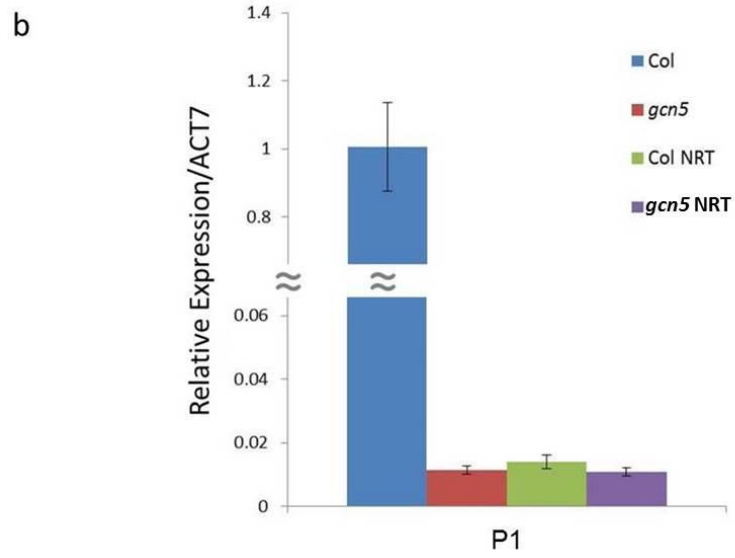
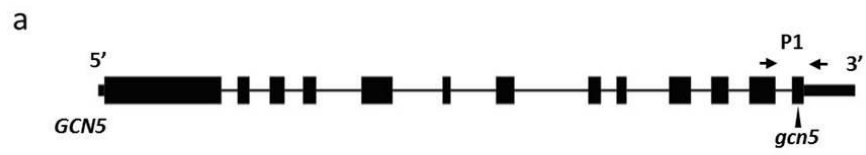


Figure 24: *GCN5* gene structure and expression in Col (WT) and *gcn5* mutant

a: A diagram showing the gene structure of *GCN5*. Black boxes: exons; lines: introns; small rectangle: untranslated regions; arrows indicate the forward and reverse primers for qPCR; triangle indicates the T-DNA insertion site of *gcn5* mutant.

b: Transcript levels of *GCN5* in WT and *gcn5* mutant. NRT represents non-reverse transcription template, as negative controls. Expression levels are relative to the expression of *ACT7*. Mean \pm SD; n=3 two-tailed Student t-test.



deformed flowers and infertility (Bertrand et al., 2003; Vlachonasios et al., 2003). I examined the *GCN5* transcript level in *gcn5* by qRT-PCR and found no significant difference relative to the negative controls (Figure 24b) (non-reverse transcription template serves as negative controls). So, I conclude that the new *gcn5* mutant is a null allele of *GCN5* in the *Col-0* background. Then, I examined the H3K27ac levels in *gcn5* and other HAT mutants by Western blot analysis. As shown in Figure 25a, only *gcn5* showed a dramatic decrease of the H3K27ac level compared to other genetic backgrounds. To examine whether GCN5 is involved in the hyperacetylation of H3K27ac in *acc1-5*, *acc1-5 gcn5* double mutants were generated by crossing heterozygous *acc1-5* plants with heterozygous *gcn5* plants. As shown in Figure 25b, *acc1-5 gcn5* double mutant exhibits less leaf fusion than that in *acc1-5*, which suggests that depleting *GCN5* can suppress the *acc1-5* leaf fusion phenotype. To examine whether the elevated H3K27ac level in *acc1-5* is also suppressed in *acc1-5 gcn5*, I compared the enrichment of H3K27ac in *acc1-5* and *acc1-5 gcn5* by performing ChIP-qPCR. As shown in Figure 25c, the H3K27ac levels at five out of six genes were significantly decreased compared to that in *acc1-5*. Those results suggest that GCN5 is involved in the sensing of acetyl-CoA abundance changes and the hyperacetylation of H3K27 on some genomic regions in *Arabidopsis*.

3.6 Global profiling of transcripts in *acc1-5*

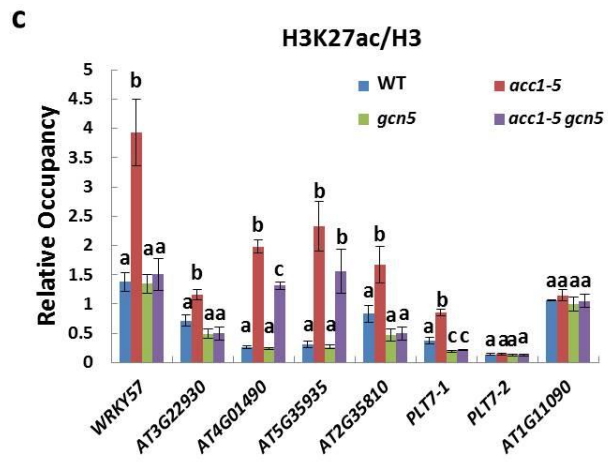
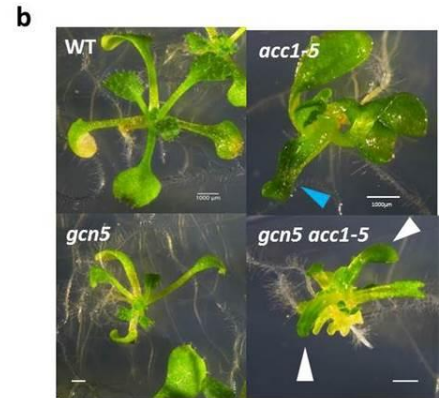
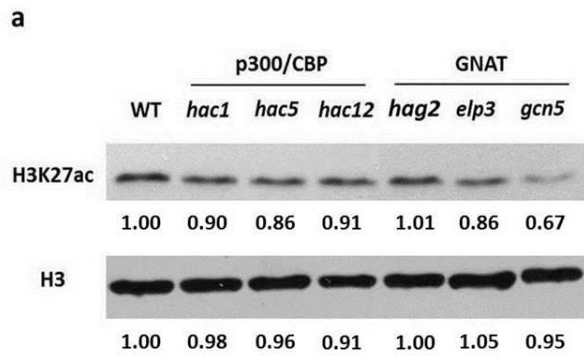
Histone modifications can regulate chromatin structures and thereby activate or repress transcription (Kurdistani and Grunstein, 2003). To assess the effect of the increased H3K27ac on global gene transcription, I performed an RNA sequencing (RNA-seq) analysis using WT and *acc1-5* plants. In total, 1,859 genes in *acc1-5* showed at least 2 fold changes ($p < 0.001$) compared to the RNA levels in WT. Among the 1,859 genes, 1,298 genes were upregulated and 561 genes were downregulated in *acc1-5*. This result suggests that the mutation in *acc1-5* has strong effects on gene activation rather than repression. As described earlier, 802 genes were hyperacetylated at H3K27 in *acc1-5*. It is interesting to know whether the hyperacetylation impacts those genes' expression. To answer this question, the transcription levels of the 802 genes in WT and *acc1-5* were

Figure 25: GCN5 is involved in hyperacetylation of H3K27 in *acc1-5*

a: Western blot analysis of total protein extracts from indicated genetic backgrounds, probed with anti-H3K27ac and anti-H3 antibodies. In all the tested genetic backgrounds, HAC1, HAC5, and HAC12 belong to CBP/p300 family and HAT1, ELP3 and GCN5 belong to GNAT family. Three independent extracts were performed for all the samples and one representative immunoblotting image is presented. The intensities of blotting signals were quantified by using ImageJ software and the average intensities from three independent extracts were shown.

b: 14 DAG seedlings from the indicated genetic backgrounds. The *gcn5* mutant shown dwarf stature, long petioles, and small leaves compared to WT. Compared to *acc1-5*, the double mutant of *gcn5 acc1-5* shown less leaf fusion and smaller leaves. White arrows indicate small leaves in the *gcn5 acc1-5* double mutant. Blue arrow indicates the fused leaves in the *acc1-5* mutant. Bar= 1mm.

c: The enrichment of H3K27ac at 8 genomic regions in Col (WT), *acc1-5*, *gcn5* and *acc1-5 gcn5*. *PLT7-2* and *AT1G11090* are used as control loci: *PLT7-2* represents a locus without H3K27ac enrichment and *AT1G11090* is a region with the same enrichment level of H3K27ac in all the 4 genetic backgrounds. Mean \pm SD; n=3. Lowercase letters indicate significant differences between genetic backgrounds, as determined by the post hoc Tukey's HSD test. $p < 0.01$

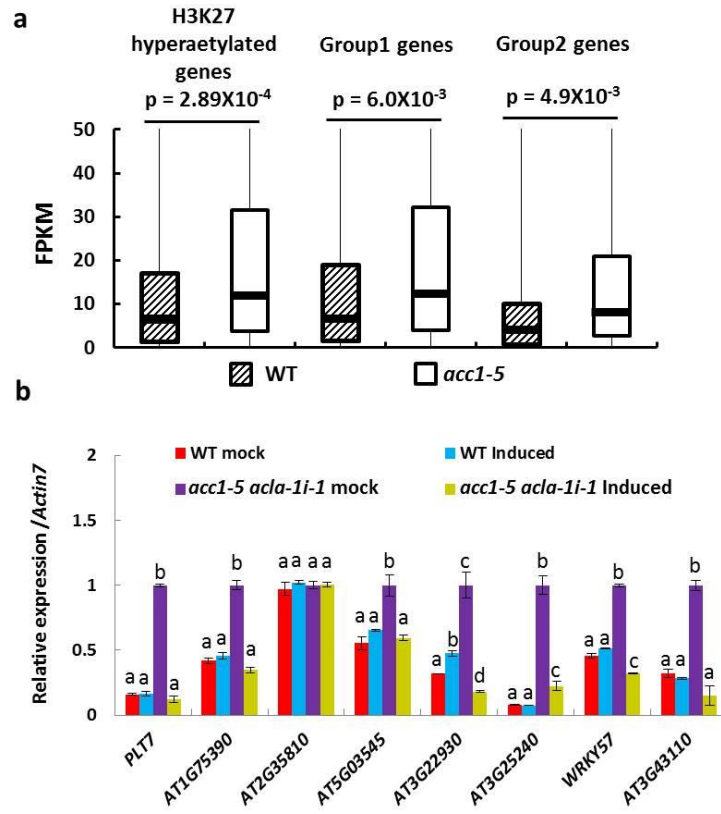


compared. As shown in Figure 26a, expression of the 802 genes that were hyperacetylated at H3K27 in *acc1-5* was significantly increased in *acc1-5* compare to that in WT. Significant increases in expression levels were also found in both subgroups (Figure 26a) (group 1 with only H3K27ac and group 2 with both H3K27ac and H3K27me3). To validate the RNA- seq data, I examined the expression levels of the selected genes in WT and *acc1-5* by performing qRT-PCR. As shown in Figure 26b, the transcript levels were significantly increased in *acc1-5* in 7 out of the 8 selected genes. Since the level of H3K27ac is associated with elevation of cytosolic acetyl-CoA, it is of interest to know whether the increase of expression in *acc1-5* was also associated to acetyl-CoA level. To test the possibility, I took advantage of the *acc1-5 acla-li-1* conditional double mutants and examined the transcript levels of the selected genes. As shown in Figure 25b, repressing *ACLA-1* in the *acc1-5* background by induced microRNA expression (*acc1-5 acla-li-1*) could restore the expression of most of the selected genes to WT levels. Collectively, these data suggest that the increased H3K27ac in *acc1-5* indeed can lead to upregulation of gene expression.

Figure 26: Hyperacetylation of H3K27 activates gene expression in *acc1-5*

a: Box plot of transcript levels of the 802 hyperacetylated genes and the two sub-groups of genes in WT and *acc1-5*. Three biological replicates are included. FPKM: fragments per kilobase of transcript per million mapped reads. Two tail, Mann-Whitney test.

b: The relative transcript levels of selected genes in WT and *acc1-5 acla-li-1* after 24h β -estradiol induction or mock treatment. Mean \pm SD; n = 3. Lowercase letters indicate significant differences between genetic backgrounds, as determined by the post hoc Tukey's HSD test. $p < 0.01$



4 DISCUSSION

4.1 Mutation of *ACC1* disrupts fatty acids elongation and causes accumulation of acetyl-CoA

In plant, as shown in Figure 2, fatty acids are mainly synthesized in the plastid and cytoplasm. After a series of decarboxylative Claisen condensation reactions, the carbon chains of fatty acids can reach up to 18 carbons in plastids. To synthesize fatty acid derivatives such as suberin, cuticle and seed oil, plastid-sourced fatty acids need to be transported into the cytoplasm for further elongation and modification (Fatland et al., 2005). Since acetyl-CoA cannot freely pass through a membrane system (Gut and Verdin, 2013), cytosolic acetyl-CoA serves as the only carbon source to elongate the carbon chain of fatty acids (Fatland et al., 2005). The limiting step of fatty acid elongation is the conversion of acetyl-CoA to malonyl-CoA which is catalyzed by ACC1. Previous studies reported that knocking out *ACC1* can dramatically decrease the levels of VLCFAs and its derivatives (Baud et al., 2003; Baud et al., 2004; Roudier et al., 2010; Lu et al., 2011b). In addition to a decrease of VLCFAs, in this work, I report that knocking out *ACC1* can also lead to an increased level of acetyl-CoA (Figure 8). Additionally, to fuel and maintain the cytosolic acetyl-CoA pool, ACL can directly cleave citrate to oxaloacetic acid and acetyl-CoA, which is currently considered as the only source of cytosolic acetyl-CoA (Fatland et al., 2005; Gut and Verdin, 2013). Dysfunctional ACL can reduce the production of cytosolic acetyl-CoA, but also impair biosynthesis of VLCFAs. The data from my conditional double mutant (*acc1-5 acla-1i*) suggest that accumulated acetyl-CoA depends on the activity of ACL rather than any shortage of VLCFAs in *acc1* (Figure 12a and 12b).

In addition to fatty acid elongation, cytosolic acetyl-CoA also can be consumed for isoprenoids synthesis (Jin et al., 2012). A previous study showed that mutants with defects in the fatty acid elongation pathway including *acc1* can accumulate a high level of cytokinin in *Arabidopsis* (Nobusawa et al., 2013). This increased cytokinin may be partially due to the accumulated acetyl-CoA channeled into the synthesis of isoprenoids. In the future, it will be interesting to investigate how to maintain the balance of acetyl-CoA utilization between isoprenoid synthesis and fatty acid elongation.

Furthermore, cytosolic acetyl-CoA can be carboxylated to malonyl-CoA by ACC1. Other than the elongation of fatty acid chains, malonyl-CoA is also involved in the biosynthesis of flavonoids, which belong to a major class of secondary plant metabolites. Flavonoids have a variety of functions ranging from flower and fruit pigmentation to regulation of polar transport of the phytohormone auxin and responses to biotic and abiotic stresses such as drought, cold and high light intensity (Winkel-Shirley, 2002; Buer et al., 2010; Martens et al., 2010; Tohge et al., 2011; Nakabayashi et al., 2014). Among these abiotic stresses, freezing tolerance has been linked to lipid compositions of the cell membrane (Uemura et al., 1995; Moellering et al., 2010). Previously, it was reported that mutation of *ACCI* can cause freezing sensitivity as it caused a shortage of cuticle after disrupting VLCFAs (Amid et al., 2012). A recent work reports that flavonoids serve as determinants of freezing tolerance and cold acclimation in *Arabidopsis* (Schulz et al., 2016). Thus, this evidence suggests that the shortage of flavonoids in *acc1* mutants may also contribute the freezing sensitivity.

4.2 Cytosolic acetyl-CoA promotes H3K27ac in *Arabidopsis*

Recent studies in animal and yeast cells have demonstrated that there is a dynamic interplay between metabolic processes and gene expression through the modification of chromatin (Wellen et al., 2009; Cai et al., 2011; Shyh-Chang et al., 2013; Lee et al., 2014). Acetyl-CoA can not only serve as a central metabolic intermediate but also provide the acetyl group for posttranslational protein acetylation, thereby regulating enzymatic activities and chromatin structures (Pietrocola et al., 2015; Shen et al., 2015). Knockdown of cytosolic ACCase in yeast and mouse hepatocytes caused the hyperacetylation of histones and extramitochondrial proteins, respectively (Galdieri and Vancura, 2012; Chow et al., 2014). In contrast, knockdown of ACL led to hypoacetylation of histone H2B, H3 and H4 in mammalian cells (Wellen et al., 2009). However, the relationship between cytosolic acetyl-CoA and histone acetylation has not been reported in plants. My study has filled a major gap in understanding whether and how cytosolic acetyl-CoA levels can affect histone acetylation in plants. Genome-wide histone acetylation profiling and transcriptomic data demonstrated that increased cytosolic acetyl-CoA in *acc1* mutants contributes to gene activation by promoting histone

hyperacetylation predominantly at lysine 27 of H3. In plants, lysine 27 of H3 appears to be more sensitive to the increased concentration of acetyl-CoA than other lysine residues of histone tails. This is different from yeast and mammalian cells, where multiple lysine residues of histone tails can be hyperacetylated when there is an increase in the level of cytosolic acetyl-CoA or the ratio of acetyl-CoA/CoA (Wellen et al., 2009; Cai et al., 2011; Galdieri and Vancura, 2012).

Lysine acetylation is normally catalyzed by acetyltransferases using acetyl-CoA as a substrate. In addition to this well-established enzyme-catalyzed acetylation, however, some acetylation may result from the direct contact of proteins with acetyl-CoA (Guan and Xiong, 2011; Hirschey et al., 2011). The reaction rate of acetyl-CoA to lysine side chains in the so-called “non-enzymatic acetylation” would be increased when acetyl-CoA level increase (Paik et al., 1970; Wagner and Payne, 2013). In addition to the direct contact between acetyl-CoA and proteins, acetylation can also be regulated by pH of subcellular environments such as the alkaline condition of the mitochondrial matrix which promotes acetylation (Wagner and Hirschey, 2014; Olia et al., 2015). In addition, acetylation especially histone acetylation is also involved in regulating intracellular pH (pH(i)). As pH(i) decreases, histones can be deacetylated by HDACs, and the released acetate anions are co-exported with protons out of the cell by monocarboxylate transporters (MCTs), preventing further reductions in pH(i) (McBrian et al., 2013). Owing to the very large amounts of acetate stored on histones, histone acetylation has been proposed to function as a pH(i) buffer (McBrian et al., 2013). However, in *acc1-5*, it appears that nonenzymatic acetylation may not contribute significantly to the hyperacetylation of H3K27. First, I observed an elevation of acetylation only at specific lysine residues (H3K27ac), while a non-enzymatic reaction would be non-specific in choosing lysine residues and thus a global hyperacetylation at multiple lysine residues would be expected. Second, when the activities of acetyltransferases were inhibited pharmacologically in *acc1* mutants, acetylation levels were restored to WT level (Figure 23), indicating the involvement of acetyltransferases.

The unexpected preference towards H3K27ac might be due to the potentially different affinities of histone acetyltransferases to the fluctuation of cytosolic acetyl-CoA levels

and the specificities of histone acetyltransferases. My genetic studies indicate that GCN5 may be one of the key HATs to promote H3K27ac at specific genomic regions in *acc1* (Figure 25a). This finding is consistent with the observation of a previous study that GCN5 promotes H3K27ac on light responsive genes (Benhamed et al., 2006). Interestingly, the decreased H3K27ac was mainly (five of six tested genomic regions) detected between *acc1* and *acc1 gcn5* but not between WT and *gcn5* (Figure 25c). This observation suggests that GCN5 is not responsible for *de novo* deposition of H3K27ac at some of the selected genes. However, the fluctuation of acetyl-CoA levels can be sensed by GCN5 and then it catalyzes H3K27ac at ectopic locations. In the future, the global occupancy of H3K27ac in *acc1-5* and *acc1-5 gcn5* should be examined to assess the genome-wide contribution of GCN5 to hyperacetylation of H3K27 in *acc1-5*.

In addition to GCN5, it has been reported that CBP/p300 proteins can mediate H3K27ac in *Drosophila* (Tie et al., 2009). In *Arabidopsis*, the CBP/p300 family contains five proteins and three of them can acetylate multiple lysine residues at H3 *in vitro* (Earley et al., 2007). This family of proteins is involved in the regulation of flowering time by affecting the expression of *FLC* (Han et al., 2007). However, there were no marked changes in H3K27ac levels after knocking out each member of the CBP/p300 family (Figure 25a). This result may be due to the potential redundancy among the *Arabidopsis* family members (Han et al., 2007). Therefore, in the future, the linkage of CBP/p300 activity and hyperacetylation of H3K27 in *acc1-5* can be examined by generating high order mutants of CBP/p300 genes in the *acc1* background. In addition, while HAM1 and HAM2 only show specificity on H4K5ac *in vitro* and *in vivo* (Earley et al., 2007; Xiao et al., 2013), it has been reported in animal cells that the concentration of acetyl-CoA not only determines the enzymatic activity of lysine acetyltransferases but also alters their specificity (Henry et al., 2013; 2015). In animal cells, although both CBP and p300 acetylate H3K14, H3K18, H3K23 in steady-state experiments with limiting H3, the specificities of p300 are up to 10^{10} -fold higher than CBP (Henry et al., 2013). Utilizing a histone tetramer as a substrate, both enzymes can also acetylate H4K5, H4K8, H4K12, and H4K16 *in vitro* (Henry et al., 2013). With limiting acetyl-CoA, p300 has the highest specificity at H4K16, where specificity is 10^{18} -fold higher than CBP (Henry et al., 2013). If the substrate concentration dependent specificity can also be demonstrated to be true *in*

in vivo, in the future, HAM1 and HAM2 also need to be examined for their potential contribution to the H3K27 hyperacetylation in *acc1*. Thus, further investigations are needed to determine how H3K27 becomes the preferred substrate for acetylation in response to the changes of cytosolic acetyl-CoA in *Arabidopsis*.

A recent study reported that treatment with the physiological donor of nitric oxide (NO) S-nitroso-glutathione (GSNO) increases the abundance of histone H3 acetylation at K9 and K14 in *Arabidopsis* (Mengel et al., 2016). This increase is triggered by NO-dependent inhibition of HDAC activity (Mengel et al., 2016). In animals, NO also participates in the regulation of histone acetylation by targeting and modifying several HDACs (Illi et al., 2008; Berghella and Puri, 2014). This evidence suggests that histone acetylation can respond dynamically to the changes of different cellular metabolites. In the *acc1* mutant, hyperacetylated genes are enriched in the biosynthesis of primary metabolites and nitrogen compounds (Figure 14d and 21a). It suggests that other metabolites, in addition to acetyl-CoA, may also have been changed in the *acc1* mutant and contribute to the hyperacetylation of H3K27 in the *acc1* mutant.

In addition to histone acetylation, the acetylation status of non-histone proteins may also be regulated during the fluctuation of acetyl-CoA levels. An example of non-histone protein acetylation is SPT6P, a component of the SAGA (Spt-Ada-Gcn5-acetyltransferase) transcriptional coactivator complex in yeast (Grant et al., 1997; Cai et al., 2011). Under limiting growth conditions, acetyl-CoA levels oscillate dynamically (Cai et al., 2011). The acetylation state of SPT6P is associated with the acetyl-CoA level. And, in turn, acetylated SPT6P can activate the SAGA complex and regulate gene expression by promoting histone acetylation (Bach et al., 2011). So, the acetylation specificity of HATs may also be determined by the acetylation of non-histone proteins. To test this possibility, in the future, the complete set of acetylated proteins (acetylome) in WT and *acc1-5* should be profiled and compared. It is expected that such a study would provide a global view of acetyl-CoA's impact on protein acetylation and its role in plant growth and development.

4.3 Interplay between H3K27ac and H3K27me3

As acetylation and trimethylation of the same lysine residues are mutually exclusive, H3K27ac has been proposed to prevent the deposition of H3K27me3 catalyzed by PRC2 and thereby antagonize polycomb-mediated silencing (Tie et al., 2009). The profiles of H3K27ac and H3K27me3 are dynamic and complementary during plant development (Charron et al., 2009; Tie et al., 2009; Jang et al., 2011). My data show that, on a genome-wide scale, H3K27ac and H3K27me3 are mainly enriched at different genes, which is consistent with the notion that H3K27ac and H3K27me3 are mutually exclusive (Tie et al., 2009). Furthermore, my data also show that the decreased deposition of H3K27me3 is accompanied with elevated H3K27ac around the TSSs in *acc1-5* (Figure 18b and 18c). This suggests that the availability of acetyl-CoA may alter the genome-wide distribution of H3K27me3 by affecting the occupancy of H3K27ac. Also, this H3K27me3-H3K27ac co-marking of genes is reminiscent of the “bivalent” genes modified by both H3K27me3 and H3K4me3 (Sachs et al., 2013). The bivalency is thought to enable the cells to respond in a timely way to developmental and environmental cues. It

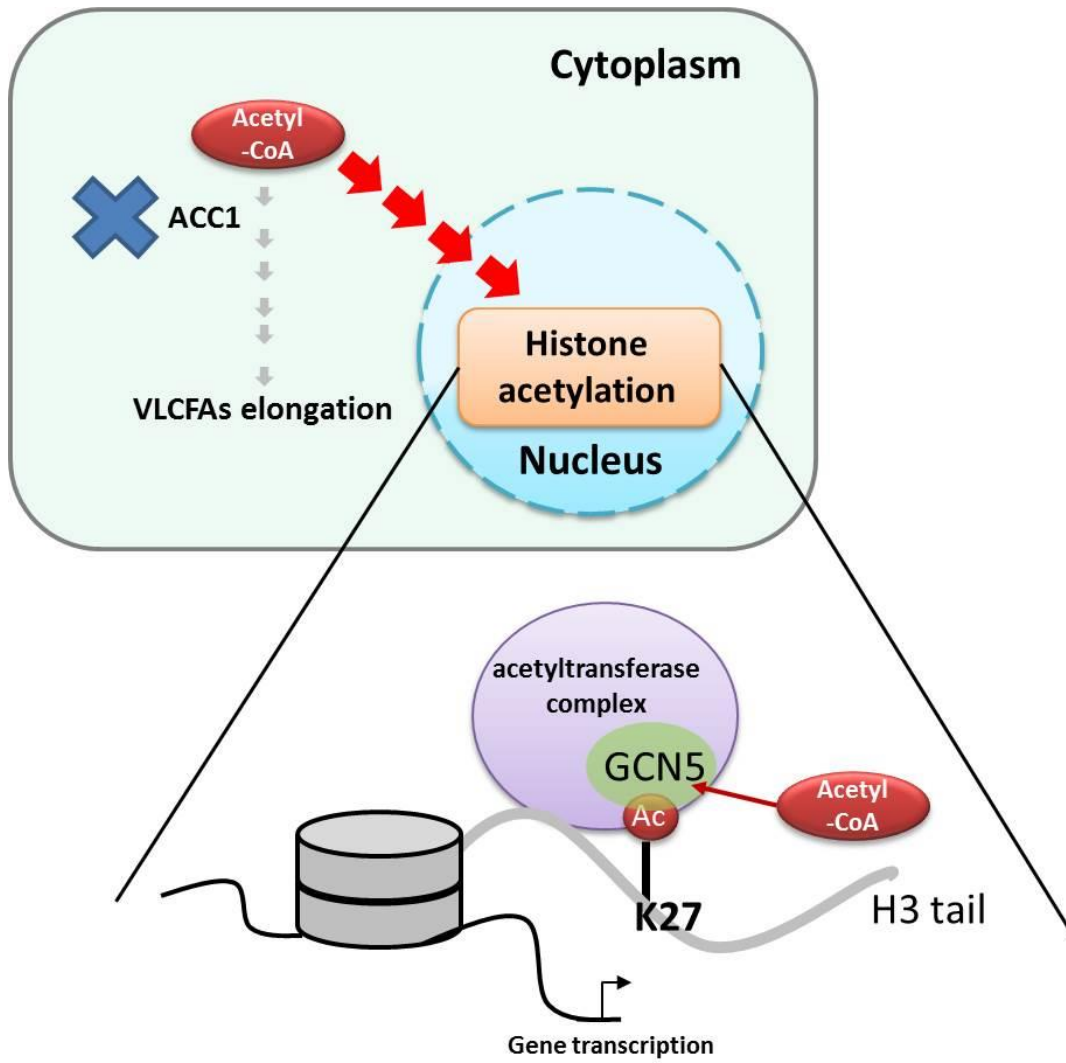
is thus tempting to speculate that the H3K27me3-H3K27ac pair plays a similar role as the “bivalent” genes at their targets (Sachs et al., 2013). However, it is worth pointing out that co-marking of H3K27me3 and H3K4me3 happens at different lysine residues of H3 tail. In my study, co-occupancy of H3K27me3 and H3K27ac was observed, but it is not clear whether the two modifications occur at two different H3 molecules in the same nucleosome. In the future, a ChIP-reChIP assay could be performed to find out whether both H3K27ac and H3K27me3 signals can be detected simultaneously at the same genomic regions or not.

4.4 Concluding remarks and perspectives

In summary, my work presented in this thesis establishes a link between metabolic signals (acetyl-CoA) and epigenetic marks (H3K27ac) that control gene regulation (Figure 27) in plants. Nuclei contain the majority of the genetic information in a cell and control most of the cellular functions through gene products, either transcripts or proteins.

Figure 27: A model showing how cytosolic acetyl-CoA affects H3K27ac in *Arabidopsis*

In plant cells, cytosolic acetyl-CoA can be consumed for biosynthesis of VLCFAs and histone acetylation in the nucleus. VLCFAs biosynthesis is controlled by ACC1, which serves as a rate limiting factor during fatty acids elongation. Knocking out *ACC1* causes shortage of VLCFAs and channels accumulated acetyl-CoA into the nucleus for histone acetylation (red arrow). Specifically, this wave of histone acetylation mainly occurs on histone H3 lysine 27 and requires the presence of GCN5 related acetyltransferase complex. Finally, the hyperacetylation of H3K27 promotes gene transcription.



The involvement of metabolic intermediates, such as acetyl-CoA level, SAM, and NADH, in epigenetic regulation of gene expression provides cells with an effective means for responding to subcellular environmental changes. This cross-talk between nuclei and subcellular environments might be one of the strategies for a cell to gradually adapt to surrounding environments. It seems that the responses of nuclei to the fluctuation of subcellular metabolites can be very specific, as shown by my work: the increased acetyl-CoA due to the disruption of fatty acids elongation affects mainly the acetylation and transcription of genes involved in fatty acids biosynthesis pathways (Figure 14e). Thus, it will be interesting to further explore how nuclei make specialized responses to various cellular changes via sensing the levels of metabolites. Understanding the mechanisms underlying the crosstalk will provide a more detailed picture about how cell and environment communicate with each other.

Appendices

Appendix A: Sequences of primers used

name	sequence
F-ACC1	GGGGACAAGTTTGTACAAAAAAGCAGGCTTCCTATGTTT TGCTATCATTTGCT
R-ACC1	GGGGACCACTTTGTACAAGAAAGCTGGGTCCAACATTTA CAACTGTGACCAA
ACLA-1D-I	GATACTAGAGTGAAAGGAGTCATTCTCTCTTTTGTATTCC
ACLA-1D-II	GAATGACTCCTTTCCTCTAGTATCAAAGAGAATCAATGA
ACLA-1D-III	GAATAACTCCTTTCAGTCTAGTTTTCACAGGTCGTGATATG
ACLA-1D-IV	GAAACTAGACTGAAAGGAGTTATTCTACATATATATTCCT
ACLA-1-A	GGGGACAAGTTTGTACAAAAAAGCAGGCTTCCTGCAAGG CGATTAAGTTGGGTAAC
ACLA-1-B	GGGGACCACTTTGTACAAGAAAGCTGGGTTCGCGGATAAC AATTTACACAGGAAACAG
LP-acc1-6	ACCTATCGTCAGCCAGTGTTTGT
RP-acc1-6	GCATCTTGCAGTTTTGCTTTCAG
LP-HAC1	CCGCATAGTATGGCTTCAGAC
RP-HAC1	GACTGACAGGTCTTTGCTTGG
LP-HAC5	ATGATCGTTCTTTGGCAAGTG
RP-HAC5	TTTGCTCGTATCCACCATAGG
LP-HAC12	AATTAATCAACCCGAGGTTCC
RP-HAC12	TTGATACAAGGCAAGCATTCC
LP-GCN5	GCTGTGGGCTAAGGGTTTATC

RP-GCN5	AGCGTAAGCGTGAGTGTAAGC
LBb1.3	ATTTTGCCGATTTTCGGAAC
qF-ACC1	CTTGGTCCTCCAGCATCTTC
qR-ACC1	CATGGCAGAGTGGGTACATC
qF-Actin7	CTCATGAAGATTCTCACTGAG
qR-Actin7	ACAACAGATAGTTCAATTCCCA
qF-ACLA-1-P1	GAGATCGAGGAGAACTGGGA
qR-ACLA-1-P1	AAGGGAAGAGTTGCGACAAG
qF-ACLA-1-P2	GCAAGTGTCATCTATGCGGA
qR-ACLA-1-P2	GCTTTTTCCATCCGGGTTTG
qF-ACLA-2	ACTCTCTGGTCAAGAATTGCCT
qR-ACLA-2	TTTTGCCACGCTTTCCGAAC
qF-ACLA-3	ATTCGCTCTGCTCAGGTGAC
qR-ACLA-3	CAAACCACTTTTCCCGCGTT
qF-ACLB-1	AGAAGGTGTTCCGGAGTCAG
qR-ACLB-1	ATAGTTCCAGCTGTGTCACCA
qF-ACLB-2	GCTTCCTGTTCAACGAATGCT
qR-ACLB-2	ATAGCGATTTTCCTCCTGCCC
qF-ELO3	ATGCGAGCTATTCGAGCCAG
qR-ELO3	CTCAGCAGGCAGTGACATGA
qF-GCN5	CGCCAGCAAAGAAAGGCAAT
qR-GCN5	ACCAGCTTCCCTTAAGCCAC
qF-HAC7	TTTTCTCCCGCCGATACTGG
qR-HAC7	AAGTCAACTGGCTTCACGCT
qF-HAC4	ATCCGCAGTCTTCGTCAGTG

qR-HAC4	TTCACAGACATGGAGCACCC
qF-HAC5	GCCAGGAGATGCTCAACAGA
qR-HAC5	CCTCCTTTGACGTAGCCGTT
qF-HAC2	TCAAGCGCCTCAAGGAAGAA
qR-HAC2	TCTGTCAGCCGAAAACACGA
qF-HAC1	AATCAGATTCACGGCGCAGA
qR-HAC1	ATGTTAATCCCTGAGCCCCC
qF-HAC12	GCACGTTTCATATTTTCAGGGGA
qR-HAC12	ACAGGCTGGAAACTTGCTGT
qF-HAM1	GCGATACTCGCTCTCACGAA
qR-HAM1	TTTCGGCGCTCGATAACCTT
qF-HAM2	ACTTCTCCCCTTTTCCGCCAG
qR-HAM2	CAGGTGGGTGCTTCAGGTCA
qF-HAF1	TCCGCAGAGATTGCAGTCAA
qR-HAF1	CTTCCATGCGAGGTTCCCTGT
qF-HAF2	TGGGTTGAACACTCTGGTGG
qR-HAF2	GCTGGCAGGCAATGTAAACC
qF-HDA19	GGAAGCACTAAGGTTACAGGAG
qR-HDA19	TTTAGGAGGAAACGCCTGCT
qF-HDA6	CAGTCAAGGGTCACGCTGAT
qR-HDA6	CGGCTCTACTCCAACAGCAA
qF-HDA7	TTGCTGGTGCTATGAGACGG
qR-HDA7	TCTGCCTGTTGGTTGGCAAT
qF-HDA9	TGCGTTCCAAGGACAAAATCT
qR-HDA9	CATCGGGTGATTTCGGACCAA

qF-HDA17	TGGCTTTCTCTATGCTTTTCACA
qR-HDA17	TCCTCCACCTCCTGTAACCA
qF-HDA5	GCGAGGGAATTTAACCCGGA
qR-HDA5	TCCATCAGTTCAACACCAACCT
qF-HDA8	TGGTTTACCGGTCTTCCAGC
qR-HDA8	CTGCGGCAATTTACACACCTT
qF-HDA15	GATGGTCCACACTTCAGAGCA
qR-HDA15	GCTAGATCAGCGCACAAACC
qF-HDA18	CGCATGTGTCCAAGTTTTGC
qR-HDA18	TCATTAGACGCCATTGACGC
qF-HDA2	GGGTTTTGTGCTTTCGCTGA
qR-HDA2	GCCGAGATCTGTTTCATGGC
qF-HDA14	CCTAAGTTCCGTGGCTCACA
qR-HDA14	TGAAGCCTCATCCATTGCCT
qF-HDA10	GGACATGCTGAATGTGGAGGAT
qR-HDA10	CAAAGAAAAATCCGGCGCAA
qF-HDT1	ACGTTTCTCAGGCATCGCTT
qR-HDT1	GCTGAGGGATGTTCTCAGTCG
qF-HDT2	AATCCCCAACATCGAGCAG
qR-HDT2	CCTTTGGCTTTGTGTCAGCC
qF-HDT3	TGGAGTTCTGGGGTGTGGAAG
qR-HDT3	GATGTGCACGAGCCTGTCTA
qF-HDT4	ACAAATTGCTGCTTTGCCTCA
qR-HDT4	CCTCGTCCAAACCCATCTCA
qF-SRT1	GCGGAGAAGCACTGCAAAAA

qR-SRT1	TGCCTCCACCTTTGAGACAC
qF-SRT2	TCAAACCAATTACCCATCAGGAGT
qR-SRT2	ATGAGCTGGTCCTGGTTGTG
qF-AT1G75390	GAAAACGCTCAGATCGTCGC
qR-AT1G75390	GTCGTTCTCCGCCTCGATAG
qF-AT2G35810	TGTCAAGTCAACGATGGCGA
qR-AT2G35810	CTCTGCGAAGGTCTCAGGTG
qF-AT5G03545	CCTTTGGCAAGCTTCGGTTC
qR-AT5G03545	CCGGAAACAAAGTAAACACGGA
qF-AT3G25240	GTTTTGAGAGCCGTGGAGGT
qR-AT3G25240	GTGACCAAGCTCTCGCAGAA
qF-AT3G43110	AAACCACAAGCGACAAAGGC
qR-AT3G43110	CGGTTAGCTTCCCCTTCGTT
F-WRKY57	TCCACCACTCCTCCGATCAT
R-WRKY57	GGTAGGTTTGACTCCGGTGG
F-AT2G22390	GGATCAGAACCCTACCGAGC
R-AT2G22390	AAATTCGATGGTGCCGTTGC
F-AT4G01490	ATCTTCAAGGATCGCCTCAGC
R-AT4G01490	TTGCTGCAGAGGTCCGATATG
F-AT5G35390	TGAGGTAAAGAGCCGCTGAA
R-AT5G35390	AGGGTTTTCTTTGGCTCCGAT
F-AT2G35810	GCGTTTAAATTCCACATCTTTGACG
R-AT2G35810	TTTTGGAACCAACCAACACA
F-PLT7-1	TTGCCGAAGGAGTTACAGGG
R-PLT7-1	CGTCGTTGATGACTCCACCA

F-PLT7-2	TTTTTCATCACAAGGGTGCCG
R-PLT7-2	CAGGCATCAGCATTGGGGTC
F-AT1G11090	TCAGATGGGTTTCGCTTGCT
R-AT1G11090	CTACGGAGGGAACATAGGCG
F-AT2G41660	ATGTCAACGGCAACTCTCGT
R-AT2G41660	CTCCCGTTGCAGTACATCGT
F-AT5G61410	GCCAACCGTTTGAGATAGCG
R-AT5G61410	GCCACGTGTGATTACGGTCT
F-Actin7	CGTTTCGCTTTCCTTAGTGTTAGCT
R-Actin7	AGCGAACGGATCTAGAGACTCACCTTG

Appendix B: Accession number and corresponding protein

Accession Number	Protein name
AT1G36160	ACC1
AT1G36170	ACC2
AT1G10670	ACLA-1
AT1G60810	ACLA-2
AT1G09430	ACLA-3
AT3G06650	ACLB-1
AT5G49460	ACLB-2
AT5G09810	ACT7
AT1G34050	ankyrin repeat family protein
AT3G22930	calmodulin-like protein
AT5G35935	copla-like retrotransposon
AT1G79000	HAC1
AT1G16710	HAC12
AT1G67220	HAC2
AT1G55970	HAC4
AT3G12980	HAC5
AT1G32750	HAF1
AT3G19040	HAF2
AT3G54610	HAG1
AT5G56740	HAG2
AT5G50320	HAG3
AT5G64610	HAM1
AT5G09740	HAM2

AT3G44660	HDA10
AT4G33470	HDA14
AT3G18520	HDA15
AT3G44490	HDA17
AT5G26040	HDA2
AT5G61060	HDA5
AT5G63110	HDA6
AT5G35600	HDA7
AT1G08460	HDA8
AT3G44680	HDA9
AT3G44750	HDT1
AT5G22650	HDT2
At5G03740	HDT3
AT2G27840	HDT4
AT1G35890	no apical meristem domain transcriptional factor
AT4G01490	non-LTR retrotransposon
AT5G65510	PLT7
AT5G61410	ribulose-5-phosphate-3-epimerase
AT1G11090	serine hydrolase
AT5G55760	SRT1
AT5G09230	SRT2
AT2G35810	unknown protein
AT1G69310	WRKY57

Appendix C: The reads information for all the ChIP-seq samples

	Total reads	mapped reads	unique mapped reads
WT H3K9ac-1	21,130,604	20,714,751	17,080,557
WT H3K9ac-2	33,981,379	27,813,947	924,781
WT H3K14ac-1	22,050,957	21,417,832	17,840,278
WT H3K14ac-2	10,003,523	8,599,774	291,210
WT H3K18ac-1	20,670,993	20,400,022	15,039,492
WT H3K18ac-2	24,509,546	23,870,324	14,578,845
WT H3K27ac-1	11,340,704	8,788,287	5,362,068
WT H3K27ac-2	6,799,442	6,025,768	3,601,419
WT H4K5ac-1	21,757,372	21,419,668	18,208,806
WT H4K5ac-2	34,722,815	32,701,966	1,013,378
WT H4K8ac-1	26,151,639	22,681,729	18,899,263
WT H4K8ac-2	35,459,661	31,484,992	1,391,083
WT H4K12ac-1	24,217,982	23,063,706	19,628,541
WT H4K12ac-2	19,436,683	18,367,166	2,111,851
WT H4K16ac-1	22,885,573	20,592,870	17,577,184
WT H4K16ac-2	14,754,957	13,026,326	1,184,177
WT input	9,770,789	9,182,326	5,529,824
<i>acc1-5</i> H3K9ac-1	22,036,665	21,095,923	17,455,404
<i>acc1-5</i> H3K9ac-2	31,393,011	26,626,714	1,008,898
<i>acc1-5</i> H3K14ac-1	21,566,673	20,360,930	18,440,037
<i>acc1-5</i> H3K14ac-2	31,910,832	18,622,321	842,081
<i>acc1-5</i> H3K18ac-1	20,238,468	19,252,492	17,059,685

<i>acc1-5</i> H3K18ac-2	25,208,402	24,526,450	15,386,323
<i>acc1-5</i> H3K27ac-1	13,982,685	11,285,915	5,595,884
<i>acc1-5</i> H3K27ac-2	14,411,629	11,911,069	6,764,021
<i>acc1-5</i> H4K5ac-1	24,507,295	23,289,333	19,851,552
<i>acc1-5</i> H4K5ac-2	36,863,086	34,271,193	1,716,691
<i>acc1-5</i> H4K8ac-1	23,211,254	17,618,669	15,171,767
<i>acc1-5</i> H4K8ac-2	28,920,997	25,808,668	1,913,369
<i>acc1-5</i> H4K12ac-1	26,530,627	24,272,537	20,629,740
<i>acc1-5</i> H4K12ac-2	20,755,388	19,333,000	1,824,613
<i>acc1-5</i> H4K16ac-1	21,898,464	19,934,039	17,134,367
<i>acc1-5</i> H4K16ac-2	17,871,224	14,682,263	1,262,860
<i>acc1-5</i> input	11,629,953	10,811,280	6,389,406
<i>acc1-5 acla-1-li</i> mock H3K27ac -1	13,610,689	10,603,637	5,062,115
<i>acc1-5 acla-1-li</i> mock H3K27ac -2	15,088,054	11,276,218	5,694,189
<i>acc1-5 acla-1-li</i> induced H3K27ac -1	14,516,502	13,231,847	8,081,749
<i>acc1-5 acla-1-li</i> induced H3K27ac -2	13,632,308	11,791,492	3,729,754
<i>acc1-5 acla-1-li</i> mock input	24,611,729	24,173,526	18,490,188
<i>acc1-5 acla-1-li</i> induced input	25,885,060	18,104,053	13,550,322

References

- Aagaard, L., Schmid, M., Warburton, P., and Jenuwein, T.** (2000). Mitotic phosphorylation of SUV39H1, a novel component of active centromeres, coincides with transient accumulation at mammalian centromeres. *Journal of Cell Science* 113, 817-829.
- Adachi, S., Nobusawa, T., and Umeda, M.** (2009). Quantitative and cell type-specific transcriptional regulation of A-type cyclin-dependent kinase in *Arabidopsis thaliana*. *Developmental Biology* 329, 306-314.
- Alvarez-Venegas, R., Pien, S., Sadler, M., Witmer, X., Grossniklaus, U., and Avramova, Z.** (2003). ATX-1, an *Arabidopsis* homolog of trithorax, activates flower homeotic genes. *Current Biology* 13, 627-637.
- Amid, A., Lytovchenko, A., Fernie, A.R., Warren, G., and Thorlby, G.J.** (2012). The sensitive to freezing3 mutation of *Arabidopsis thaliana* is a cold-sensitive allele of homomeric acetyl-CoA carboxylase that results in cold-induced cuticle deficiencies. *Journal of Experimental Botany* 63, 5289-5299.
- Austin, R.S., Vidaurre, D., Stamatiou, G., Breit, R., Provart, N.J., Bonetta, D., Zhang, J., Fung, P., Gong, Y., Wang, P.W., McCourt, P., and Guttman, D.S.** (2011). Next-generation mapping of *Arabidopsis* genes. *The Plant Journal* 67, 715-725.
- Bach, L., Gissot, L., Marion, J., Tellier, F., Moreau, P., Satiat-Jeunemaitre, B., Palauqui, J.C., Napier, J.A., and Faure, J.D.** (2011). Very-long-chain fatty acids are required for cell plate formation during cytokinesis in *Arabidopsis thaliana*. *Journal of Cell Science* 124, 3223-3234.
- Bach, L., Michaelson, L.V., Haslam, R., Bellec, Y., Gissot, L., Marion, J., Da Costa, M., Boutin, J.P., Miquel, M., Tellier, F., Domergue, F., Markham, J.E., Beaudoin, F., Napier, J.A., and Faure, J.D.** (2008). The very-long-chain hydroxy fatty acyl-CoA dehydratase PASTICCINO2 is essential and limiting for plant development. *Proceedings of the National Academy of Sciences of the United States of America* 105, 14727-14731.
- Baek, S.H.** (2011). When signaling kinases meet histones and histone modifiers in the nucleus. *Molecular Cell* 42, 274-284.
- Baud, S., Guyon, V., Kronenberger, J., Wulleme, S., Miquel, M., Caboche, M., Lepiniec, L., and Rochat, C.** (2003). Multifunctional acetyl-CoA carboxylase 1 is essential for very long chain fatty acid elongation and embryo development in *Arabidopsis*. *The Plant Journal* 33, 75-86.
- Baud, S., Bellec, Y., Miquel, M., Bellini, C., Caboche, M., Lepiniec, L., Faure, J.D., and Rochat, C.** (2004). *gurke* and *pasticcino3* mutants affected in embryo development are impaired in acetyl-CoA carboxylase. *EMBO Report* 5, 515-520.

- Baumbusch, L.O., Thorstensen, T., Krauss, V., Fischer, A., Naumann, K., Assalkhou, R., Schulz, I., Reuter, G., and Aalen, R.B.** (2001). The *Arabidopsis thaliana* genome contains at least 29 active genes encoding SET domain proteins that can be assigned to four evolutionarily conserved classes. *Nucleic Acids Research* 29, 4319-4333.
- Benhamed, M., Bertrand, C., Servet, C., and Zhou, D.X.** (2006). *Arabidopsis* GCN5, HD1, and TAF1/HAF2 interact to regulate histone acetylation required for light-responsive gene expression. *Plant Cell* 18, 2893-2903.
- Berger, S.L.** (2007). The complex language of chromatin regulation during transcription. *Nature* 447, 407-412.
- Berghella, L., and Puri, P.L.** (2014). Nitric oxide and histone acetylation-shaping craniofacial development. *Chemistry and Biology* 21, 565-566.
- Bernatavichute, Y.V., Zhang, X., Cokus, S., Pellegrini, M., and Jacobsen, S.E.** (2008). Genome-wide association of histone H3 lysine nine methylation with CHG DNA methylation in *Arabidopsis thaliana*. *PloS One* 3, e3156.
- Berr, A., Shafiq, S., and Shen, W.H.** (2011). Histone modifications in transcriptional activation during plant development. *Biochimica et Biophysica Acta* 1809, 567-576.
- Bertrand, C., Bergounioux, C., Domenichini, S., Delarue, M., and Zhou, D.X.** (2003). *Arabidopsis* histone acetyltransferase AtGCN5 regulates the floral meristem activity through the WUSCHEL/AGAMOUS pathway. *The Journal of Biological Chemistry* 278, 28246-28251.
- Bertrand, C., Benhamed, M., Li, Y.F., Ayadi, M., Lemonnier, G., Renou, J.P., Delarue, M., and Zhou, D.X.** (2005). *Arabidopsis* HAF2 gene encoding TATA-binding protein (TBP)-associated factor TAF1, is required to integrate light signals to regulate gene expression and growth. *The Journal of Biological Chemistry* 280, 1465-1473.
- Biel, M., Kretsovali, A., Karatzali, E., Papamatheakis, J., and Giannis, A.** (2004). Design, synthesis, and biological evaluation of a small-molecule inhibitor of the histone acetyltransferase Gcn5. *Angewandte Chemie* 43, 3974-3976.
- Bordoli, L., Netsch, M., Luthi, U., Lutz, W., and Eckner, R.** (2001). Plant orthologs of p300/CBP: conservation of a core domain in metazoan p300/CBP acetyltransferase-related proteins. *Nucleic Acids Research* 29, 589-597.
- Boycheva, I., Vassileva, V., and Iantcheva, A.** (2014). Histone acetyltransferases in plant development and plasticity. *Current Genomics* 15, 28-37.
- Bratzel, F., Lopez-Torrejón, G., Koch, M., Del Pozo, J.C., and Calonje, M.** (2010). Keeping cell identity in *Arabidopsis* requires PRC1 RING-finger homologs that catalyze H2A monoubiquitination. *Current biology* 20, 1853-1859.
- Brownell, J.E., and Allis, C.D.** (1996). Special HATs for special occasions: linking histone acetylation to chromatin assembly and gene activation. *Current Opinion in Genetics & Development* 6, 176-184.

- Brundrett, M.C., Kendrick, B., and Peterson, C.A.** (1991). Efficient lipid staining in plant material with sudan red 7B or fluorol yellow 088 in polyethylene glycol-glycerol. *Biotechnic and Histochemistry* 66, 111-116.
- Buer, C.S., Imin, N., and Djordjevic, M.A.** (2010). Flavonoids: new roles for old molecules. *Journal of Integrative Plant Biology* 52, 98-111.
- Cai, L., Sutter, B.M., Li, B., and Tu, B.P.** (2011). Acetyl-CoA induces cell growth and proliferation by promoting the acetylation of histones at growth genes. *Molecular Cell* 42, 426-437.
- Cartagena, J.A., Matsunaga, S., Seki, M., Kurihara, D., Yokoyama, M., Shinozaki, K., Fujimoto, S., Azumi, Y., Uchiyama, S., and Fukui, K.** (2008). The *Arabidopsis* SDG4 contributes to the regulation of pollen tube growth by methylation of histone H3 lysines 4 and 36 in mature pollen. *Developmental Biology* 315, 355-368.
- Chance, B., Estabrook, R.W., and Ghosh, A.** (1964). Damped sinusoidal oscillations of cytoplasmic reduced pyridine nucleotide in yeast cells. *Proceedings of the National Academy of Sciences of the United States of America* 51, 1244-1251.
- Charron, J.B., He, H., Elling, A.A., and Deng, X.W.** (2009). Dynamic landscapes of four histone modifications during deetiolation in *Arabidopsis*. *Plant Cell* 21, 3732-3748.
- Chen, D., Molitor, A., Liu, C., and Shen, W.H.** (2010). The *Arabidopsis* PRC1-like ring-finger proteins are necessary for repression of embryonic traits during vegetative growth. *Cell Research* 20, 1332-1344.
- Chen, Y., Sprung, R., Tang, Y., Ball, H., Sangras, B., Kim, S.C., Falck, J.R., Peng, J., Gu, W., and Zhao, Y.** (2007). Lysine propionylation and butyrylation are novel post-translational modifications in histones. *Molecular & Cellular Proteomics* 6, 812-819.
- Chow, J.D., Lawrence, R.T., Healy, M.E., Dominy, J.E., Liao, J.A., Breen, D.S., Byrne, F.L., Kenwood, B.M., Lackner, C., Okutsu, S., Mas, V.R., Caldwell, S.H., Tomsig, J.L., Cooney, G.J., Puigserver, P.B., Turner, N., James, D.E., Villen, J., and Hoehn, K.L.** (2014). Genetic inhibition of hepatic acetyl-CoA carboxylase activity increases liver fat and alters global protein acetylation. *Molecular Metabolism* 3, 419-431.
- Clarke, J.D.** (2009). Cetyltrimethyl ammonium bromide (CTAB) DNA miniprep for plant DNA isolation. *Cold Spring Harbor Protocols* 2009, 5177.
- Cohen, H.Y., Miller, C., Bitterman, K.J., Wall, N.R., Hekking, B., Kessler, B., Howitz, K.T., Gorospe, M., de Cabo, R., and Sinclair, D.A.** (2004). Calorie restriction promotes mammalian cell survival by inducing the SIRT1 deacetylase. *Science* 305, 390-392.
- Curtis, M.D., and Grossniklaus, U.** (2003). A gateway cloning vector set for high-throughput functional analysis of genes in planta. *Plant Physiology* 133, 462-469.

- Dai, L., Peng, C., Montellier, E., Lu, Z., Chen, Y., Ishii, H., Debernardi, A., Buchou, T., Rousseaux, S., Jin, F., Sabari, B.R., Deng, Z., Allis, C.D., Ren, B., Khochbin, S., and Zhao, Y.** (2014). Lysine 2-hydroxyisobutyrylation is a widely distributed active histone mark. *Nature Chemical Biology* 10, 365-370.
- Dang, L., White, D.W., Gross, S., Bennett, B.D., Bittinger, M.A., Driggers, E.M., Fantin, V.R., Jang, H.G., Jin, S., Keenan, M.C., Marks, K.M., Prins, R.M., Ward, P.S., Yen, K.E., Liao, L.M., Rabinowitz, J.D., Cantley, L.C., Thompson, C.B., Vander Heiden, M.G., and Su, S.M.** (2009). Cancer-associated IDH1 mutations produce 2-hydroxyglutarate. *Nature* 462, 739-744.
- Dangl, M., Brosch, G., Haas, H., Loidl, P., and Lusser, A.** (2001). Comparative analysis of HD2 type histone deacetylases in higher plants. *Planta* 213, 280-285.
- Dhalluin, C., Carlson, J.E., Zeng, L., He, C., Aggarwal, A.K., and Zhou, M.M.** (1999). Structure and ligand of a histone acetyltransferase bromodomain. *Nature* 399, 491-496.
- Dong, G., Ma, D.P., and Li, J.** (2008). The histone methyltransferase SDG8 regulates shoot branching in *Arabidopsis*. *Biochemical and Biophysical Research Communications* 373, 659-664.
- Earley, K.W., Shook, M.S., Brower-Toland, B., Hicks, L., and Pikaard, C.S.** (2007). In vitro specificities of *Arabidopsis* co-activator histone acetyltransferases: implications for histone hyperacetylation in gene activation. *The Plant Journal* 52, 615-626.
- Earley, K.W., Haag, J.R., Pontes, O., Opper, K., Juehne, T., Song, K., and Pikaard, C.S.** (2006). Gateway-compatible vectors for plant functional genomics and proteomics. *The Plant Journal* 45, 616-629.
- Eberharter, A., Lechner, T., Goralik-Schramel, M., and Loidl, P.** (1996). Purification and characterization of the cytoplasmic histone acetyltransferase B of maize embryos. *FEBS Letters* 386, 75-81.
- Fatland, B.L., Nikolau, B.J., and Wurtele, E.S.** (2005). Reverse genetic characterization of cytosolic acetyl-CoA generation by ATP-citrate lyase in *Arabidopsis*. *Plant Cell* 17, 182-203.
- Fatland, B.L., Ke, J., Anderson, M.D., Mentzen, W.I., Cui, L.W., Allred, C.C., Johnston, J.L., Nikolau, B.J., and Wurtele, E.S.** (2002). Molecular characterization of a heteromeric ATP-citrate lyase that generates cytosolic acetyl-coenzyme A in *Arabidopsis*. *Plant Physiology* 130, 740-756.
- Faure, J.D., Vittorioso, P., Santoni, V., Fraissier, V., Prinsen, E., Barlier, I., Van Onckelen, H., Caboche, M., and Bellini, C.** (1998). The PASTICCINO genes of *Arabidopsis thaliana* are involved in the control of cell division and differentiation. *Development* 125, 909-918.
- Feinberg, A.P.** (2007). Phenotypic plasticity and the epigenetics of human disease. *Nature* 447, 433-440.

- Frey, P.A., Hegeman, A.D., and Ruzicka, F.J.** (2008). The Radical SAM Superfamily. *Critical Reviews in Biochemistry and Molecular Biology* 43, 63-88.
- Frye, R.A.** (2000). Phylogenetic classification of prokaryotic and eukaryotic Sir2-like proteins. *Biochemical and Biophysical Research Communications* 273, 793-798.
- Fuchs, J., Demidov, D., Houben, A., and Schubert, I.** (2006). Chromosomal histone modification patterns--from conservation to diversity. *Trends in Plant Science* 11, 199-208.
- Galdieri, L., and Vancura, A.** (2012). Acetyl-CoA carboxylase regulates global histone acetylation. *The Journal of Biological Chemistry* 287, 23865-23876.
- Gendler, K., Paulsen, T., and Napoli, C.** (2008). ChromDB: the chromatin database. *Nucleic Acids Research* 36, D298-302.
- Gendrel, A.V., Lippman, Z., Martienssen, R., and Colot, V.** (2005). Profiling histone modification patterns in plants using genomic tiling microarrays. *Nature Methods* 2, 213-218.
- Grant, P.A., Duggan, L., Cote, J., Roberts, S.M., Brownell, J.E., Candau, R., Ohba, R., Owen-Hughes, T., Allis, C.D., Winston, F., Berger, S.L., and Workman, J.L.** (1997). Yeast Gcn5 functions in two multisubunit complexes to acetylate nucleosomal histones: characterization of an Ada complex and the SAGA (Spt/Ada) complex. *Genes and Development* 11, 1640-1650.
- Guan, K.L., and Xiong, Y.** (2011). Regulation of intermediary metabolism by protein acetylation. *Trends in Biochemical Sciences* 36, 108-116.
- Guarente, L.** (2013). Calorie restriction and sirtuins revisited. *Genes & Development* 27, 2072-2085.
- Gut, P., and Verdin, E.** (2013). The nexus of chromatin regulation and intermediary metabolism. *Nature* 502, 489-498.
- Han, S.K., Song, J.D., Noh, Y.S., and Noh, B.** (2007). Role of plant CBP/p300-like genes in the regulation of flowering time. *The Plant Journal* 49, 103-114.
- Hardie, D.G.** (2011). AMP-activated protein kinase: an energy sensor that regulates all aspects of cell function. *Genes & Development* 25, 1895-1908.
- Hassan, A.H., Prochasson, P., Neely, K.E., Galasinski, S.C., Chandy, M., Carrozza, M.J., and Workman, J.L.** (2002). Function and selectivity of bromodomains in anchoring chromatin-modifying complexes to promoter nucleosomes. *Cell* 111, 369-379.
- Hellens, R., Mullineaux, P., and Klee, H.** (2000). Technical Focus: a guide to *Agrobacterium* binary Ti vectors. *Trends in Plant Science* 5, 446-451.
- Henry, R.A., Kuo, Y.M., and Andrews, A.J.** (2013). Differences in specificity and selectivity between CBP and p300 acetylation of histone H3 and H3/H4. *Biochemistry* 52, 5746-5759.

- Henry, R.A., Kuo, Y.M., Bhattacharjee, V., Yen, T.J., and Andrews, A.J.** (2015). Changing the selectivity of p300 by acetyl-CoA modulation of histone acetylation. *ACS Chemical Biology* 10, 146-156.
- Hicke, L.** (2001). Protein regulation by monoubiquitin. *Molecular Cell Biology* 2, 195-201.
- Hirschey, M.D., Shimazu, T., Huang, J.Y., Schwer, B., and Verdin, E.** (2011). SIRT3 regulates mitochondrial protein acetylation and intermediary metabolism. *Cold Spring Harbor Symposia on Quantitative Biology* 76, 267-277.
- Hollender, C., and Liu, Z.** (2008). Histone deacetylase genes in *Arabidopsis* development. *Journal of Integrative Plant Biology* 50, 875-885.
- Illi, B., Dello Russo, C., Colussi, C., Rosati, J., Pallaoro, M., Spallotta, F., Rotili, D., Valente, S., Ragone, G., Martelli, F., Biglioli, P., Steinkuhler, C., Gallinari, P., Mai, A., Capogrossi, M.C., and Gaetano, C.** (2008). Nitric oxide modulates chromatin folding in human endothelial cells via protein phosphatase 2A activation and class II histone deacetylases nuclear shuttling. *Circulation Research* 102, 51-58.
- Jackson, J.P., Johnson, L., Jasencakova, Z., Zhang, X., PerezBurgos, L., Singh, P.B., Cheng, X., Schubert, I., Jenuwein, T., and Jacobsen, S.E.** (2004). Dimethylation of histone H3 lysine 9 is a critical mark for DNA methylation and gene silencing in *Arabidopsis thaliana*. *Chromosoma* 112, 308-315.
- Jang, I.C., Chung, P.J., Hemmes, H., Jung, C., and Chua, N.H.** (2011). Rapid and reversible light-mediated chromatin modifications of *Arabidopsis* phytochrome A locus. *Plant Cell* 23, 459-470.
- Jin, H., Song, Z., and Nikolau, B.J.** (2012). Reverse genetic characterization of two paralogous acetoacetyl CoA thiolase genes in *Arabidopsis* reveals their importance in plant growth and development. *The Plant Journal* 70, 1015-1032.
- Kajiwara, T., Furutani, M., Hibara, K., and Tasaka, M.** (2004). The GURKE gene encoding an acetyl-CoA carboxylase is required for partitioning the embryo apex into three subregions in *Arabidopsis*. *Plant & Cell Physiology* 45, 1122-1128.
- Kim, D., Perte, G., Trapnell, C., Pimentel, H., Kelley, R., and Salzberg, S.L.** (2013). TopHat2: accurate alignment of transcriptomes in the presence of insertions, deletions and gene fusions. *Genome Biology* 14, R36.
- Klevecz, R.R., Bolen, J., Forrest, G., and Murray, D.B.** (2004). A genomewide oscillation in transcription gates DNA replication and cell cycle. *Proceedings of the National Academy of Sciences of the United States of America* 101, 1200-1205.
- Klose, R.J., and Zhang, Y.** (2007). Regulation of histone methylation by demethylination and demethylation. *Molecular Cell Biology* 8, 307-318.

- Kohler, C., Hennig, L., Bouveret, R., Gheyselinck, J., Grossniklaus, U., and Gruissem, W.** (2003). *Arabidopsis* MSII is a component of the MEA/FIE Polycomb group complex and required for seed development. *The EMBO Journal* 22, 4804-4814.
- Kornet, N., and Scheres, B.** (2009). Members of the GCN5 histone acetyltransferase complex regulate PLETHORA-mediated root stem cell niche maintenance and transit amplifying cell proliferation in *Arabidopsis*. *Plant Cell* 21, 1070-1079.
- Kurdistani, S.K., and Grunstein, M.** (2003). Histone acetylation and deacetylation in yeast. *Molecular Cell Biology* 4, 276-284.
- Kurihara, D., Matsunaga, S., Omura, T., Higashiyama, T., and Fukui, K.** (2011). Identification and characterization of plant Haspin kinase as a histone H3 threonine kinase. *BMC Plant Biology* 11, 73.
- Kurihara, D., Matsunaga, S., Kawabe, A., Fujimoto, S., Noda, M., Uchiyama, S., and Fukui, K.** (2006). Aurora kinase is required for chromosome segregation in tobacco BY-2 cells. *The Plant Journal* 48, 572-580.
- Langmead, B., Trapnell, C., Pop, M., and Salzberg, S.L.** (2009). Ultrafast and memory-efficient alignment of short DNA sequences to the human genome. *Genome Biology* 10, R25.
- Latrasse, D., Benhamed, M., Henry, Y., Domenichini, S., Kim, W., Zhou, D.X., and Delarue, M.** (2008). The MYST histone acetyltransferases are essential for gametophyte development in *Arabidopsis*. *BMC Plant Biology* 8, 121.
- Lee, J.V., Carrer, A., Shah, S., Snyder, N.W., Wei, S., Venneti, S., Worth, A.J., Yuan, Z.F., Lim, H.W., Liu, S., Jackson, E., Aiello, N.M., Haas, N.B., Rebbeck, T.R., Judkins, A., Won, K.J., Chodosh, L.A., Garcia, B.A., Stanger, B.Z., Feldman, M.D., Blair, I.A., and Wellen, K.E.** (2014). Akt-dependent metabolic reprogramming regulates tumor cell histone acetylation. *Cell Metabolism* 20, 306-319.
- Li, B., Carey, M., and Workman, J.L.** (2007). The role of chromatin during transcription. *Cell* 128, 707-719.
- Li, C., Chen, C., Gao, L., Yang, S., Nguyen, V., Shi, X., Siminovitch, K., Kohalmi, S.E., Huang, S., Wu, K., Chen, X., and Cui, Y.** (2015). The *Arabidopsis* SWI2/SNF2 chromatin Remodeler BRAHMA regulates polycomb function during vegetative development and directly activates the flowering repressor gene SVP. *PLoS Genetics* 11, e1004944.
- Li, H., Ilin, S., Wang, W., Duncan, E.M., Wysocka, J., Allis, C.D., and Patel, D.J.** (2006). Molecular basis for site-specific read-out of histone H3K4me3 by the BPTF PHD finger of NURF. *Nature* 442, 91-95.
- Lindegren, G., Hwang, Y.L., Oshima, Y., and Lindegren, C.C.** (1965). Genetical mutants induced by ethyl methanesulfonate in *Saccharomyces*. *Canadian Journal of Genetics and Cytology* 7, 491-499.

- Liu, C., Lu, F., Cui, X., and Cao, X.** (2010). Histone methylation in higher plants. *Annual Review of Plant Biology* 61, 395-420.
- Long, J.A., Ohno, C., Smith, Z.R., and Meyerowitz, E.M.** (2006). TOPLESS regulates apical embryonic fate in *Arabidopsis*. *Science* 312, 1520-1523.
- Lu, C., and Thompson, C.B.** (2012). Metabolic regulation of epigenetics. *Cell Metabolism* 16, 9-17.
- Lu, C., Ward, P.S., Kapoor, G.S., Rohle, D., Turcan, S., Abdel-Wahab, O., Edwards, C.R., Khanin, R., Figueroa, M.E., Melnick, A., Wellen, K.E., O'Rourke, D.M., Berger, S.L., Chan, T.A., Levine, R.L., Mellinghoff, I.K., and Thompson, C.B.** (2012). IDH mutation impairs histone demethylation and results in a block to cell differentiation. *Nature* 483, 474-478.
- Lu, F., Cui, X., Zhang, S., Jenuwein, T., and Cao, X.** (2011a). *Arabidopsis* REF6 is a histone H3 lysine 27 demethylase. *Nature Genetics* 43, 715-719.
- Lu, Q., Tang, X., Tian, G., Wang, F., Liu, K., Nguyen, V., Kohalmi, S.E., Keller, W.A., Tsang, E.W., Harada, J.J., Rothstein, S.J., and Cui, Y.** (2010). *Arabidopsis* homolog of the yeast TREX-2 mRNA export complex: components and anchoring nucleoporin. *The Plant Journal* 61, 259-270.
- Lu, S., Zhao, H., Parsons, E.P., Xu, C., Kosma, D.K., Xu, X., Chao, D., Lohrey, G., Bangarusamy, D.K., Wang, G., Bressan, R.A., and Jenks, M.A.** (2011b). The glossyhead1 allele of ACC1 reveals a principal role for multidomain acetyl-coenzyme A carboxylase in the biosynthesis of cuticular waxes by *Arabidopsis*. *Plant Physiology* 157, 1079-1092.
- Luger, K., Mader, A.W., Richmond, R.K., Sargent, D.F., and Richmond, T.J.** (1997). Crystal structure of the nucleosome core particle at 2.8 Å resolution. *Nature* 389, 251-260.
- Lusser, A., Brosch, G., Loidl, A., Haas, H., and Loidl, P.** (1997). Identification of maize histone deacetylase HD2 as an acidic nucleolar phosphoprotein. *Science* 277, 88-91.
- Lusser, A., Eberharter, A., Loidl, A., Goralik-Schramel, M., Horngacher, M., Haas, H., and Loidl, P.** (1999). Analysis of the histone acetyltransferase B complex of maize embryos. *Nucleic Acids Research* 27, 4427-4435.
- Madiraju, P., Pande, S.V., Prentki, M., and Madiraju, S.R.** (2009). Mitochondrial acetylcarnitine provides acetyl groups for nuclear histone acetylation. *Epigenetics* 4, 399-403.
- Malapeira, J., Khaitova, L.C., and Mas, P.** (2012). Ordered changes in histone modifications at the core of the *Arabidopsis* circadian clock. *Proceedings of the National Academy of Sciences of the United States of America* 109, 21540-21545.
- Marmorstein, R.** (2001). Structure and function of histone acetyltransferases. *Cellular and Molecular Life Sciences* 58, 693-703.

- Martens, S., Preuss, A., and Matern, U.** (2010). Multifunctional flavonoid dioxygenases: flavonol and anthocyanin biosynthesis in *Arabidopsis thaliana*. *Phytochemistry* 71, 1040-1049.
- Mathieu, O., Probst, A.V., and Paszkowski, J.** (2005). Distinct regulation of histone H3 methylation at lysines 27 and 9 by CpG methylation in *Arabidopsis*. *The EMBO Journal* 24, 2783-2791.
- McBrian, M.A., Behbahan, I.S., Ferrari, R., Su, T., Huang, T.W., Li, K., Hong, C.S., Christofk, H.R., Vogelauer, M., Seligson, D.B., and Kurdistani, S.K.** (2013). Histone acetylation regulates intracellular pH. *Molecular Cell* 49, 310-321.
- Mengel, A., Ageeva, A., Georgii, E., Bernhardt, J., Wu, K., Durner, J., and Lindermayr, C.** (2016). Nitric oxide modulates histone acetylation at stress genes by inhibition of histone deacetylases. *Plant Physiology*.
- Mikkelsen, T.S., Hanna, J., Zhang, X., Ku, M., Wernig, M., Schorderet, P., Bernstein, B.E., Jaenisch, R., Lander, E.S., and Meissner, A.** (2008). Dissecting direct reprogramming through integrative genomic analysis. *Nature* 454, 49-55.
- Min, J., Zhang, Y., and Xu, R.M.** (2003a). Structural basis for specific binding of Polycomb chromodomain to histone H3 methylated at Lys 27. *Genes & Development* 17, 1823-1828.
- Min, J., Feng, Q., Li, Z., Zhang, Y., and Xu, R.M.** (2003b). Structure of the catalytic domain of human DOT1L, a non-SET domain nucleosomal histone methyltransferase. *Cell* 112, 711-723.
- Moellering, E.R., Muthan, B., and Benning, C.** (2010). Freezing tolerance in plants requires lipid remodeling at the outer chloroplast membrane. *Science* 330, 226-228.
- Nakabayashi, R., Yonekura-Sakakibara, K., Urano, K., Suzuki, M., Yamada, Y., Nishizawa, T., Matsuda, F., Kojima, M., Sakakibara, H., Shinozaki, K., Michael, A.J., Tohge, T., Yamazaki, M., and Saito, K.** (2014). Enhancement of oxidative and drought tolerance in *Arabidopsis* by overaccumulation of antioxidant flavonoids. *The Plant Journal* 77, 367-379.
- Nicol, J.W., Helt, G.A., Blanchard, S.G., Jr., Raja, A., and Loraine, A.E.** (2009). The Integrated Genome Browser: free software for distribution and exploration of genome-scale datasets. *Bioinformatics* 25, 2730-2731.
- Nobusawa, T., Okushima, Y., Nagata, N., Kojima, M., Sakakibara, H., and Umeda, M.** (2013). Synthesis of very-long-chain fatty acids in the epidermis controls plant organ growth by restricting cell proliferation. *PLoS Biology* 11, e1001531.
- Olia, A.S., Barker, K., McCullough, C.E., Tang, H.Y., Speicher, D.W., Qiu, J., LaBaer, J., and Marmorstein, R.** (2015). Nonenzymatic Protein Acetylation Detected by NAPPA Protein Arrays. *ACS Chemical Biology* 10, 2034-2047.
- Oliver, D.J., Nikolau, B.J., and Syrkin Wurtele, E.** (2009). Acetyl-CoA-Life at the metabolic nexus. *Plant Science* 176, 597-601.

- Ossowski, S., Schwab, R., and Weigel, D.** (2008). Gene silencing in plants using artificial microRNAs and other small RNAs. *The Plant Journal* 53, 674-690.
- Paik, W.K., Pearson, D., Lee, H.W., and Kim, S.** (1970). Nonenzymatic acetylation of histones with acetyl-CoA. *Biochim Biophys Acta* 213, 513-522.
- Pandey, R., Muller, A., Napoli, C.A., Selinger, D.A., Pikaard, C.S., Richards, E.J., Bender, J., Mount, D.W., and Jorgensen, R.A.** (2002). Analysis of histone acetyltransferase and histone deacetylase families of *Arabidopsis thaliana* suggests functional diversification of chromatin modification among multicellular eukaryotes. *Nucleic Acids Research* 30, 5036-5055.
- Parthun, M.R., Widom, J., and Gottschling, D.E.** (1996). The major cytoplasmic histone acetyltransferase in yeast: links to chromatin replication and histone metabolism. *Cell* 87, 85-94.
- Pickart, C.M.** (2001). Mechanisms underlying ubiquitination. *Annual Review of Biochemistry* 70, 503-533.
- Pien, S., and Grossniklaus, U.** (2007). Polycomb group and trithorax group proteins in *Arabidopsis*. *Biochimica et Biophysica Acta* 1769, 375-382.
- Pien, S., Fleury, D., Mylne, J.S., Crevillen, P., Inze, D., Avramova, Z., Dean, C., and Grossniklaus, U.** (2008). *ARABIDOPSIS* TRITHORAX1 dynamically regulates FLOWERING LOCUS C activation via histone 3 lysine 4 trimethylation. *Plant Cell* 20, 580-588.
- Pietrocola, F., Galluzzi, L., Bravo-San Pedro, J.M., Madeo, F., and Kroemer, G.** (2015). Acetyl coenzyme A: a central metabolite and second messenger. *Cell Metabolism* 21, 805-821.
- Ponting, C.P., Blake, D.J., Davies, K.E., Kendrick-Jones, J., and Winder, S.J.** (1996). ZZ and TAZ: new putative zinc fingers in dystrophin and other proteins. *Trends in Biochemical Sciences* 21, 11-13.
- Ramirez F., Ryan D. P., Gruning B., Bhardwaj V., Kilpert F., Richter A. S., Heyne S., Dundar F., and Manke T.** (2016). deepTools2: a next generation web server for deep-sequencing data analysis. *Nucleic acids research* 44, 160-165.
- Roth, S.Y., Denu, J.M., and Allis, C.D.** (2001). Histone acetyltransferases. *Annual Review of Biochemistry* 70, 81-120.
- Roudier, F., Gissot, L., Beaudoin, F., Haslam, R., Michaelson, L., Marion, J., Molino, D., Lima, A., Bach, L., Morin, H., Tellier, F., Palauqui, J.C., Bellec, Y., Renne, C., Miquel, M., Dacosta, M., Vignard, J., Rochat, C., Markham, J.E., Moreau, P., Napier, J., and Faure, J.D.** (2010). Very-long-chain fatty acids are involved in polar auxin transport and developmental patterning in *Arabidopsis*. *Plant Cell* 22, 364-375.
- Roudier, F., Ahmed, I., Berard, C., Sarazin, A., Mary-Huard, T., Cortijo, S., Bouyer, D., Caillieux, E., Duvernois-Berthet, E., Al-Shikhley, L., Giraut, L., Despres, B., Drevensek, S., Barneche, F., Derozier, S., Brunaud, V., Aubourg, S., Schnittger, A., Bowler, C., Martin-Magniette, M.L., Robin, S., Caboche,**

- M., and Colot, V.** (2011). Integrative epigenomic mapping defines four main chromatin states in *Arabidopsis*. *The EMBO Journal* 30, 1928-1938.
- Sachs, M., Onodera, C., Blaschke, K., Ebata, K.T., Song, J.S., and Ramalho-Santos, M.** (2013). Bivalent chromatin marks developmental regulatory genes in the mouse embryonic germline in vivo. *Cell Reports* 3, 1777-1784.
- Sack, M.N., and Finkel, T.** (2012). Mitochondrial Metabolism, Sirtuins, and Aging. *Cold Spring Harbor Perspectives in Biology* 4.
- Salmon-Divon, M., Dvinge, H., Tammoja, K., and Bertone, P.** (2010). PeakAnalyzer: genome-wide annotation of chromatin binding and modification loci. *BMC Bioinformatics* 11, 415.
- Schulz, E., Tohge, T., Zuther, E., Fernie, A.R., and Hinch, D.K.** (2016). Flavonoids are determinants of freezing tolerance and cold acclimation in *Arabidopsis thaliana*. *Scientific Reports* 6, 34027.
- Schwab, R., Ossowski, S., Riester, M., Warthmann, N., and Weigel, D.** (2006). Highly specific gene silencing by artificial microRNAs in *Arabidopsis*. *Plant Cell* 18, 1121-1133.
- Sequeira-Mendes, J., Araguez, I., Peiro, R., Mendez-Giraldez, R., Zhang, X., Jacobsen, S.E., Bastolla, U., and Gutierrez, C.** (2014). The Functional Topography of the *Arabidopsis* Genome Is Organized in a Reduced Number of Linear Motifs of Chromatin States. *Plant Cell* 26, 2351-2366.
- Servet, C., Conde e Silva, N., and Zhou, D.X.** (2010). Histone acetyltransferase AtGCN5/HAG1 is a versatile regulator of developmental and inducible gene expression in *Arabidopsis*. *Molecular Plant* 3, 670-677.
- Shen, Y., Wei, W., and Zhou, D.-X.** (2015). Histone Acetylation Enzymes Coordinate Metabolism and Gene Expression. *Trends in Plant Science* 20, 614-621.
- Shyh-Chang, N., Locasale, J.W., Lyssiotis, C.A., Zheng, Y., Teo, R.Y., Ratanasirintraoort, S., Zhang, J., Onder, T., Unternaehrer, J.J., Zhu, H., Asara, J.M., Daley, G.Q., and Cantley, L.C.** (2013). Influence of threonine metabolism on S-adenosylmethionine and histone methylation. *Science* 339, 222-226.
- Slavov, N., Macinskis, J., Caudy, A., and Botstein, D.** (2011). Metabolic cycling without cell division cycling in respiring yeast. *Proceedings of the National Academy of Sciences of the United States of America* 108, 19090-19095.
- Springer, N.M., Napoli, C.A., Selinger, D.A., Pandey, R., Cone, K.C., Chandler, V.L., Kaeppler, H.F., and Kaeppler, S.M.** (2003). Comparative analysis of SET domain proteins in maize and *Arabidopsis* reveals multiple duplications preceding the divergence of monocots and dicots. *Plant Physiology* 132, 907-925.
- Sterner, D.E., and Berger, S.L.** (2000). Acetylation of histones and transcription-related factors. *Microbiology and Molecular Biology Reviews* 64, 435-459.
- Sutendra, G., Kinnaird, A., Dromparis, P., Paulin, R., Stenson, T.H., Haromy, A., Hashimoto, K., Zhang, N., Flaim, E., and Michelakis, E.D.** (2014). A nuclear

pyruvate dehydrogenase complex is important for the generation of acetyl-CoA and histone acetylation. *Cell* 158, 84-97.

- Takahashi, H., McCaffery, J.M., Irizarry, R.A., and Boeke, J.D.** (2006). Nucleocytosolic acetyl-coenzyme a synthetase is required for histone acetylation and global transcription. *Molecular Cell* 23, 207-217.
- Tan, M., Luo, H., Lee, S., Jin, F., Yang, J.S., Montellier, E., Buchou, T., Cheng, Z., Rousseaux, S., Rajagopal, N., Lu, Z., Ye, Z., Zhu, Q., Wysocka, J., Ye, Y., Khochbin, S., Ren, B., and Zhao, Y.** (2011). Identification of 67 histone marks and histone lysine crotonylation as a new type of histone modification. *Cell* 146, 1016-1028.
- Tanaka, M., Kikuchi, A., and Kamada, H.** (2008). The *Arabidopsis* histone deacetylases HDA6 and HDA19 contribute to the repression of embryonic properties after germination. *Plant Physiology* 146, 149-161.
- Tang, X., Lim, M.H., Pelletier, J., Tang, M., Nguyen, V., Keller, W.A., Tsang, E.W., Wang, A., Rothstein, S.J., Harada, J.J., and Cui, Y.** (2012). Synergistic repression of the embryonic programme by SET DOMAIN GROUP 8 and EMBRYONIC FLOWER 2 in *Arabidopsis* seedlings. *Journal of Experimental Botany* 63, 1391-1404.
- Tang, X., Hou, A., Babu, M., Nguyen, V., Hurtado, L., Lu, Q., Reyes, J.C., Wang, A., Keller, W.A., Harada, J.J., Tsang, E.W., and Cui, Y.** (2008). The *Arabidopsis* BRAHMA chromatin-remodeling ATPase is involved in repression of seed maturation genes in leaves. *Plant Physiology* 147, 1143-1157.
- Tian, L., Wang, J., Fong, M.P., Chen, M., Cao, H., Gelvin, S.B., and Chen, Z.J.** (2003). Genetic control of developmental changes induced by disruption of *Arabidopsis* histone deacetylase 1 (AtHD1) expression. *Genetics* 165, 399-409.
- Tie, F., Banerjee, R., Stratton, C.A., Prasad-Sinha, J., Stepanik, V., Zlobin, A., Diaz, M.O., Scacheri, P.C., and Harte, P.J.** (2009). CBP-mediated acetylation of histone H3 lysine 27 antagonizes *Drosophila* Polycomb silencing. *Development* 136, 3131-3141.
- Tohge, T., Kusano, M., Fukushima, A., Saito, K., and Fernie, A.R.** (2011). Transcriptional and metabolic programs following exposure of plants to UV-B irradiation. *Plant Signaling & Behavior* 6, 1987-1992.
- Trapnell, C., Williams, B.A., Pertea, G., Mortazavi, A., Kwan, G., van Baren, M.J., Salzberg, S.L., Wold, B.J., and Pachter, L.** (2010). Transcript assembly and quantification by RNA-Seq reveals unannotated transcripts and isoform switching during cell differentiation. *Nature Biotechnology* 28, 511-515.
- Trojer, P., and Reinberg, D.** (2007). Facultative heterochromatin: is there a distinctive molecular signature. *Molecular Cell* 28, 1-13.
- Tsuchiya, Y., Pham, U., Hu, W., Ohnuma, S., and Gout, I.** (2014). Changes in acetyl CoA levels during the early embryonic development of *Xenopus laevis*. *PloS One* 9, e97693.

- Tu, B.P., Kudlicki, A., Rowicka, M., and McKnight, S.L.** (2005). Logic of the yeast metabolic cycle: temporal compartmentalization of cellular processes. *Science* 310, 1152-1158.
- Tu, B.P., Mohler, R.E., Liu, J.C., Dombek, K.M., Young, E.T., Synovec, R.E., and McKnight, S.L.** (2007). Cyclic changes in metabolic state during the life of a yeast cell. *Proceedings of the National Academy of Sciences of the United States of America* 104, 16886-16891.
- Turck, F., Roudier, F., Farrona, S., Martin-Magniette, M.L., Guillaume, E., Buisine, N., Gagnot, S., Martienssen, R.A., Coupland, G., and Colot, V.** (2007). *Arabidopsis* TFL2/LHP1 specifically associates with genes marked by trimethylation of histone H3 lysine 27. *PLoS Genetics* 3, e86.
- Uemura, M., Joseph, R.A., and Steponkus, P.L.** (1995). Cold acclimation of *Arabidopsis thaliana*. *Plant Physiology* 109, 15-30.
- Venkatesh, S., and Workman, J.L.** (2015). Histone exchange, chromatin structure and the regulation of transcription. *Molecular Cell Biology* 16, 178-189.
- Verdin, E., and Ott, M.** (2015). 50 years of protein acetylation: from gene regulation to epigenetics, metabolism and beyond. *Molecular Cell Biology* 16, 258-264.
- Verreault, A., Kaufman, P.D., Kobayashi, R., and Stillman, B.** (1998). Nucleosomal DNA regulates the core-histone-binding subunit of the human Hat1 acetyltransferase. *Current Biology* 8, 96-108.
- Vlachonasios, K.E., Thomashow, M.F., and Triezenberg, S.J.** (2003). Disruption mutations of ADA2b and GCN5 transcriptional adaptor genes dramatically affect *Arabidopsis* growth, development, and gene expression. *Plant Cell* 15, 626-638.
- Wagner, G.R., and Payne, R.M.** (2013). Widespread and enzyme-independent Nepsilon-acetylation and Nepsilon-succinylation of proteins in the chemical conditions of the mitochondrial matrix. *The Journal of Biological Chemistry* 288, 29036-29045.
- Wagner, G.R., and Hirsche, M.D.** (2014). Nonenzymatic protein acylation as a carbon stress regulated by sirtuin deacylases. *Molecular Cell* 54, 5-16.
- Wang, J., Alexander, P., Wu, L., Hammer, R., Cleaver, O., and McKnight, S.L.** (2009). Dependence of mouse embryonic stem cells on threonine catabolism. *Science* 325, 435-439.
- Ward, P.S., Patel, J., Wise, D.R., Abdel-Wahab, O., Bennett, B.D., Collier, H.A., Cross, J.R., Fantin, V.R., Hedvat, C.V., Perl, A.E., Rabinowitz, J.D., Carroll, M., Su, S.M., Sharp, K.A., Levine, R.L., and Thompson, C.B.** (2010). The common feature of leukemia-associated IDH1 and IDH2 mutations is a neomorphic enzyme activity converting alpha-ketoglutarate to 2-hydroxyglutarate. *Cancer Cell* 17, 225-234.
- Waterworth, W.M., Drury, G.E., Blundell-Hunter, G., and West, C.E.** (2015). *Arabidopsis* TAF1 is an MRE11-interacting protein required for resistance to

genotoxic stress and viability of the male gametophyte. *The Plant Journal* 84, 545-557.

- Weake, V.M., and Workman, J.L.** (2008). Histone ubiquitination: triggering gene activity. *Molecular Cell* 29, 653-663.
- Wellen, K.E., Hatzivassiliou, G., Sachdeva, U.M., Bui, T.V., Cross, J.R., and Thompson, C.B.** (2009). ATP-citrate lyase links cellular metabolism to histone acetylation. *Science* 324, 1076-1080.
- Winkel-Shirley, B.** (2002). Biosynthesis of flavonoids and effects of stress. *Current Opinion in Plant Biology* 5, 218-223.
- Wu, K., Tian, L., Malik, K., Brown, D., and Miki, B.** (2000). Functional analysis of HD2 histone deacetylase homologues in *Arabidopsis thaliana*. *The Plant Journal* 22, 19-27.
- Xiao, J., Zhang, H., Xing, L., Xu, S., Liu, H., Chong, K., and Xu, Y.** (2013). Requirement of histone acetyltransferases HAM1 and HAM2 for epigenetic modification of FLC in regulating flowering in *Arabidopsis*. *Journal of Plant Physiology* 170, 444-451.
- Xie, Z., Dai, J., Dai, L., Tan, M., Cheng, Z., Wu, Y., Boeke, J.D., and Zhao, Y.** (2012). Lysine succinylation and lysine malonylation in histones. *Molecular & Cellular Proteomics* 11, 100-107.
- Xing, S., and Poirier, Y.** (2012). The protein acetylome and the regulation of metabolism. *Trends in Plant Science* 17, 423-430.
- Xu, L., and Shen, W.H.** (2008). Polycomb silencing of KNOX genes confines shoot stem cell niches in *Arabidopsis*. *Current Biology* 18, 1966-1971.
- Xu, L., Zhao, Z., Dong, A., Soubigou-Taconnat, L., Renou, J.P., Steinmetz, A., and Shen, W.H.** (2008). Di- and tri- but not monomethylation on histone H3 lysine 36 marks active transcription of genes involved in flowering time regulation and other processes in *Arabidopsis thaliana*. *Molecular and Cellular Biology* 28, 1348-1360.
- Yanai, Y., Kawasaki, T., Shimada, H., Wurtele, E.S., Nikolau, B.J., and Ichikawa, N.** (1995). Genomic organization of 251 kDa acetyl-CoA carboxylase genes in *Arabidopsis*: tandem gene duplication has made two differentially expressed isozymes. *Plant & Cell Physiology* 36, 779-787.
- Yang, H., Yang, T., Baur, J.A., Perez, E., Matsui, T., Carmona, J.J., Lamming, D.W., Souza-Pinto, N.C., Bohr, V.A., Rosenzweig, A., de Cabo, R., Sauve, A.A., and Sinclair, D.A.** (2007). Nutrient-sensitive mitochondrial NAD⁺ levels dictate cell survival. *Cell* 130, 1095-1107.
- Ye, T., Krebs, A.R., Choukrallah, M.A., Keime, C., Plewniak, F., Davidson, I., and Tora, L.** (2011). seqMINER: an integrated ChIP-seq data interpretation platform. *Nucleic Acids Research* 39, e35.

- Zang, C., Schones, D.E., Zeng, C., Cui, K., Zhao, K., and Peng, W.** (2009). A clustering approach for identification of enriched domains from histone modification ChIP-Seq data. *Bioinformatics* 25, 1952-1958.
- Zhang, K., Sridhar, V.V., Zhu, J., Kapoor, A., and Zhu, J.K.** (2007a). Distinctive core histone post-translational modification patterns in *Arabidopsis thaliana*. *PLoS One* 2, e1210.
- Zhang, X., Henriques, R., Lin, S.S., Niu, Q.W., and Chua, N.H.** (2006). *Agrobacterium*-mediated transformation of *Arabidopsis thaliana* using the floral dip method. *Nature Protocols* 1, 641-646.
- Zhang, X., Bernatavichute, Y.V., Cokus, S., Pellegrini, M., and Jacobsen, S.E.** (2009). Genome-wide analysis of mono-, di- and trimethylation of histone H3 lysine 4 in *Arabidopsis thaliana*. *Genome Biology* 10, R62.
- Zhang, X., Clarenz, O., Cokus, S., Bernatavichute, Y.V., Pellegrini, M., Goodrich, J., and Jacobsen, S.E.** (2007b). Whole-genome analysis of histone H3 lysine 27 trimethylation in *Arabidopsis*. *PLoS Biology* 5, e129.
- Zhang, Y.** (2003). Transcriptional regulation by histone ubiquitination and deubiquitination. *Genes & Development* 17, 2733-2740.
- Zhang, Y., Liu, T., Meyer, C.A., Eeckhoute, J., Johnson, D.S., Bernstein, B.E., Nussbaum, C., Myers, R.M., Brown, M., Li, W., and Liu, X.S.** (2008). Model-based analysis of ChIP-Seq (MACS). *Genome Biology* 9, R137.
- Zhao, Z., and Shen, W.H.** (2004). Plants contain a high number of proteins showing sequence similarity to the animal SUV39H family of histone methyltransferases. *Annals of the New York Academy of Sciences* 1030, 661-669.
- Zuo, J., Niu, Q.W., and Chua, N.H.** (2000). Technical advance: An estrogen receptor-based transactivator XVE mediates highly inducible gene expression in transgenic plants. *The Plant Journal* 24, 265-273.

Curriculum Vitae

Name: Chen Chen

Post-secondary Education and Degrees: Yangtze University
Jingzhou, Hubei, China
2002-2006 B.A.

Sun Yat-Sen University
Guangzhou, Guangdong, China
2008-2011 M.A.

The University of Western Ontario
London, Ontario, Canada
2012-2017 Ph.D.

Honors and Awards: Chinese Government Scholarship for Abroad Doctoral Study
2012-2015

Related Work Experience: Teaching Assistant
The University of Western Ontario
2012-2016

Publications:

- Li, C., **Chen, C.**, Gao, L., Yang, S., Nguyen, V., Shi, X., Siminovitch, K., Kohalmi, S.E., Huang, S., Wu, K., Chen, X., and Cui, Y. (2015). The *Arabidopsis* SWI2/SNF2 chromatin Remodeler BRAHMA regulates polycomb function during vegetative development and directly activates the flowering repressor gene SVP. *PLoS Genetics* 11, e1004944.
- Li, C., Gu, L., Gao, L., **Chen, C.**, Wei, C.Q., Qiu, Q., Chien, C.W., Wang, S., Jiang, L., Ai, L.F., Chen, C.Y., Yang, S., Nguyen, V., Qi, Y., Snyder, M.P., Burlingame, A.L., Kohalmi, S.E., Huang, S., Cao, X., Wang, Z.Y., Wu, K., Chen, X., and Cui, Y. (2016). Concerted genomic targeting of H3K27 demethylase REF6 and chromatin-remodeling ATPase BRM in *Arabidopsis*. *Nature Genetics* 48, 687-693.
- Zhou, Y., Tan, B., Luo, M., Li, Y., Liu, C., **Chen, C.**, Yu, C.W., Yang, S., Dong, S., Ruan, J., Yuan, L., Zhang, Z., Zhao, L., Li, C., Chen, H., Cui, Y., Wu, K., and Huang, S. (2013). HISTONE DEACETYLASE19 interacts with HSL1 and participates in the repression of seed maturation genes in *Arabidopsis* seedlings. *Plant Cell* 25, 134-148.

Presentation:

Chen, C., Tian G., Saatian B., Austin R.S., Kohalmi, S.E. and Cui, Y. (2014)
Identification of a new acetyl-CoA carboxylase 1 mutant allele responsible for the derepression of seed storage proteins. 25th International Conference on *Arabidopsis* Research, Vancouver, Canada